NAS9-12524
T-754
Line Item No. 7
MA-129T

R-9401
NASA CR-
141688

FINAL REPORT

HIGH-TEMPERATURE EARTH-STORABLE PROPELLANT ACOUSTIC CAVITY TECHNOLOGY

May 1974

by

C. L. Oberg, W. S. Hines, and A. Y. Falk

Rocketdyne Division
ROCKWELL INTERNATIONAL
6633 Canoga Avenue
Canoga Park, California

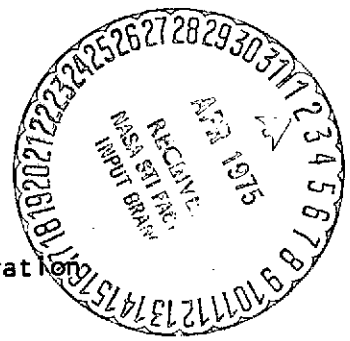

prepared for

National Aeronautics and Space Administration
Lyndon B. Johnson Space Center
R. C. Kahl, Technical Monitor

R-9401

FINAL REPORT
HIGH-TEMPERATURE EARTH-STORABLE PROPELLANT ACOUSTIC CAVITY TECHNOLOGY

Prepared by

C. L. Oberg

W. S. Hines

A. Y. Falk

Prepared for

National Aeronautics and Space Administration
Lyndon B. Johnson Space Center
R. C. Kahl, Technical Monitor

Contract NAS9-12524

May 1974

Rocketdyne Division,
Rockwell International
6633 Canoga Avenue
Canoga Park, California 91304

FOREWORD

The technology program described herein was sponsored by the National Aeronautics and Space Administration, Lyndon B. Johnson Space Center, Houston, Texas, under Contract NAS9-12524. The study was conducted during the 16-month period from July 1972 to October 1973. The NASA Technical Monitor was Mr. W. L. Brasher, initially, and, subsequently, Mr. R. C. Kahl. At Rocketdyne, Mr. L. P. Combs was Program Manager and Dr. C. L. Oberg was Project Engineer. Dr. Oberg was assisted by Mr. W. S. Hines and Dr. A. Y. Falk.

This report has been assigned Rocketdyne report number R-9401.

ABSTRACT

Design criteria, methods and data, have been developed to permit effective design of acoustic cavities for use in regeneratively cooled OME-type engines. This information was developed experimentally from two series of motor firings with high-temperature fuel during which the engine stability was evaluated under various conditions and with various cavity configurations. Supplementary analyses and acoustic model testing were used to aid cavity design and interpretation of results.

Results from this program clearly indicate that dynamic stability in regeneratively cooled OME-type engines can be ensured through the use of acoustic cavities. Moreover, multiple modes of instatility were successfully suppressed with the cavity.

CONTENTS

Introduction 1
Cavity and Motor Hardware Design 3
  General Approach 3
  Cavity Selection and Design 3
  Injector and Hardware Configurations 16
  Injector 18
  Thrust Chamber 18
  BLC Injector 23
  Stability Rating Bombs 23
  Test Stand 25
  Experimental Measurements 25
Experimental Results 33
  Stability Results From Single-Mode Test Results 33
Conclusions 73
Appendix A
Iterative Equations for Prediction of Cavity Damping From a Circumferentially Nonuniform Radially Directed Cavity 75
Appendix B
Derivation of Expression for Spatial Average Temperature in Axial Cavities 79
References 81

ILLUSTRATIONS

1. Comparison of Stability Results From Testing Unbaffled LMA Engine With Predicted Stability Trends 5
2. Thrust Chamber Assembly Used for Heated Fuel Acoustic Cavity Testing 6
3. Predicted Cavity Damping for the First and Second Tangential Modes 8
4. Predicted Cavity Damping for the First Radial and Third Tangential Modes 9
5. Cavity Configurations Used for First Series of Tests 11
6. Resonant Frequencies From Bench Model Tests 14
7. Effective Cavity Depth From Bench Model Tests 15
8. Thrust Chamber Assembly Used for Heated Fuel Acoustic Cavity Testing 17
9. Injector Like-Double No. 2, Showing Face Pattern and Injector Portion of Semi-Axial Cavity 19
10. Photograph of Like Doublet No. 2 Injector With Central Bomb Attachment Location and Fuel Manifold 20
11a. Thrust Chambers Used for Test Firing Program 21
11b. Thrust Chambers Used for Test Firing Program 22
12. Stability Rating Bomb 24
13. Photograph of Thrust Chamber Assembly Mounted on the Test Stand 26
14. Schematic of Lima Test Stand Showing Propellant Feed Systems and Instrumentation 27
15a. MMH Tank and Pressurant System 28
15b. N_2O_4 Tank and Pressurant System 28
16. Pressure Response From a Bomb Disturbance Exhibiting 2640- and 440-Hz Oscillation 37
17. Pressure Response From a Bomb Disturbance Exhibiting 3000-Hz Instability 38
18. Pressure Response From a Bomb Disturbance Exhibiting Stable Behavior 39
19. Comparison of Stability Results With Predicted Trends for Primary Cavity, $\Gamma\hat{p}/\gamma p_o = 0.15$ 42
20. Comparison of Stability Results With Predicted Trends for Primary Cavity, $\Gamma\hat{p}/\gamma p_o = 0.30$ 43
21. Comparison of Stability Results From Multimode Test Series With Predicted Trends for Circumferentially Uniform Secondary Cavity . 52
22. Variation of c* Efficiency (Based on Chamber Pressure) With Mixture Ratio 57
23. Variation of Cavity Gas Temperature With Depth in Radial Primary Cavities 62
24. Variation of Cavity Gas Temperature in Depth in Axial Primary Cavities 63
25. Variation of Measured Cavity Gas Temperature With Mixture Ratio During Runs 177-185 65
26. Variation of Gas Temperature With Depth for Axial Cavities 67
27. Variation of Gas Temperature With Effective Depth for Radial Cavities 68

TABLES

1. Locations of High-Frequency Pressure Transducers and Bomb Installations 24
2. Instrumentation for OME Stability Rating Firings 29
3. Thermocouple Locations in Axial Cavities During Single Mode Test Series 31
4. Thermocouple Locations in Axial Cavities During Multimode Test Series With Excursions in Chamber Pressure, Mixture Ratio, and Fuel Temperature 31
5. Location of Cavity Thermocouples for Radial Cavity Tests 32
6. Completed Test Matrix for Single Mode Test Series 34
7. Summary of Stability Results From Single Mode Test Series 35
8. Bomb Stability Results From Single Mode Test Series 40
9. Test Matrix for Multimode Suppression Testing 45
10. Summary of Stability Results From Multimode Suppression Test Series 46
11. Summary of Bomb Stability Results From Multimode Suppression Test Series 48
12. Summary of Performance Measured During OME Stability Rating Tests 54
13. Summary of Axial Cavity Gas Temperature Results (Runs 43 through 53) 59
14. Summary of Radial Cavity Gas Temperature Results (Runs 54 through 69) 60
15. Summary of Axial Cavity Gas Temperature Results (Runs 174 through 191) 61
16. Acoustic Cavity Gas Temperature Measurements During N_2O_4 MMH Motor Firings With an Unlike Doublet Injector 64
17. Correlation Coefficients for Acoustic Cavity Temperature Distributions 70

INTRODUCTION

Acoustic cavities, used either independently or in conjunction with baffles, have been demonstrated to be an effective method of suppressing acoustic modes of combustion instability in rocket engines. In propulsion applications with requirements for both long-duration firings and reusability, cavities have an advantage over baffles because they are easier to cool and, therefore, less subject to failure from either burnout or thermal cycling. Acoustic cavities, therefore, are particularly attractive for use in the orbit maneuvering engine (OME).

The effectiveness of acoustic cavities for preventing acoustic modes of combustion instability has been demonstrated under some circumstances. Extensive tests have been made with LM ascent engine-type hardware, an unbaffled injector, and the N_2O_4/N_2H_4-UDMH (50-50) propellant combination (Ref. 1). Dynamic stability was demonstrated with a relatively wide range of cavity configurations. Moreover, analytical design techniques have been developed for the design of these cavities (Ref. 1). Nevertheless, the stability of an engine with or without acoustic cavities cannot be predicted analytically with confidence.

The analytical design techniques utilized by Rocketdyne are based on a prediction of the damping contributed by the acoustic cavity without defining the driving effect of the combustion or other contributory processes. The assumption is made that an engine will be stable if the calculated damping from the acoustic cavity alone is made "large enough." However, the required amount of damping is not predicted. Thus, the analytical model provides guidelines for cavity design by indicating those configurations that will provide the greatest stabilizing influence, but stability rating tests are needed to actually define the configurations that will stabilize the engine. In addition, the gas density and sound velocity that exist in the acoustic cavity must be measured or predicted before the cavity damping can be predicted.

Acoustic cavities can be used most effectively and efficiently in the development of any engine if test data are available from stability-rating tests made under conditions that approximate those that exist in that engine. These are needed to predict the gas density and sound velocity that exist in the cavity and, also, to predict the cavity damping requirement.

The purpose of the program described herein was to develop the information necessary to allow effective use of acoustic cavities in regeneratively cooled OME systems. When the program was begun, the data from the extensive testing with the LMA (lunar module ascent)-type hardware were available to aid in the design of cavities for the OME case, but all of these tests had been made with ambient temperature propellants and with operating conditions near those of the LMA engine. Of principal concern was the effect at the high fuel temperature (associated with regenerative cooling). Therefore, this program was begun to evaluate the effectiveness of acoustic cavities under conditions closer to those of the OME.

In addition, it became evident during the program that acoustic cavities to suppress multiple modes of instability, rather than only the first tangential mode which had been encountered previously, were needed for the OME application. Therefore, a portion of the effort was directed toward multimode suppression with acoustic cavities as well.

CAVITY AND MOTOR HARDWARE DESIGN

GENERAL APPROACH

The purpose of this program was to develop the neçessary design criteria, methods, and data to permit efficient and effective use of acoustic cavities in regeneratively cooled OME-type engines. This information was developed experimentally from two series of motor firings with high-temperature fuel during which the engine stability was evaluated under various conditions and with various cavity configurations. A Rocketdyne-owned like-doublet injector and thrust chamber of one of the OME size and type were used for this testing with the NTO/MMH propellant combination. Stability rating bombs were used to evaluate engine stability with three bombs being used for each motor firing. Acoustic cavities with two resonant frequencies were used to obtain multimode suppression, i.e., suppression of more than one mode of instability. One cavity or set of cavities, the "primary" cavity, was intended to suppress the first tangential mode of instability. A second cavity, the "secondary" cavity, was intended to suppress the first radial and third tangential modes of instability. These three modes were shown to occur when insufficient cavity suppression was used. Supplementary analysis and acoustic model testing were used to aid cavity design and interpretation of results.

During the first series of tests, multiple cavity configurations were tested to define roughly the range of cavity configurations that would stabilize the engine. These tests were made with cavities designed to suppress all three modes of instability, the first and third tangential modes and the first radial mode. However, principal attention was directed toward evaluating the suppression of the first tangential mode. During these tests, the effects on engine stability of variations in mixture ratio, fuel injection temperature and the configuration (size and orientation) of the primary cavity, designed to damp the first tangential mode, were determined. A second cavity was installed to suppress the first radial and third tangential modes of instability; this cavity was not changed during this test series. The second cavity was used to allow for possible interaction between the primary and secondary cavities and, further, to ensure that the results obtained for the first tangential mode were not obscured or altered by the occurrence of the higher order modes. These tests were made without BLC, but this did not prevent meeting the objectives of this series.

The second series of tests was directed toward assessing the ability to suppress multiple modes of instability simultaneously with acoustic cavities. This testing was directed toward evaluating the influence of variations in secondary cavity (to suppress higher frequency modes) configuration, BLC flowrate, and mixture ratio on engine stability. A fixed primary cavity configuration, based on results from the first series, was used for all of these tests.

CAVITY SELECTION AND DESIGN

The cavity configurations to be tested during the first series of tests were selected to both demonstrate adequate stability of the first tangential mode with properly designed cavities and, also, roughly define the stability margin. The selection was based primarily on experimental results obtained previously with

the unbaffled LM hardware (Ref. 1) and on predicted cavity damping trends obtained through use of the analytical model for cavity damping (Ref. 1). Most of these experimental results are summarized in Fig. 1 which includes stability results from ~100 motor firings with 25 conventional cavity configurations and ~190 bomb disturbances. Theoretical curves of constant cavity damping coefficient also are shown.

The results shown in Fig. 1 provided an indication of the required damping and cavity dimensions. However, it was considered likely that the heated fuel could increase the damping requirements so that a more limited range of cavity dimensions would stabilize the engine; for example, the required damping coefficient could increase from 400 to 600 sec^{-1}. In addition, although the diameters of the LM and company-owned OME-type thrust chamber were nearly equal, the contraction ratio of the latter chamber is lower, which is predicted to worsen stability (Ref. 2). Nonetheless, the cavity configurations in the central portion of this stable range should provide the greatest damping and, therefore, were likely to stabilize the engine with heated fuel. However, the heated fuel could also alter the cavity temperature distribution and, thus, gas density and sound velocity. This change in temperature would affect the dimensional requirements of the cavity as well, principally cavity depth (or tuning).

To meet the program objectives, two cavity configurations were selected which were expected to provide near maximum damping. Secondly, two additional configurations were selected to define roughly the limits of the stable region.

The like-doublet injector used during the first series of tests initially included a semi-axial acoustic cavity along the periphery of the injector, as shown in Fig. 2. The cavities to be tested were all located in this vicinity, with either radial (not illustrated) or semi-axial entrances, as shown. However, the cavities could not extend radially outward more than 1.5 inches because of the bolt circle (see Fig. 2).

Two major factors were considered in selecting the cavity configurations to be tested. One was how to introduce damping most efficiently for two (or more) modes of instability while evaluating the effects of cavity variations on the primary, first tangential, mode. The second was how to define the range of cavity sizes that would stabilize the engine, with respect to the first tangential mode, with only four different cavity configurations (restricted by the cost of testing).

Two potential methods of introducing "dual-mode" damping were explored. The first was based on the use of L-shaped resonators. Previous analytical results (Ref. 1) and preliminary acoustic model (bench test) results indicated that two basic resonant frequencies could be developed in an L-shaped resonator and that the proximity of these two resonant frequencies to each other could be controlled by adjusting the relative lengths of the two branches of the L. This result suggests that a single L-shaped resonator could be tuned to suppress two modes of instability, by adjusting the two resonant frequencies to correspond to the normal mode instability frequencies. However, later bench model test results did not show evidence of one of these basic resonant frequencies. Nevertheless, because this concept offered the attractive potential for dual-mode suppression with a single resonator, additional analysis was done to define the resonance characteristics more fully.

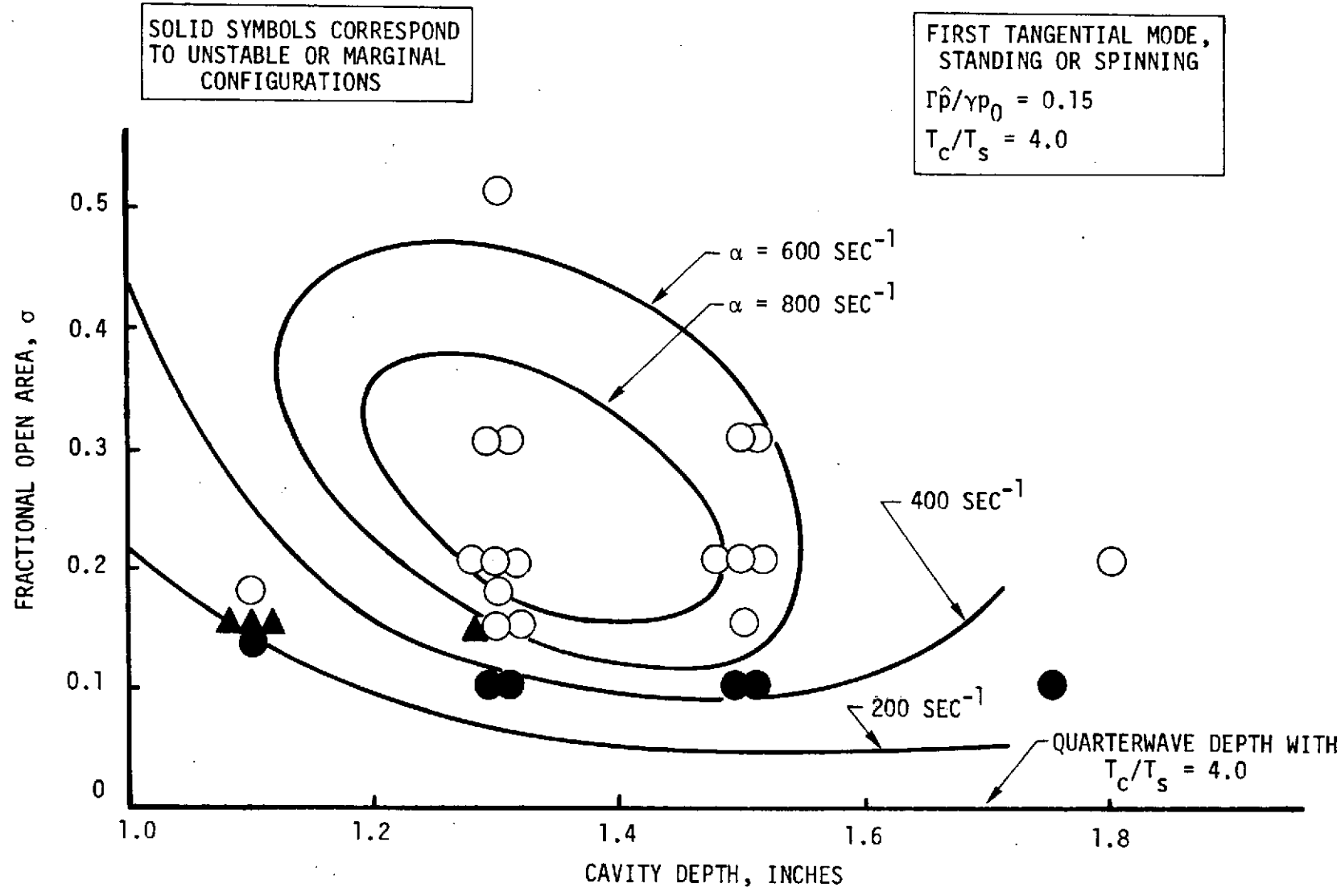

Figure 1. Comparison of Stability Results From Testing Unbaffled LMA Engine With Predicted Stability Trends

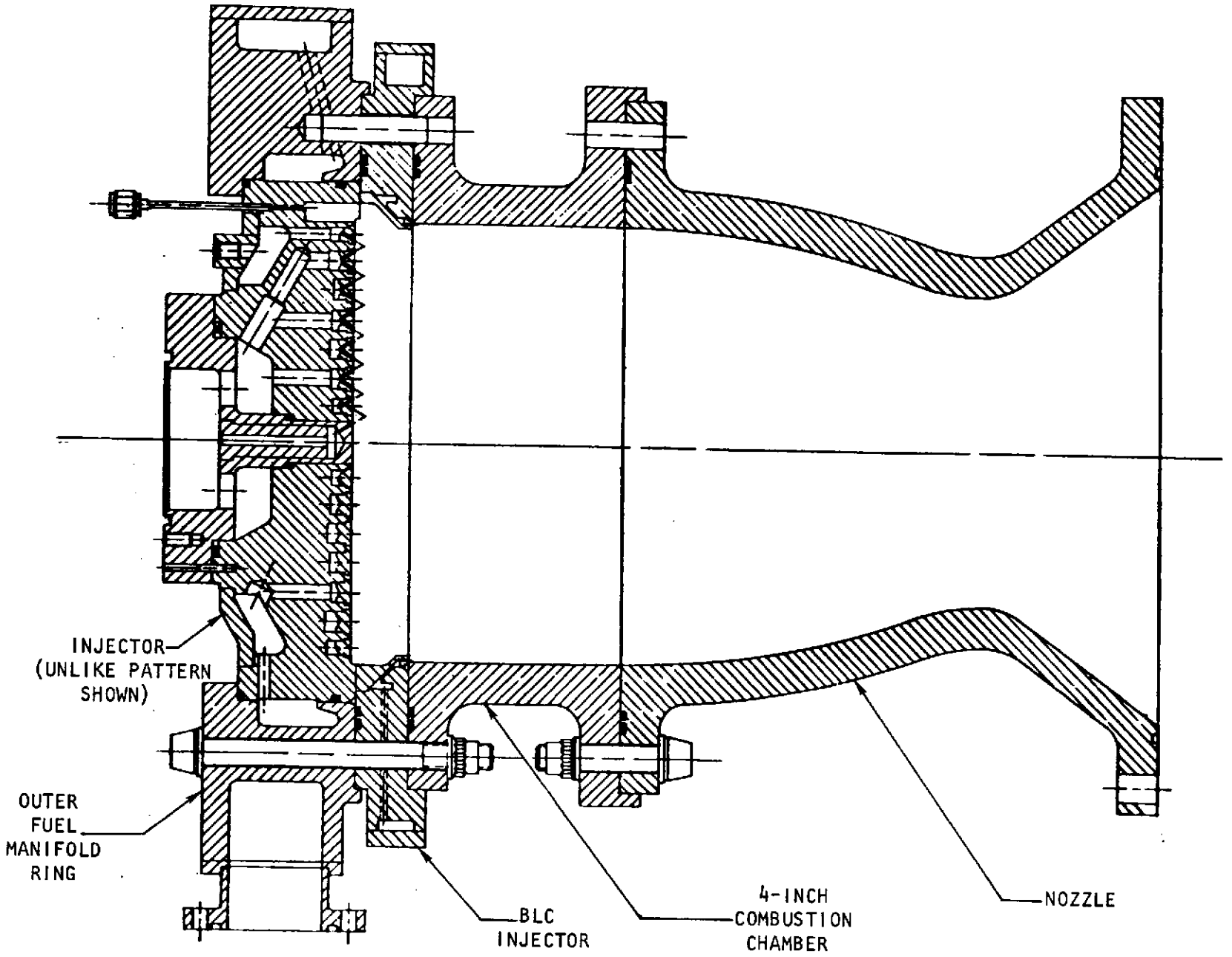

Figure 2. Thrust Chamber Assembly Used for Heated Fuel Acoustic Cavity Testing

Additional, and more definitive, calculations were made of the resonant frequencies. This investigation showed that one of the two basic resonant frequencies was due to a nonphysical or extraneous root to the characteristic equation used to predict the resonant frequencies, and only one basic resonant frequency was predicted. This analysis was based on a variational-iterational solution to an integral form of the wave equation (Ref. 3) which led to a characteristic equation of the form:

$$\int u(p_a - p_b)dS = 0$$

where p_a and p_b are approximate expressions for the oscillatory pressure on each side of an interface joining the two braches of the L, and u is the oscillatory velocity normal to this interface. Physically significant solutions are obtained only when $p_a \simeq p_b$. A nonphysical or extraneous solution is obtained (conceptually at least) when $u = 0$. Therefore, it was necessary to evaluate whether or not a solution to the characteristic equation is acceptable by comparing p_a and p_b. When this comparison was made, it was clear that one of the basic resonant frequencies obtained from the characteristic equation should be rejected and dual-mode damping should not be expected. Further, the results showed the basic resonant frequency to correspond closely to a quarterwave resonance based on the average cavity depth, i.e., the wave is efficiently transmitted around the corner.

Therefore, a second method was selected for achieving dual-mode suppression, which was to use two individual resonator sizes, arranged in two individual rows of each size for convenience in fabrication. One of the resonator sizes was chosen to suppress the first radial and the third tangential modes, which have nearly the same frequency and often are encountered together. The size of the other resonator was varied, but was chosen to suppress the first tangential mode.

Because the two cavities are not independent of one another, a series of damping calculations was made to aid in final selection of the cavity sizes. The cavity damping model was modified to specifically include two discrete resonator rows (previously an averaging procedure had been used). This modified model was used to calculate the anticipated damping for the lowest several modes (first, second, and third tangential modes and the first radial mode) over a range of cavity sizes. The sound velocities in each of the two cavities were assumed equal for these calculations. The variation of the first tangential mode damping with cavity depth was calculated for a primary (first tangential mode) cavity width of 0.5 inch and secondary cavity dimensions of 0.2-inch wide by 0.9-inch deep. Results from these calculations are shown in Fig. 3 . The calculated damping for the second tangential mode is also shown in Fig. 3. The sound velocity ratio, $c_s/c = 0.664$, was estimated from limited stability results obtained with the same and similar motor hardware during company-funded testing. The influence of the secondary cavity on the primary (first tangential) mode is evident but is not very significant. Similarly, the variation of the radial mode damping with depth of the secondary cavity was calculated with a secondary cavity width of 0.2 inch and primary cavity dimensions of 0.5-inch wide by 1.8-inch deep. These results are shown in Fig. 4, along with calculated damping for the third tangential mode (with a single resonator). In this case, the influence of the second resonator is more significant, but still not very large. Note that the radial mode damping is roughly one-half of the third tangential mode damping, which is primarily due to differences in the pressure distributions between the two modes and the location of the resonators relative to the maximum pressure regions.

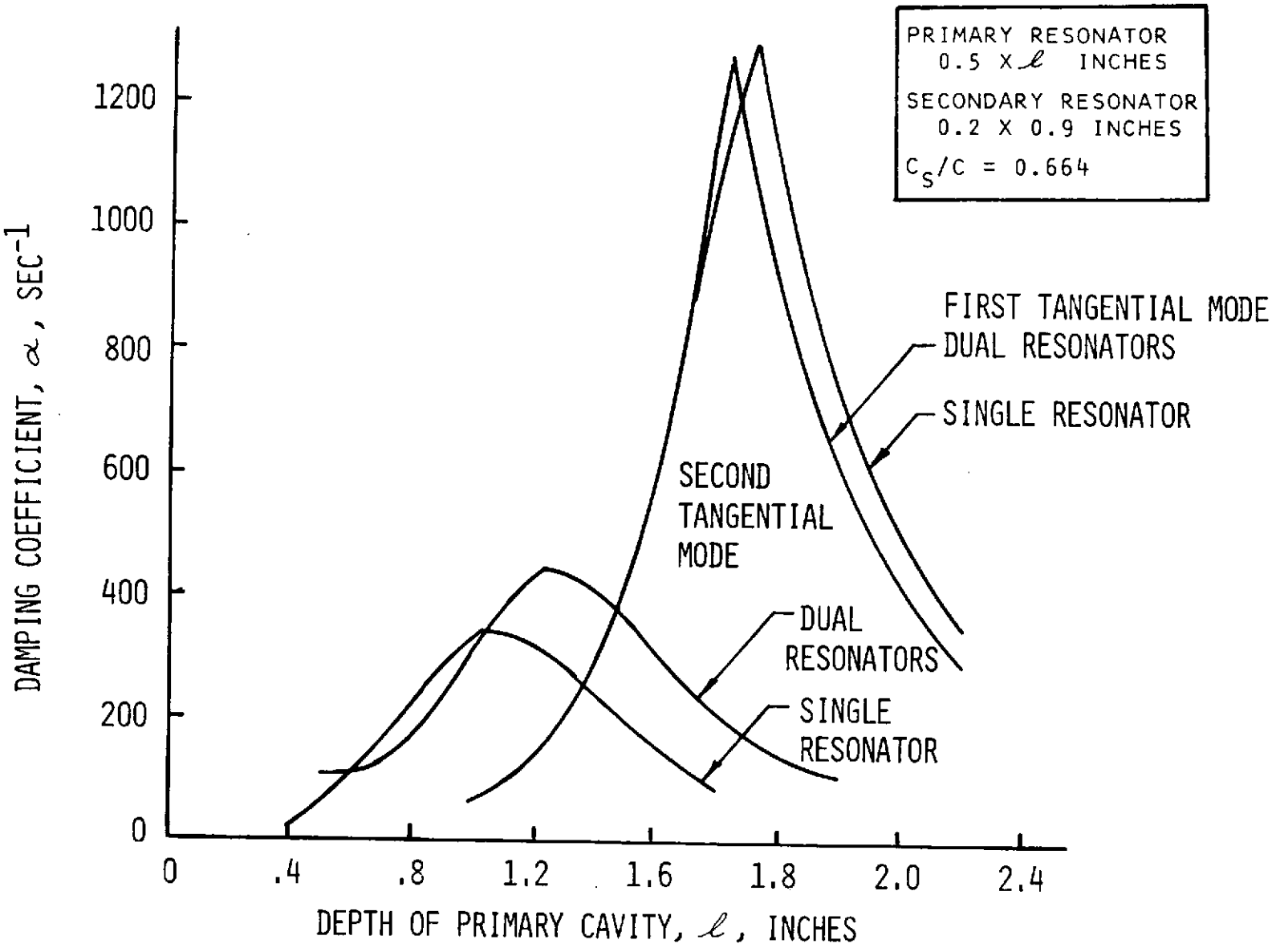

Figure 3. Predicted Cavity Damping for the First and Second Tangential Modes

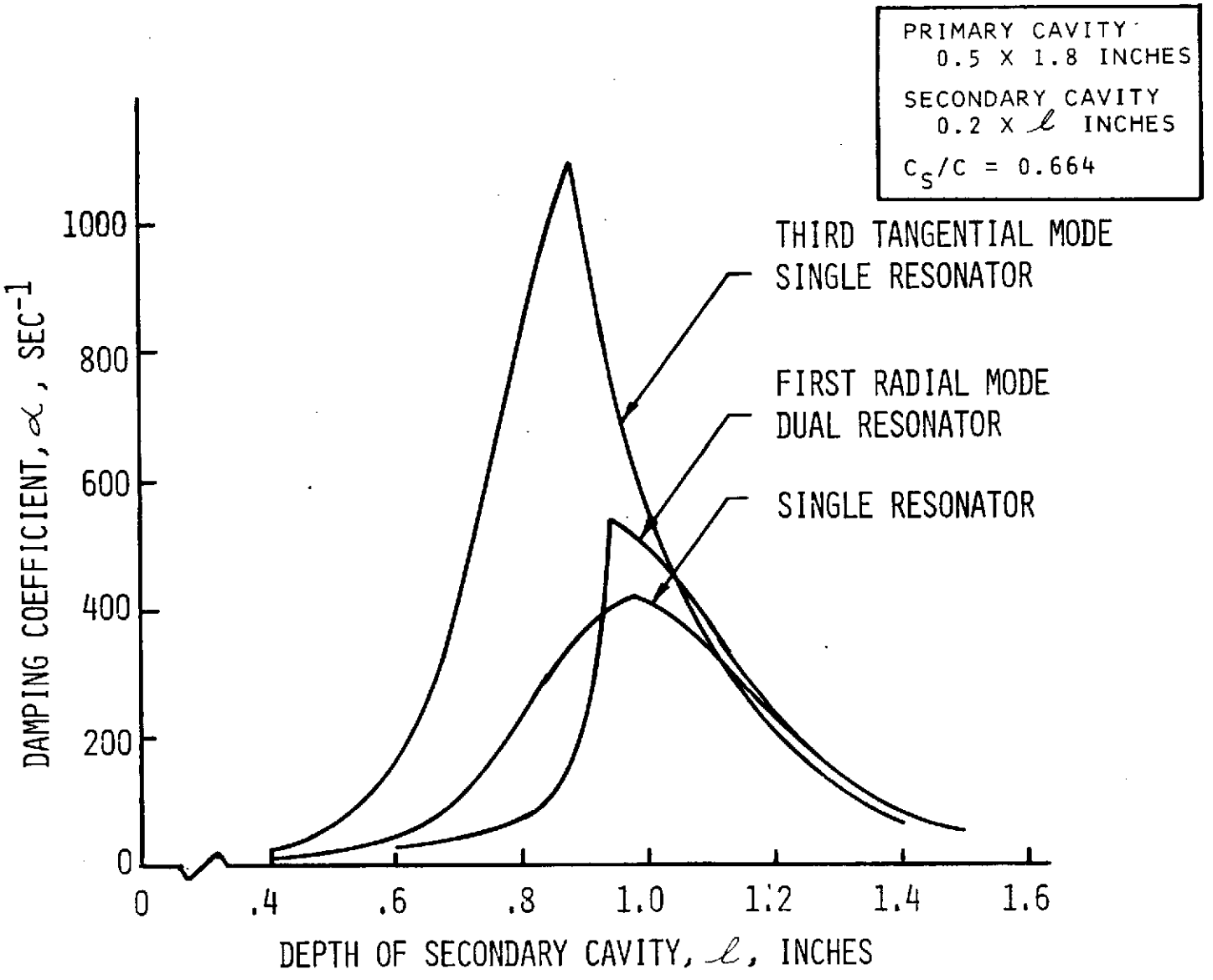

Figure 4. Predicted Cavity Damping for the First Radial and Third Tangential Modes

Probably the most practical type of cavity configuration is the semi-axial configuration shown in the chamber drawing (Fig. 2). Therefore, it would have been desirable to utilize this general configuration for all tests. Unfortunately, the space available in this region of the injector was limited by the proximity of the fuel passages in the injector. Semi-axial cavity dimensions greater than ~1.9 x 0.56 inches were not possible without drastic rework of the injector to move the fuel passages. However, because axial and radial cavities appeared to be largely equivalent from a stability standpoint, the radial arrangement was attractive for roughly defining the range of cavity dimensions, which would stabilize the engine. Moreover, the radial cavity variations could be obtained less expensively through the use of cavity rings than axial variations. Consequently, a radial cavity configuration of the type shown in Fig. 5 was selected for much of the testing. One configuration of the semi-axial type was also tested; it is also shown in Fig. 5. It appeared best to omit the film coolant for these tests, which were of short duration, because of the downstream secondary (higher frequency) cavity. An L-shaped arrangement was required because of the bolt circle at 1.5 inches from the chamber wall.

The following nominal cavity configurations were selected for testing:

Cavity	Effective Depth, inches	Physical Depth, inches	Width, inches	Fractional Open Area, σ
No. 1 Axial	1.9	1.3	0.5	0.225
No. 1 Radial	1.9	1.1+0.8	0.3	0.133
No. 2 Radial	1.8	0.9+0.9	0.5	0.222
No. 3 Radial	1.4	0.9+0.5	0.5	0.222

As explained below, the indicated effective depth of the semi-axial cavity corresponds to a physical depth of 1.3 inches from the injector face.

The indicated effective depths for the radial cavities are obtained with L-shaped resonators with the following dimensions:

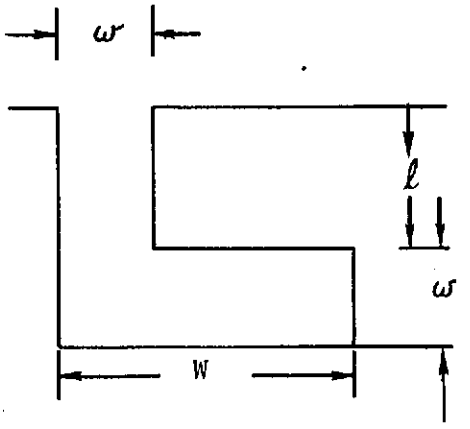

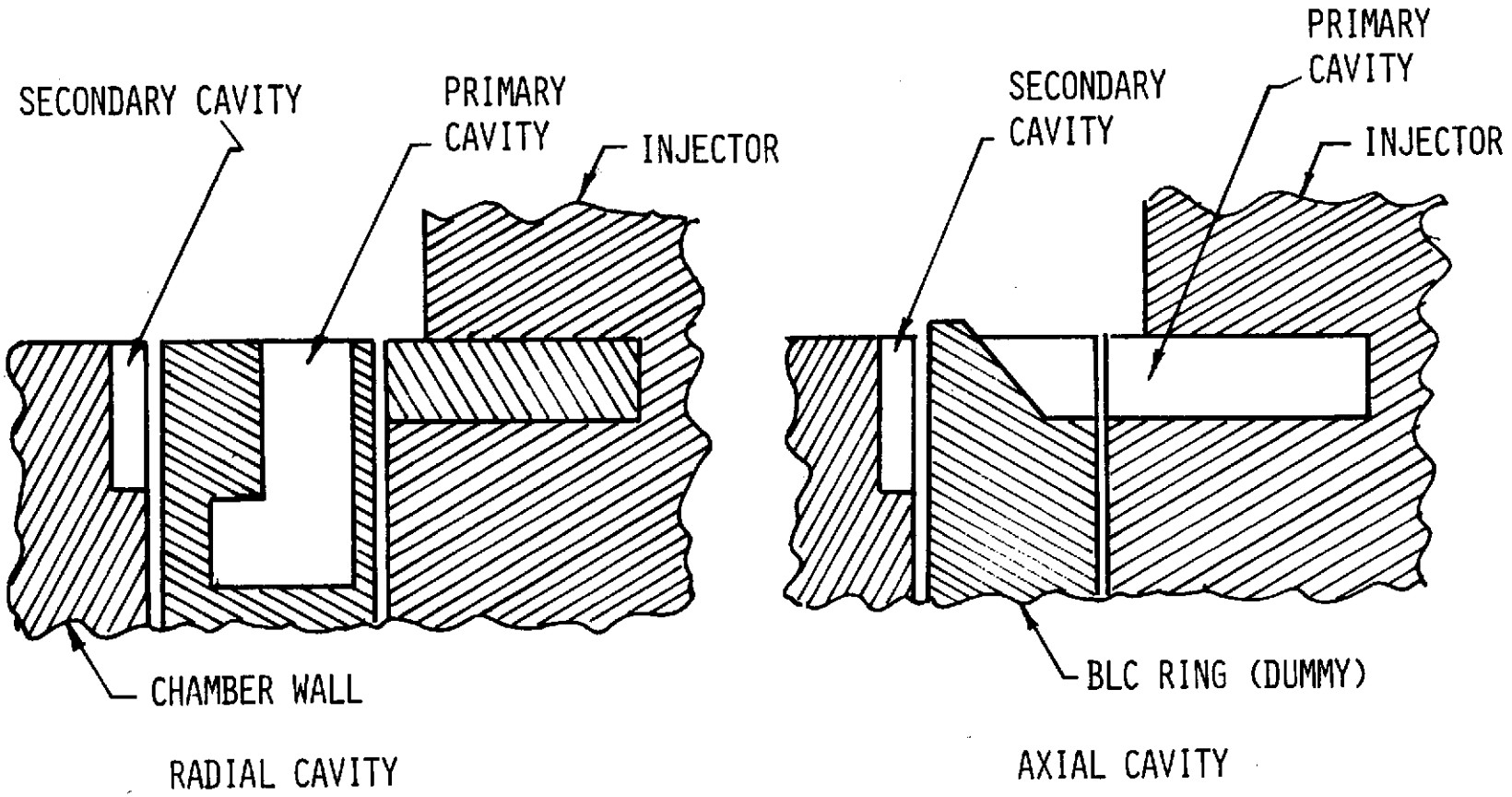

Figure 5. Cavity Configurations Used for First Series of Tests

Cavity	Effective Depth, inches	ω, inches	ℓ, inches	W, inches	Fractional Open Area, σ
No. 1 Radial	1.9	0.3	1.1	0.8	0.133
No. 2 Radial	1.8	0.5	0.9	0.9	0.222
No. 3 Radial	1.4	0.5	0.9	0.5	0.222

The semi-axial cavity configuration had been build into the injector. It had been tested previously, but only a few bomb tests were made with heated fuel and the data were much too limited to justify testing another configuration. This cavity extended 1.3 inches back from the injector face, with a width in this region of 0.5 inch, and had a contoured entrance as shown in Fig. 5 . Bench scale acoustic model tests were made to determine the effective depth of this entrance region. The results indicate the entrance region contributes 0.57 inch to the effective depth.

Acoustic Model Tests

The entrance region of the semi-axial cavity contributes to the effective depth of the cavity but this contribution is not readily predictable. Therefore, a limited number of acoustic model tests were made to measure that contribution. For these measurements, a three-times scale, two-dimensional model of the cavity was made from Lucite and the variation of the resonant frequencies was measured as the cavity dimensions were changed. The model is sketched below:

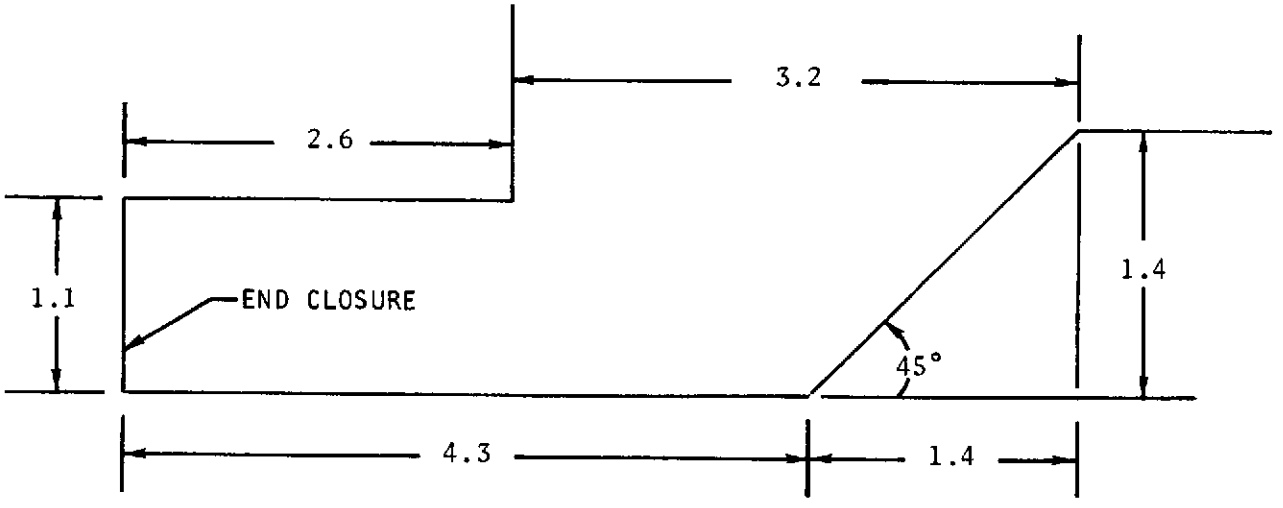

The model was approximately 1.0-inch high (the omitted third dimension in the sketch) with Lucite sheets on the top and bottom. The depth and width dimensions were varied by moving or replacing the end closure. An acoustic driver and microphone were inserted from the top near the end closure. The resonant frequency

was determined by observing the maximum microphone output as the driving frequency was varied. Tests were also made with similarly sized quarterwave resonators that did not have the angular entrance of the semi-axial configuration.

The measured variations in resonant frequency are shown in Fig. 6. The variation in effective depth with depth of the uniform width portion of the cavity is shown in Fig. 7, where the effective depth was calculated from $\ell_e = c/(4\ f_o)$ and the measured resonant frequencies.

The effective depths of the quarterwave resonators are greater than the physical depths because of end effects, i.e., end correction. Because an effective depth for the semi-axial resonator, exclusive of the end correction, was needed, the quarterwave end corrections were used as approximations for the angular case. The results indicate the angular entrance region contributes $\sim$0.42 inch with a 0.36-inch-wide resonator, and $\sim$0.57 inch with a 0.5-inch-wide resonator. These values were used to estimate the effective slot depth of the semi-axial cavities.

Cavity Selection for Multimode Suppression Test Series

Results from the first series of tests indicated the size of primary cavity required to prevent the first tangential mode of instability. Therefore, the second test series was directed toward defining the requirements for suppressing the higher frequency modes while simultaneously suppressing the first tangential mode. The use of two cavity sizes was again chosen to achieve the multimode suppression. Further, to impose a reasonable practical constraint, all cavities were assumed to be located along the periphery of the injector and confined to a spatial region 0.5-inch wide (radially) and 1.3-inches deep (from the injector face).

A basic cavity configuration was selected that allowed various combinations of primary and secondary cavities to be obtained through the use of filler blocks. This basic configuration is sketched below:

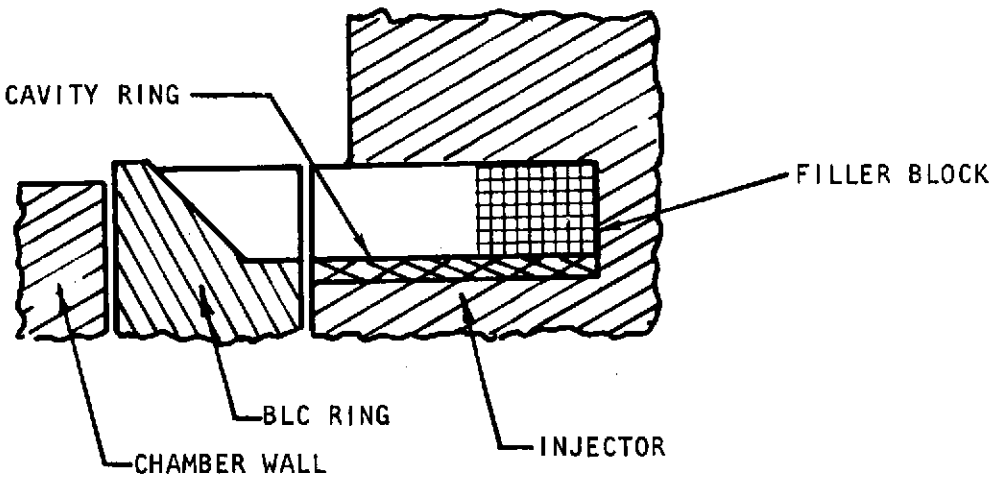

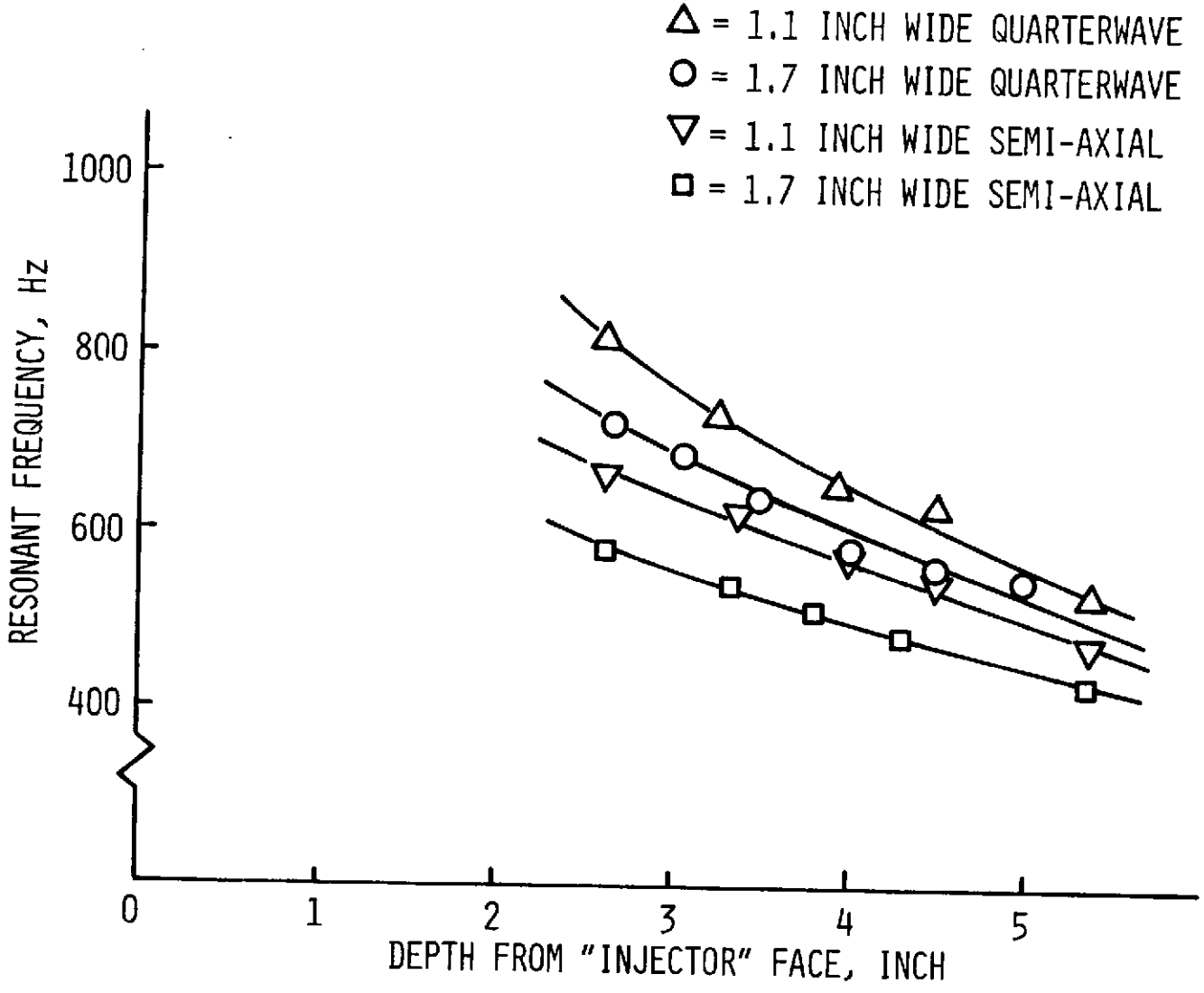

Figure 6. Resonant Frequencies From Bench Model Tests

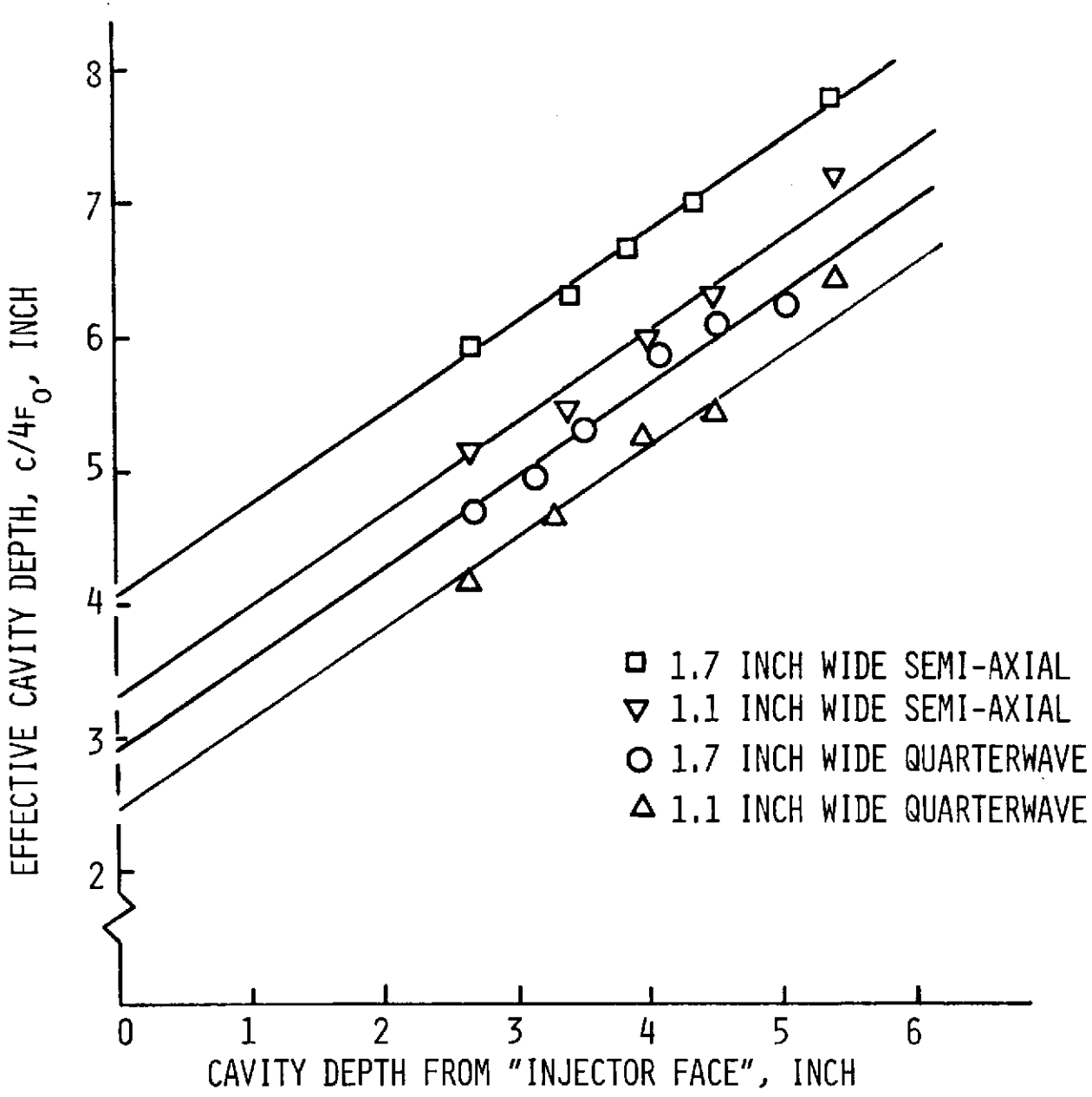

Figure 7. Effective Cavity Depth From Bench Model Tests

The basic cavity configuration is the same as that originally built into the injector and was formed by the BLC ring (entrance region), the cavity ring, and the injector. The overall cavity was divided into 12 compartments by partitions built into the cavity ring. Filler blocks were attached at the closed end of some of the individual cavities to reduce the cavity depth and increase the resonant frequency. The use of filler blocks with single basic ring structure allowed considerable flexibility in the cavity configurations to be tested.

A number of cavity configurations were selected for testing. Based on the results from the first series of tests, a primary cavity depth (effective depth) of 1.75 inches was chosen (a physical depth of 1.15 inches from the injector face). Assuming the cavity gas sound velocities were the same in both the primary and secondary cavities, a corresponding cavity depth for the secondary cavity of 0.92 inch was chosen, based on the analytical predictions for maximum cavity damping. A set of filler-block configurations was then chosen to allow several open area fractions (ratio of cavity open area to injector face area) and cavity depths of the secondary cavity to be tested. These were chosen to allow definition of the range of secondary cavity sizes that will prevent the third tangential and first radial modes.

INJECTOR AND HARDWARE CONFIGURATIONS

Rocketdyne-owned injector and thrust chamber of the OME-type were used for this program. This hardware was designed to operate under the nominal conditions listed below:

Propellant Combination	N_2O_4/MMH
Overall Mixture Ratio	1.65
Chamber Pressure, psia	125
Thrust, pounds	6000
Throat Diameter, inches	5.8
Contraction Ratio	2:1
Expansion Ratio	3:1
BLC Flowrate, percent	2 to 5

This program was directed toward ensuring stability in a regeneratively cooled engine, with an injected fuel temperature in the neighborhood of 200 F (the exact temperature depending upon the BLC flowrate employed to reduce chamber wall heat load). Therefore, the MMH used in the stability test program was preheated to nominal temperatures of 200 or 250 F in an external heat exchanger before each firing.

The overall layout of the workhorse thrust chamber assembly is shown schematically in Fig. 8. The major subassemblies which bolt together to form the engine are described in the following paragraphs.

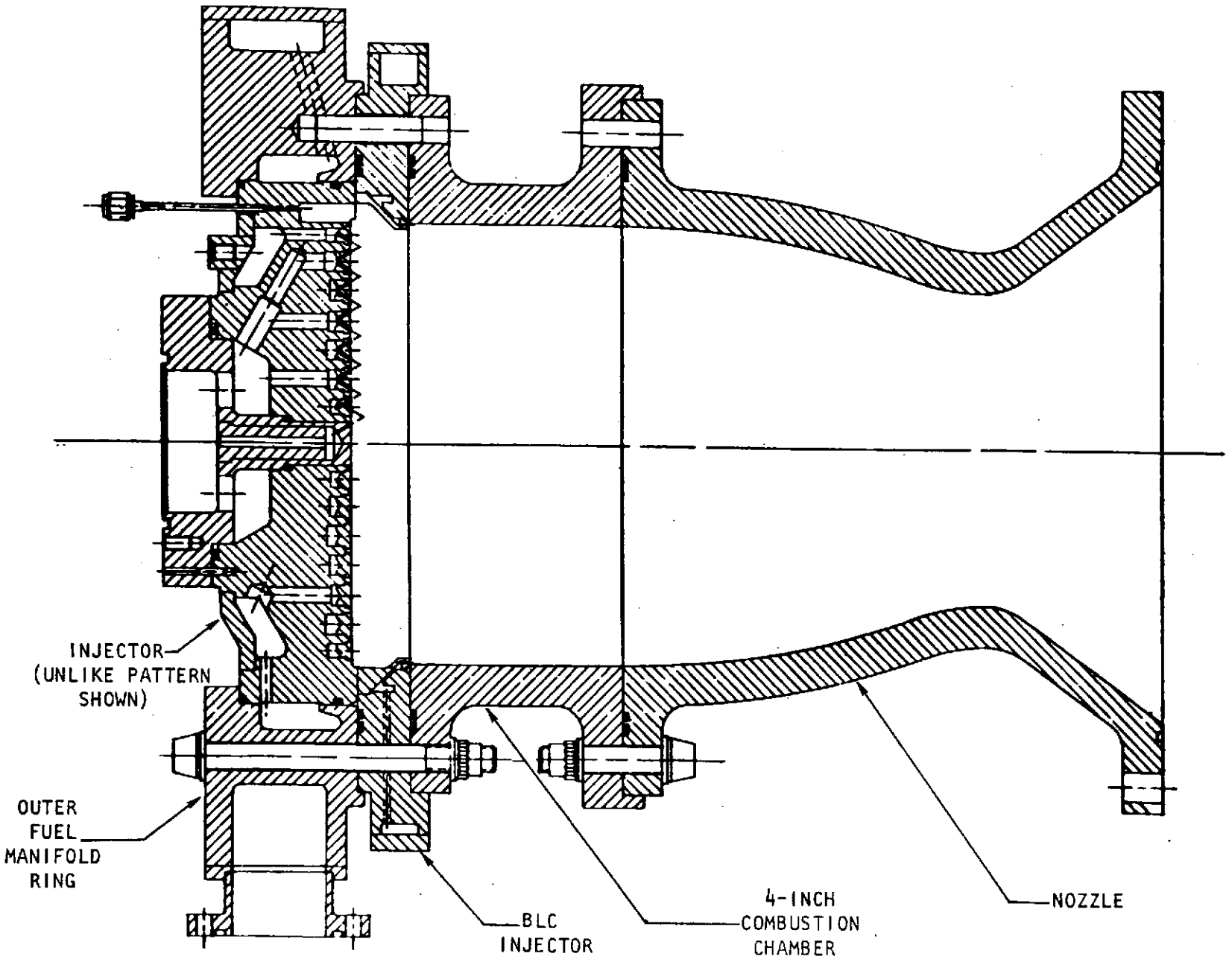

Figure 8. Thrust Chamber Assembly Used for Heated Fuel Acoustic Cavity Testing

INJECTOR

The injector used for the cavity stability testing is shown in Fig. 9. This injector, identified as like doublet No. 2, has 286 pairs of fuel and oxidizer like-double elements in 10 circumferential rows. Fuel is fed from an outer ring manifold (Fig. 8) radially inward through two secondary manifolds and then through downcomers into ring manifolds immediately behind the injector face. Oxidizer is fed from a dome manifold into a secondary manifold and then through downcomers into ring manifolds alternating with the fuel manifolds at the injector face. The spray fans of all elements are oriented with their major transverse dimension in the radial direction and with the fans of each fuel/oxidizer like-doublet pair impinging at an angle of 34 degrees, chosen to promote maximum propellant spray mixing. The orifice diameters of the fuel and oxidizer elements of the inner nine rings are a uniform 0.0251 and 0.0308 inch, respectively. The orifice diameters in the outer ring are 0.0263 and 0.0323, fuel and oxidizer, respectively. During previous company-funded performance tests, the like doublet No. 2 configuration (Fig. 9) delivered c* efficiencies of approximately 94 to 95 percent, with a combustion chamber length (injector face-to-nozzle throat) of 12 inches.

For the present program, the injector was modified slightly by the attachment of a fitting which permitted installation of a thermally detonated stability rating bomb at the center of the injector face (to promote the first radial mode of instability). The modified injector is shown in Fig. 10.

THRUST CHAMBER

The uncooled steel thrust chamber consisted of a 4.0-inch-long cylindrical section, and a nozzle section, shown in Fig. 11a and 11b. The cylindrical section has a constant inside diameter of 8.20 inches; the nozzle converges from the chamber diameter to a throat diameter of 5.82 inches over a distance of 6.91 inches, and then diverges to an exit diameter of approximately 10.1 inches over a length of 3.33 inches.

The cylindrical section contained a radial acoustic cavity 0.80-inch deep by 0.20-inch wide, which was partitioned into 10 compartments to minimize the circumferential flow of hot gas. This cavity was sized to damp the first radial and third tangential acoustic modes of the chamber during the first test series. The cavities in and adjacent to the injector were sized to damp the first tangential mode. After completion of the first test series, this first radial/third tangential mode cavity was eliminated by first machining out the radial dams and then filling the resultant slot with a closely fitting steel ring insert.

The flanged connections between the combustor and nozzle sections and between the combustor section and either the film-coolant injector or radial cavity spacer sections were sealed by sets of double O-rings.

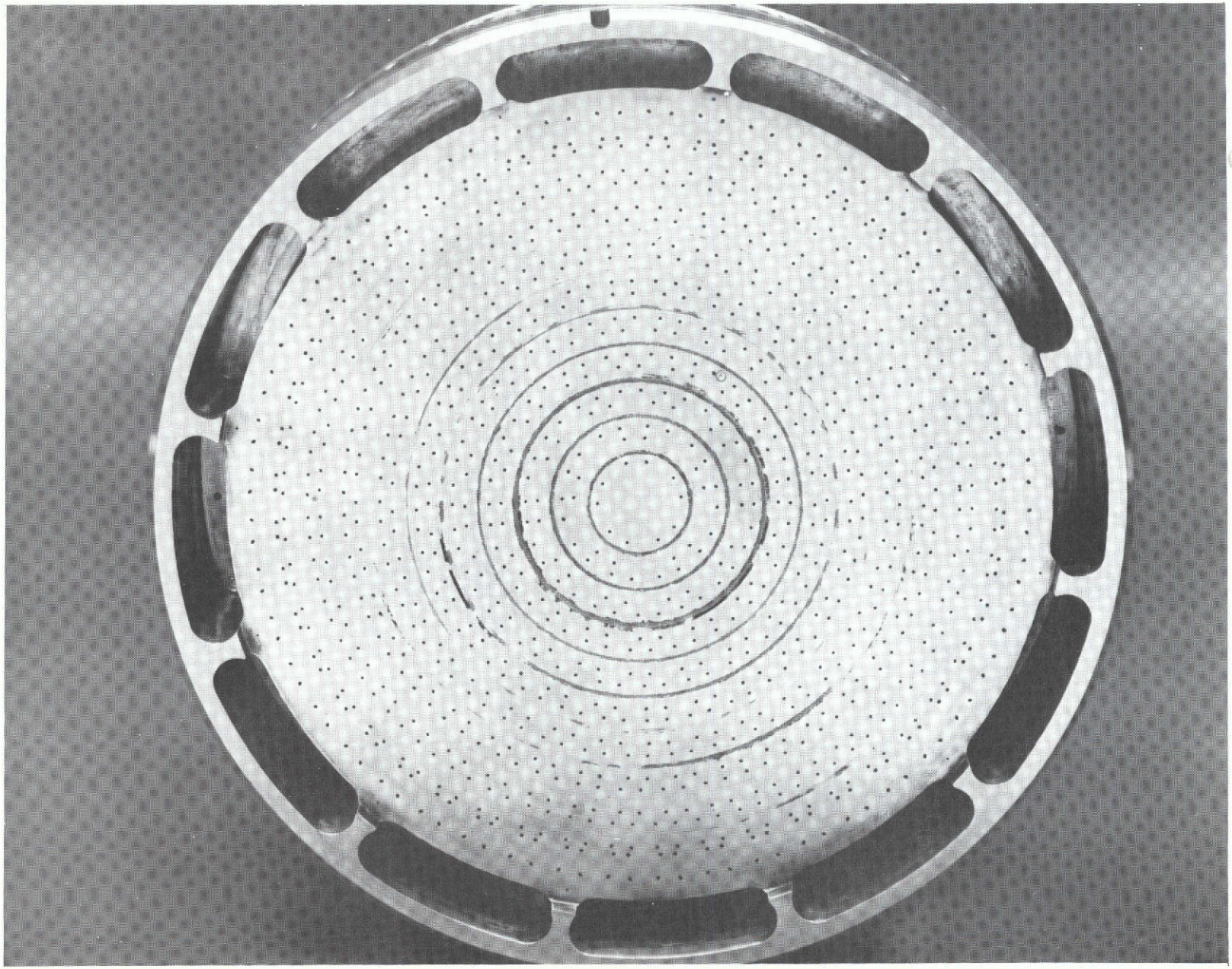

1S042-2/2/73-C1A

Figure 9. Injector Like-Doublet No. 2, Showing Face Pattern and Injector Portion of Semi-Axial Cavity

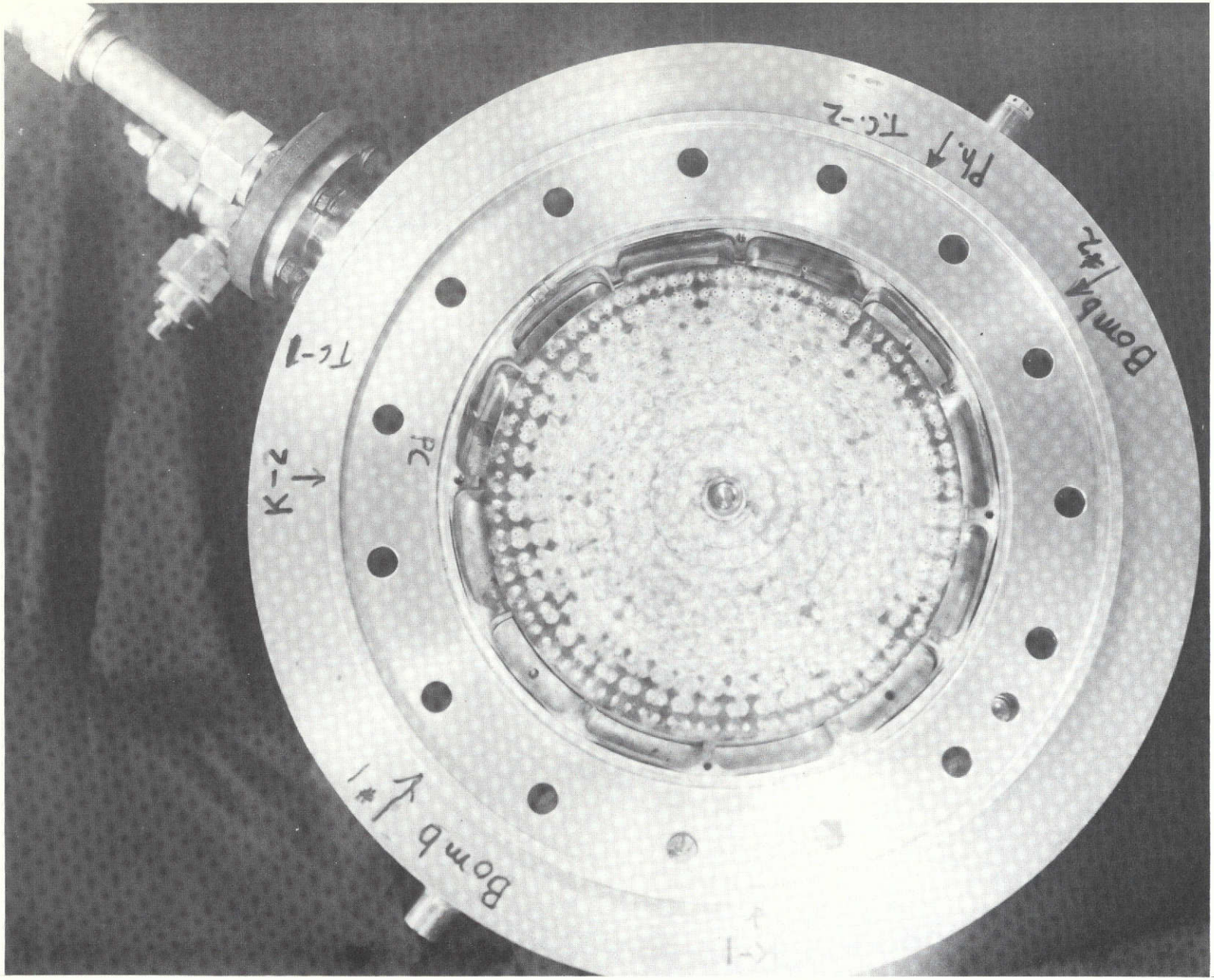

5AA36-7/30/73-S1

Figure 10. Photograph of Like Doublet No. 2 Injector With Central Bomb Attachment Location and Fuel Manifold

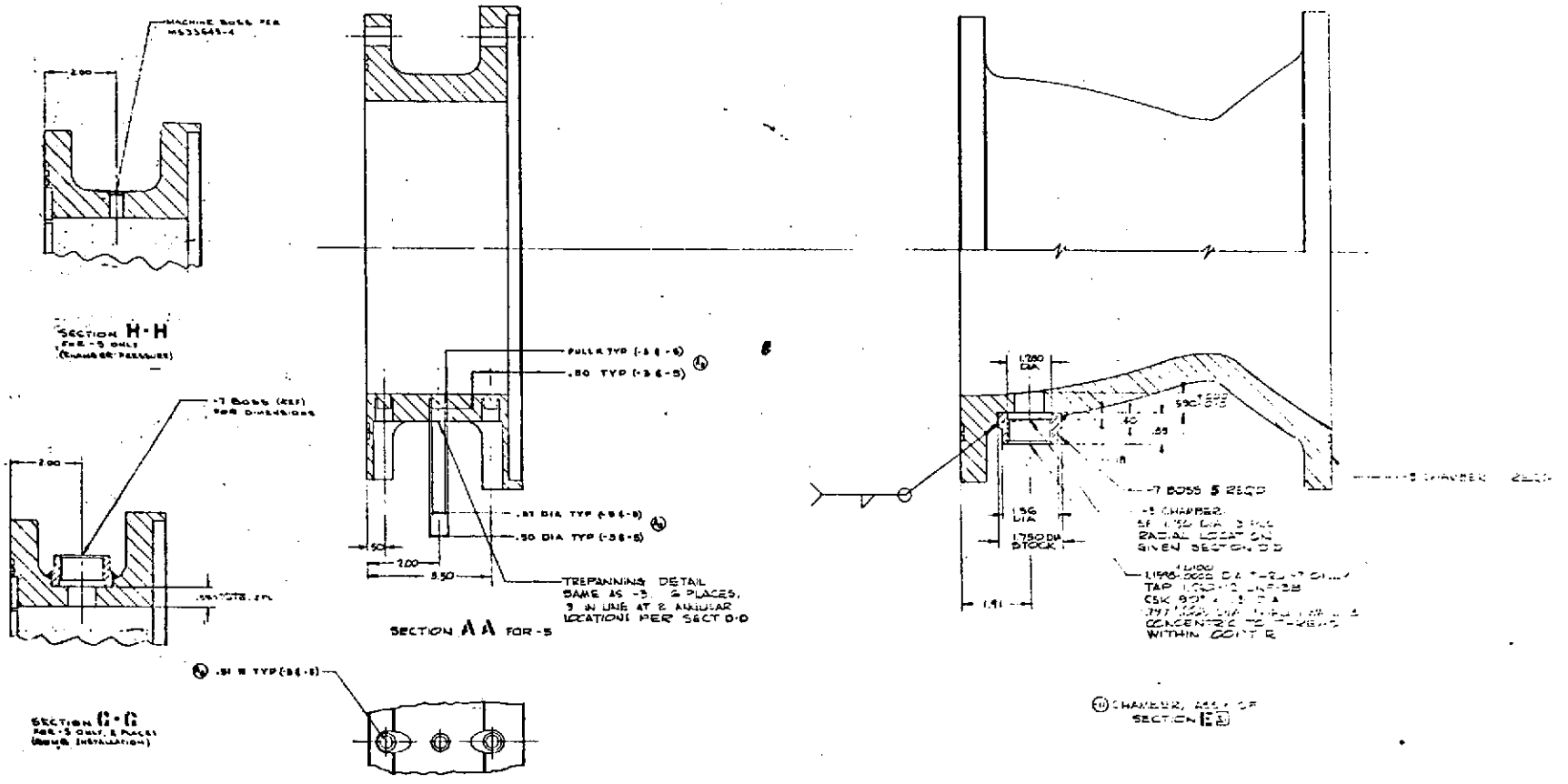

Figure 11a. Thrust Chambers Used for Test Firing Program

Figure 11b. Thrust Chamber Used for Test Firing Program

The two chamber sections were instrumented with a total of 26 thermal isolation plugs for measurement of local chamber wall heat flux through the transient temperature response of thermocouples attached to their outer (back wall) surface. Extensive measurements of heat flux were made with the thrust chamber during previous testing, and a limited number of heat transfer measurements also were made during the firings of this program.

Three ports for either Photocon Model 307 or Kistler Model 614A high-frequency pressure transducers were located in each chamber section at the positions shown in Table 1 . Two bomb ports also were located in the cylindrical section, with three additional ports in the nozzle section at positions shown in Table 1 .

BLC INJECTOR

This thrust chamber was designed for use with a film coolant to reduce the heat load to the chamber and nozzle walls. This BLC (boundary layer coolant) was introduced from a ring injector located between the main injector and the cylindrical chamber section, as shown in Fig. 8 . The BLC ring also provided contoured entrances to the acoustic cavities located along the periphery of the main injector.

In the BLC, the fuel is introduced through a circumferentially tapered outer ring manifold and flows radially inward to a coaxial inner manifold through a set of 30 evenly spaced downcomers. This dual manifold system serves both to pass the fuel through the flange bolt circle and distribute the BLC flow uniformly to the inner manifold prior to its injection into the chamber. The BLC fuel is then injected tangentially along the chamber wall through 90, uniformly spaced, 0.021-inch-diameter orifices located approximately 1.20 inches downstream of the injector face. As shown in Fig. 8 , the location of the film-coolant orifices minimizes the accumulation of liquid fuel which may act as a monopropellant in the axial acoustic cavities.

During the initial single mode test series, no film coolant was used and the BLC injector was replaced by either a blank or dummy BLC ring, or radial cavity rings. The BLC injector was replaced by the dummy ring during nonfilm-cooled firings because of its low thermal capacity and the resultant possibility of overheating when no BLC flow was providing internal regenerative cooling.

STABILITY RATING BOMBS

Stability rating bombs were used to evaluate engine stability. These bombs were equivalent to those used previously for acoustic cavity testing under NASA contract NAS9-9866 (Ref. 1). The bomb configuration is shown in Fig. 12. Three 6.5-grain bombs were utilized in each test. Two of these, inserted through the side wall of the combustor spacer section, were detonated electrically. The third bomb, which was positioned in a fitting at the injector face, was initiated thermally by the hot combustion gases. The bombs were mounted in a steel fitting which sealed the 1/4-inch tubing and located the center of the bomb charge approximately 1.5 inch from the chamber wall.

TABLE 1. LOCATIONS OF HIGH-FREQUENCY PRESSURE TRANSDUCERS AND BOMB INSTALLATIONS

Installation	Angular Location,† degrees	Axial Location (Axial Cavity Tests), inches	Axial Location (Radial Cavity Tests), inches
Photocon* No. 1	12	2.85	3.90
Photocon* No. 2	108	2.85	3.90
Photocon No. 3	228	2.85	3.90
Bomb No. 1	60	3.11	4.16
Bomb No. 2	252	3.11	4.16
Bomb No. 3	---**	~1.5 to 2.0	~1.5 to 2.0

†Angular reference shown in Fig. 11b.
*Modified to accommodate Kistler transducers before multimode test series
**Center of injector face

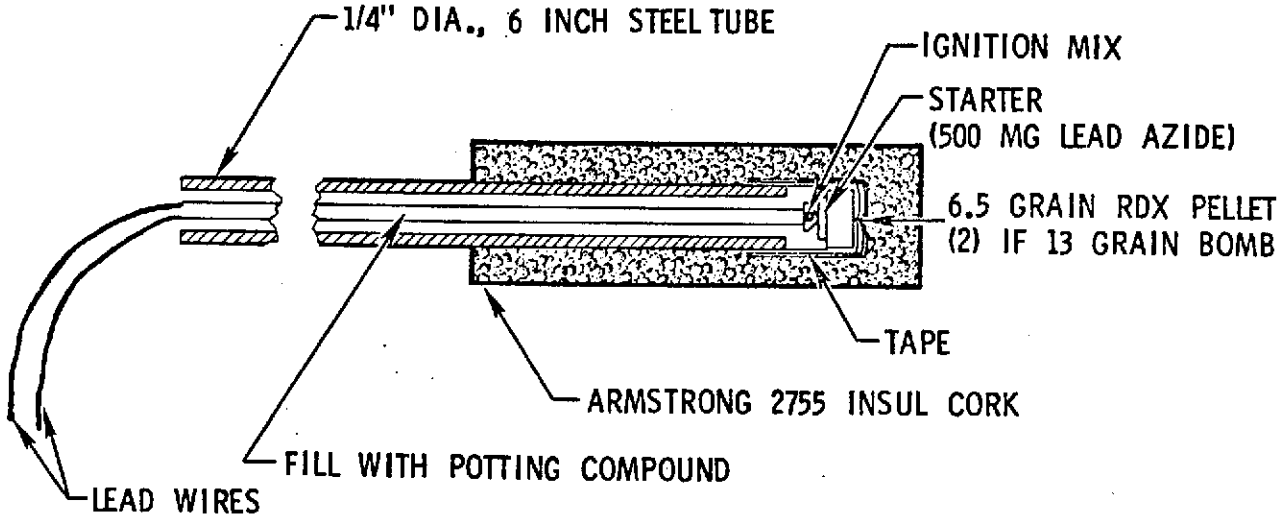

Figure 12. Stability Rating Bomb

The same bombs were used for the injector face mounting location by cutting off the electrical leads and approximately 5.5 inches of the stainless-steel tubing. In this case, the center of the charge was located approximately 2.0 inches downstream from the injector face. Three cork insulation thicknesses (0.050, 0.10, and 0.156 inch) were tested in the first series of firings to determine the thickness that allowed bomb detonation at approximately 1 to 2 seconds from the start of a firing. Based on these data, the 0.10-inch-thick insulation was selected for use in a majority of the remaining tests.

The electrically initiated bombs were sequenced for initiation approximately 1.5 and 2.0 seconds into the test. Thus, all three bombs were planned for initiation between 1 and 2 seconds from the start of the test. Based on extensive previous cavity stability testing, this was thought to be sufficient to allow reasonably constant engine and cavity operating conditions to be established. Generally, longer term transients have not been experienced at Rocketdyne.

TEST STAND

The motor firings were performed on Lima stand in Rocketdyne's Propulsion Research Area (PRA). A photograph of the workhorse thrust chamber installed on this test stand is shown in Fig. 13. Simplified schematic representations of the overall propellant flow system and of the MMH and N_2O_4 tank pressurization systems are shown in Fig. 14 and 15. High-pressure gaseous nitrogen was used both to pressurize the propellant tanks and to purge the thrust chamber and injector manifolds between firings. The test stand was operated remotely from a console in a nearby concrete blockhouse.

Fuel Heater

To model the fuel injection temperatures typical of a regeneratively cooled engine, the required weight of MMH for a single test was batch heated to 200 or 250 F, nominally, in a coil-in-shell heat exchanger located immediately upstream of the fuel engine main valve. In this heater, hot water flowing inside four concentric coils of 0.250-inch-OD stainless steel tubing is used to provide a temperature-limited heat source for moderate amounts of the thermally unstable MMH. As shown in Fig. 14, the water is circulated in a closed system from a steel reservoir tank through either the heat exchanger or a bypass loop and back to the reservoir. An alternate supply of cold water could be introduced into the system to quickly cool the heat exchanger and permit test personnel to inspect the hardware and replace stability rating bombs between firings.

EXPERIMENTAL MEASUREMENTS

The instrumentation list for the motor firings is given in Table 2 . The numbers listed in the second and third columns of this table specify the location of the measurement in terms of the similar numbers in Fig. 14 and 15, the stand and propellant system schematics. Temperatures, flowrates, and low-frequency pressures were measured with thermocouples, turbine flowmeters, and Taber strain gage transducers, respectively. The electrical outputs from the various transducers were recorded on either a Beckman digital data system with 100 channels, on direct-reading potentiometers, or on two oscillographs. The high-frequency pressure

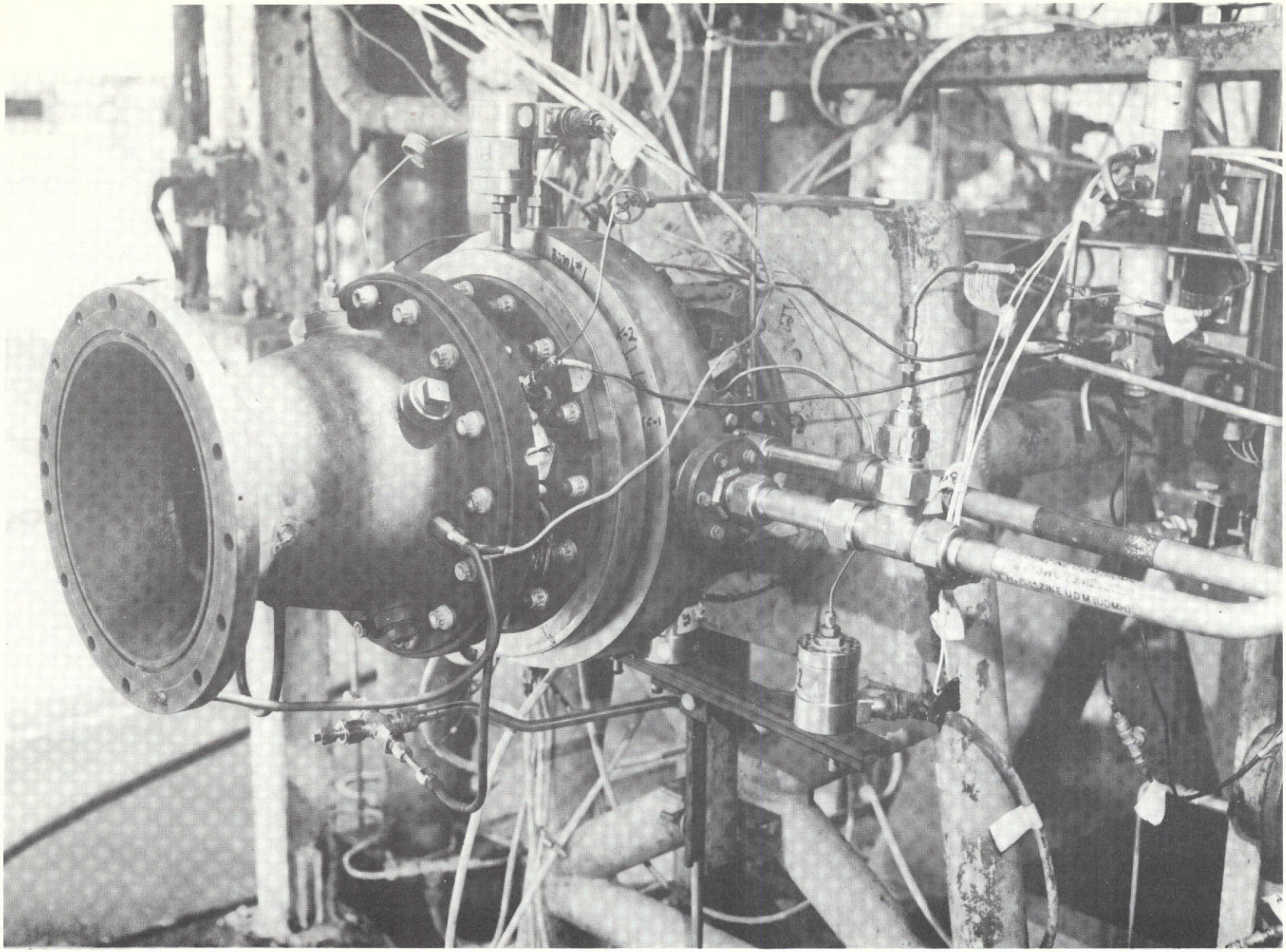

5Z224-8/30/73-S1

Figure 13. Photograph of Thrust Chamber Assembly Mounted on the Test Stand

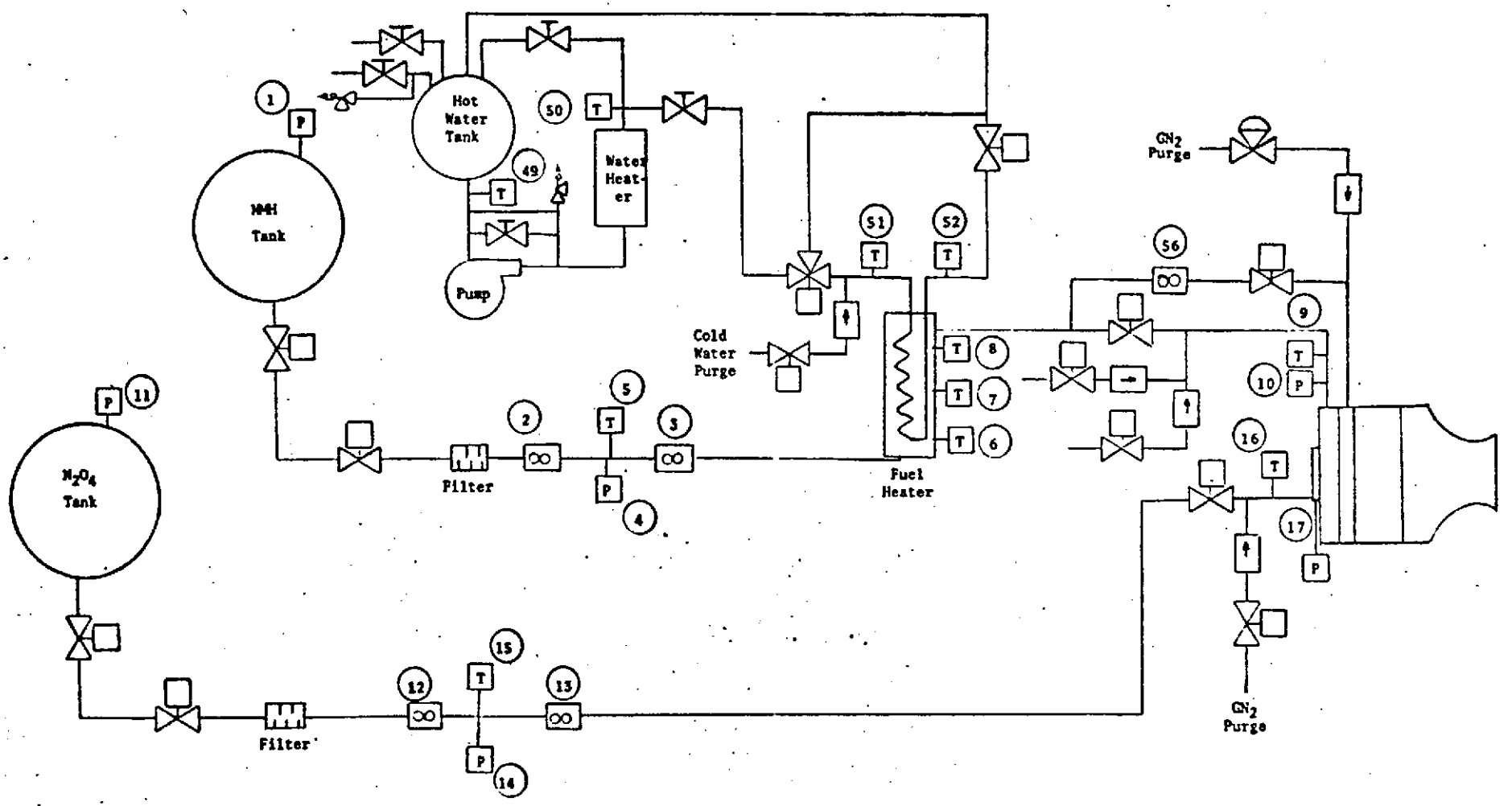

Figure 14. Schematic of Lima Test Stand Showing Propellant Feed Systems and Instrumentation

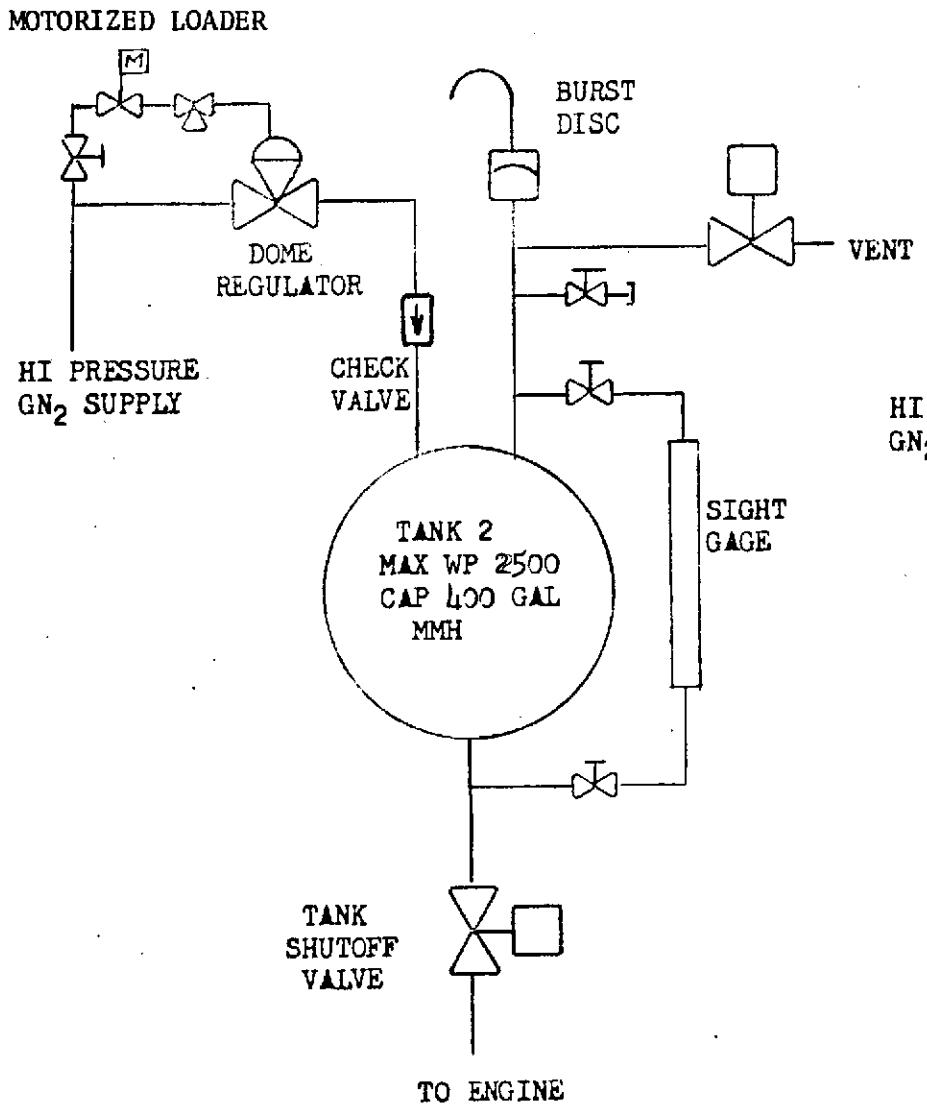

Figure 15a. MMH Tank and Pressurant System

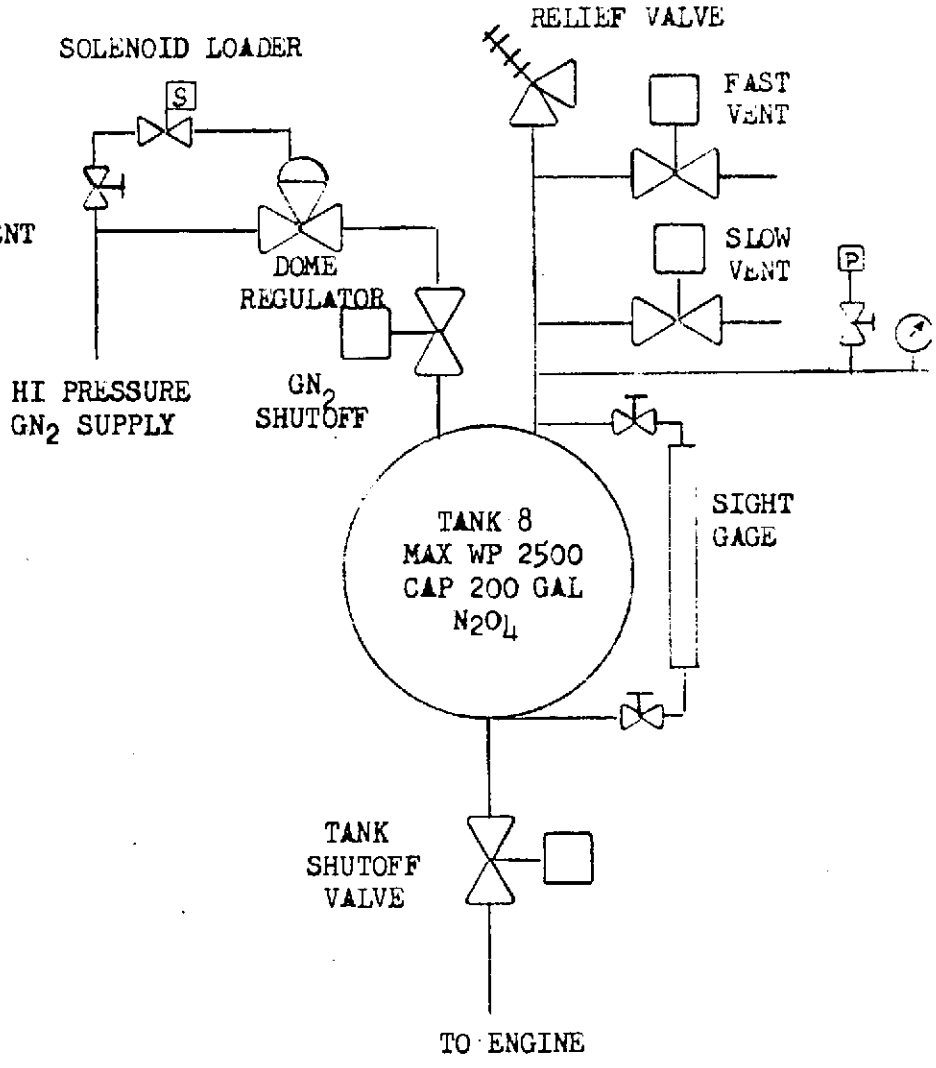

Figure 15b. N_2O_4 Tank and Pressurant System

TABLE 2 . INSTRUMENTATION FOR OME STABILITY RATING FIRINGS

Parameter	Transducer	Location		Recording
		Fig.	Fig.	
Fuel System				
Tank Pressure	Taber	(1)		DRP
Flowrate	Flowmeter (2 measurements)	(2),(3)		BDD, DRP, OSC
Line Pressure	Taber	(4)		BDD, DRP
Line Temperature	1/C T/C	(5)		BDD, DRP
Heater Temperature	1/C T/C (3 measurements)	(6),(7),(8)		DRP
Injection Temperature	1/C T/C	(9)		BDD, DRP
Injection Pressure	Taber		(2)	BDD, DRP, OSC
Oxidizer System				
Tank Pressure	Taber	(11)		DRP
Flowrate	Flowmeter (2 measurements)	(12),(13)		BDD, DRP, OSC
Line Pressure	Taber	(I4)		BDD, DRP
Line Temperature	1/C T/C	(15)		BDD, DRP
Injection Temperature	1/C T/C	(16)		BDD, DRP
Injection Pressure	Taber		(1)	BDD, DRP, OSC
Thrust Chamber				
Chamber Pressure	Taber (2 measurements)			BDD, DRP, OSC, TAPE
Pressure Oscillation	Photocon or Kistler (3 measurements)		(5)	OSC, TAPE
Cavity Temperature	T/C (up to 10 measurements)		(4)	BDD, DRP
Wall Temperature	1/C T/C (up to 8 measurements)		(7)	BDD, DRP
Miscellaneous				
Water Tank Temperature	1/C T/C	(18)		DRP
Water Heater Temperature	1/C T/C	(19)		DRP
Water Temperature at Fuel Heater	1/C T/C (2 measurements)	(20)(21)		DRP
Reference Junction Temperature	1/C T/C			BDD
Fuel Main Valve Power and Travel				BDD
Oxidizer Main Valve Power and Travel				BDD
MMH Film-Coolant (BLC) Flowrate	Flowmeter	(22)		BDD, DRP, OSC

Key

Taber - Taber strain gage pressure pickup
T/C - Thermocouple
1/C - Iron constantan
BDD - Beckman Digital Data System
DRP - Direct Reading Potentiometer
OSC - Oscillograph
TAPE - Magnetic Recording Tape

oscillations initiated in each test by stability rating bombs were measured with either water-cooled Photocon Model 307 or helium-bleed-cooled Kistler Model 614A transducers. High-frequency data were recorded on both a high-speed oscillograph and on magnetic tape. Duplicate measurements were made of the key performance parameters, fuel and oxidizer flowrates, and chamber pressure.

The locations of the three high-frequency pressure transducers in the walls of the combustor section are listed in Table 1. The axial locations are referenced to the injector face, while the angular locations are referenced in accordance with Fig. 11b. It should be noted that the transducers have two possible distances from the injector, depending on whether a particular test was made with the BLC ring or with one of the radial cavity segments (Fig. 5). Table 1 also shows the location of the three rating bombs. The two wall-mounted bombs and the high-frequency instrumentation were located at approximately the same axial station.

The gas temperatures in the acoustic cavities were measured with up to 10 exposed junction thermocouple probes. Sheathed thermocouples were used which thermally isolated (approximately) the thermocouple from the cavity wall and allowed the gas temperature to be measured. Either W-5% Rh/W-26% Rh or chromel/alumel thermocouples were used. Locations of the thermocouples within the cavities (which varied during the two test series) are listed in Tables 3 through 5. For the axial cavities, thermocouple location is defined in terms of the depth (D) and distance from the nearest radial dam (η); for the L-shaped radial cavities, the location is given in terms of the radial (Δr) and axial (z) distances from the center of the cavity opening, together with a specification of whether the thermocouple is located in the angular plane of symmetry of the cavity compartment (CL), or within approximately 0.15 inch of the radial dams separating the cavity compartments (NW).

As mentioned previously, the combustor and nozzle sections of the chamber were instrumented with 26 thermal isolation buttons. These buttons were used to measure heat flux during a lengthy series of performance evaluation firings performed before the initiation of the stability tests of this program. As a result of this prior firing history of the uncooled steel chamber, substantial fatigue of the thin circular webs connecting the buttons to the adjacent main wall structure had occurred at the start of the stability test program. Consequently, these buttons could be used for local heat flux measurement in only the first few firings of the program before it was necessary to weld them into the main chamber wall structure.

TABLE 3. THERMOCOUPLE LOCATIONS IN AXIAL CAVITIES DURING SINGLE MODE TEST SERIES

Thermocouple	Distance from Dam (η), inch	Depth from Injector Face (D), inch
T_{AX} -1	0.1	0.0
T_{AX} -2	1.0	0.1
T_{AX} -3	0.1	0.3
T_{AX} -4	1.0	0.5
T_{AX} -5	0.1	0.7
T_{AX} -6	0.1	0.2
T_{AX} -7	1.0	0.4
T_{AX} -8	0.1	0.5
T_{AX} -9	1.0	0.7
T_{AX} -10	0.1	0.8

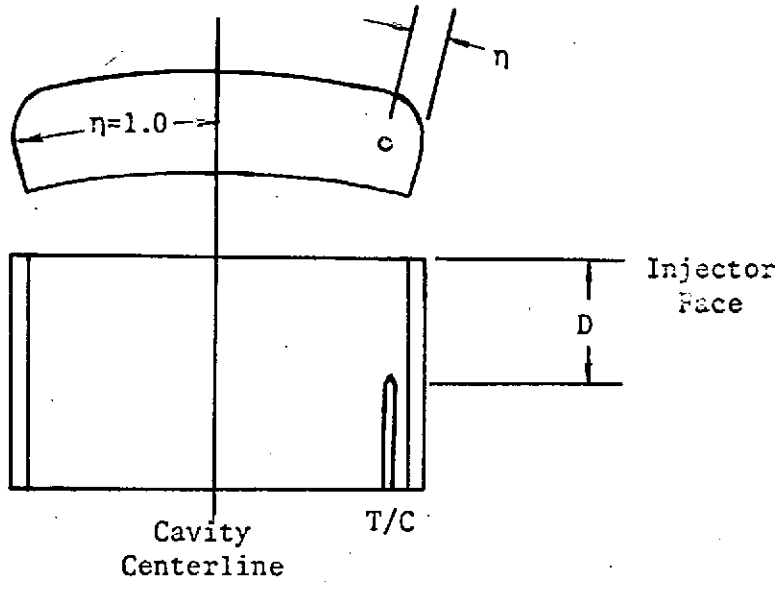

TABLE 4. THERMOCOUPLE LOCATIONS IN AXIAL CAVITIES DURING MULTIMODE TEST SERIES WITH EXCURSIONS IN CHAMBER PRESSURE, MIXTURE RATIO, AND FUEL TEMPERATURE

Thermocouple	Distance from Dam (η), inch	Depth from Injector Face (D), inch
T_{AX} -1	0.1	1.00
T_{AX} -2	1.0	0.60
T_{AX} -3	0.1	1.00
T_{AX} -4	1.0	0.60
T_{AX} -5	0.1	0.40
T_{AX} -6	0.1	0.80

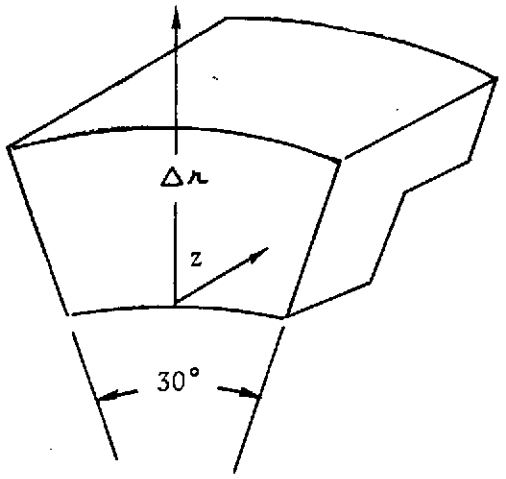

Δr = radial distance from cavity opening

z = distance from upstream edge of cavity

TABLE 5. LOCATION OF CAVITY THERMOCOUPLES FOR RADIAL CAVITY TESTS

Cavity	Thermocouple Designation	Δr	z	θ *
Radial No. 1	T_R -1	0.3	0.15	NW
	-2	1.0	0.15	NW
	-3	0.5	0.15	NW
	-4	0.1	0.15	CL
	-5	1.25	0.55	NW
	-6	1.25	0.35	NW
	-7	1.2	0.15	CL
	-8	0.8	0.15	NW
	-9	0.5	0.15	NW
	-10	1.3	0.15	NW
Radial No. 2	-1	0.2	0.27	NW
	-2	1.0	↓	NW
	-3	0.5	↓	NW
	-4	0.1	↓	CL
	-5	1.2	↓	NW
	-6	0.3	↓	NW
	-7	1.2	↓	CL
	-8	0.8	↓	NW
	-9	0.5	↓	NW
	-10	1.3	0.27	NW
Radial No. 3	-1	0.3	0.27	NW
	-2	1.0	↓	NW
	-3	0.5	↓	NW
	-4	0.1	↓	CL
	-5	1.2	↓	NW
	-6	0.3	↓	NW
	-7	1.2	↓	CL
	-8	0.8	↓	NW
	-9	0.5	↓	NW
	-10	1.3	0.27	NW

*NW = near sidewall location

CL = centerline or midwidth location

EXPERIMENTAL RESULTS

STABILITY RESULTS FROM SINGLE-MODE TEST SERIES

The purpose of the first series of tests was to demonstrate stability with a practical cavity configuration and to roughly define the range of cavity configurations that would prevent a first tangential mode of instability. A secondary cavity was installed to provide suppression for the first radial and third tangential modes of instability. This secondary cavity was used to allow for any interactive effects between the primary and secondary cavities and, also, to prevent occurrence of the higher frequency modes which could cause uncertainty relative to the first-tangential mode results. The secondary cavity was not changed during the test series. Furthermore, no attempt was made at this time to ensure that the first radial and/or third tangential modes would occur without the secondary cavity.

The most important stability-related parameters were considered to be cavity dimensions, mixture ratio, and fuel temperature. Chamber pressure and film-coolant flowrate appeared to have a less significant effect on the first tangential mode during previous tests with the unbaffled LMA-type hardware (Ref. 1); therefore, these were not being varied. Twenty-seven tests were made with four different cavity configurations.

The completed test matrix for this series of tests is shown in Table 6 . All of these tests were made with the like-doublet injector (LD No. 2) in the uncooled OME-type thrust chamber (described previously) with the NTO/MMH propellant combination. The indicated nominal mixture ratios correspond to the core mixture ratios that would be obtained with 2.5-percent BLC and overall mixture ratios of 1.55, 1.65, and 1.75. The fuel was heated to temperatures representative of the injection temperatures of a regeneratively cooled engine. Chamber pressure and thrust were fixed for all tests at 125 psia and 6000 pounds, nominally. Combustion stability was determined by monitoring the chamber response to a series of three bomb-induced disturbances during each test.

The dimensions of the secondary cavity remained fixed for all tests at 0.2 by 0.8 inch. This cavity was located in the cylindrical chamber section downstream of the film-coolant ring. For this reason, the film coolant was omitted for these tests, which were of short duration (~3 to 4 seconds). In a practical design, the secondary cavity would probably be located upstream of the film-coolant injection. Omission of the film coolant was not expected to significantly affect the cavity stabilization because previous tests with the unbaffled LMA hardware (under Contract NAS9-9866) showed no measurable effects.

Stability results from this series of tests are summarized in Table 7 . Configurations were classified, for the indicated operating conditions, as stable, marginal, or unstable if: (1) all bomb disturbances damped to within ±5 percent of chamber pressure in less than 20 milliseconds, (2) any disturbance required more than 20 milliseconds to damp, or (3) any disturbance failed to damp. Two, or possibly three, modes of instability were encountered. The 3000-Hz oscillation encountered with the radial No. 1 cavity was identified as the first tangential

TABLE 6. COMPLETED TEST MATRIX FOR SINGLE MODE TEST SERIES

Objective	No.* of Tests	Acoustic Cavity**				Mixture Ratio			Fuel Temperature, F	
		No. 1 Axial	No. 1 Radial	No. 2 Radial	No. 3 Radial	1.57	1.77	1.97	200	250
Thorough Evaluation of Practical Cavity	2	X					X		X	
	3	X				X			X	
	1	X						X	X	
	2	X					X			X
	2	X				X				X
	1	X						X		X
Define Stable Region	3		X				X		X	
	2		X				X			X
	3			X			X		X	
	2			X			X			X
	3				X		X		X	
	3				X		X			X
Total Tests	27									

*Three bombs were planned for each test unless the first one initiated an instability.

**Secondary cavity of fixed dimensions designed to suppress the first radial and third tangential modes was used during all tests.

TABLE 7. SUMMARY OF STABILITY RESULTS FROM SINGLE MODE TEST SERIES

Configuration	No. of Tests/Bombs	Nominal Mixture Ratio	Fuel Nominal Temperature, F	Maximum Damp Time, msec	Stability	No. of Instabilities/ No. of Bombs	Frequencies, Hz
Axial (0.5 x 1.9)	2/6	1.57	200	6	Stable	0/6	
	3/7	1.77	200	∞	Unstable*	1/7	2640 + 440
	1/3	1.97	200	28	Marginal*	1/3	2380
	2/6	1.57	250	7	Stable	0/6	
	2/6	1.77	250	8	Stable	0/6	
	1/2	1.97	250	7	Stable	0/2	
Radial No. 1 (0.3 x 1.9)	3/8	1.57	200	95	Marginal	3/8	3000
	2/5	1.57	250	55	Marginal	2/5	3000
Radial No. 2 (0.5 x 1.8)	3/9	1.57	200	6	Stable	0/9	
	2/6	1.57	250	7	Stable	0/6	
Radial No. 3 (0.5 x 1.4)	3/8	1.57	200	∞	Unstable*	1/8	2600 + 420
	3/6	1.57	250	6	Stable	0/6	
Total	27/72						

*Apparently stable to first tangential mode.

mode. A similar frequency had been encountered during previous company-funded tests with an unlike doublet injector in this thrust chamber. Calculated frequencies for the lowest several acoustic modes, calculated from the normal mode expressions for a closed cylinder and the 3060 Hz average frequency for the first tangential mode observed during company-funded tests, are listed below:

INSTABILITY MODE FREQUENCIES BASED ON 3060 Hz FOR FIRST TANGENTIAL MODE

Mode	Frequency, Hz
First longitudinal	2107
First tangential	3060
First-tangential-first longitudinal	3715
Second tangential	5076
First radial	6369
Third tangential	6983

Another mode of instability with a frequency near 2600 Hz was encountered that does not appear to correspond to any of the chamber acoustic modes. This mode has not been identified positively but it is suggested that it is a feed system-coupled, high-frequency mode. Such modes have been encountered previously at Rocketdyne, e.g., the Extended Range Lance (XRL) booster engine. The XRL problem was identified with a fluid resonance within the ring grooves of the injector and was eliminated by placing dams in the ring grooves to prevent the resonance. Therefore, it has been tentatively concluded that the 2600-Hz oscillation is due to a similar mode. A more nearly conclusive identification would require analysis of the coupled modes of the chamber and feed system. In two instances, this mode of instability continued until the end of the test and a number of instances of similar oscillation were encountered that damped (several during the second test series). The frequency tended to be lower when the oscillation damped, ~2400 Hz.

A 430-Hz oscillation also occurred, but only after the 2600-Hz oscillation had been initiated and never occurred without it. Therefore, these two modes appear related. An example of this behavior is shown in Fig. 16 .

Examples of the pressure histories obtained from unstable (3000 Hz) and stable tests as a result of bomb disturbances are shown in Fig. 17 and 18.

Results from a detailed analysis of the bomb-induced transients are summarized in Table 8 , including overpressures, damp times, and rates of pressure rise.

Comparisons of predicted stability trends and measured stability are shown in Fig. 19 and 20. Measured results from both the OME-type hardware and the Rocketdyne unbaffled LMA hardware are shown. Data from the latter hardware have been adjusted for the differences in instability frequencies and estimated cavity sound velocities, i.e., LMA cavity depths have been increased by the factor 1.295.

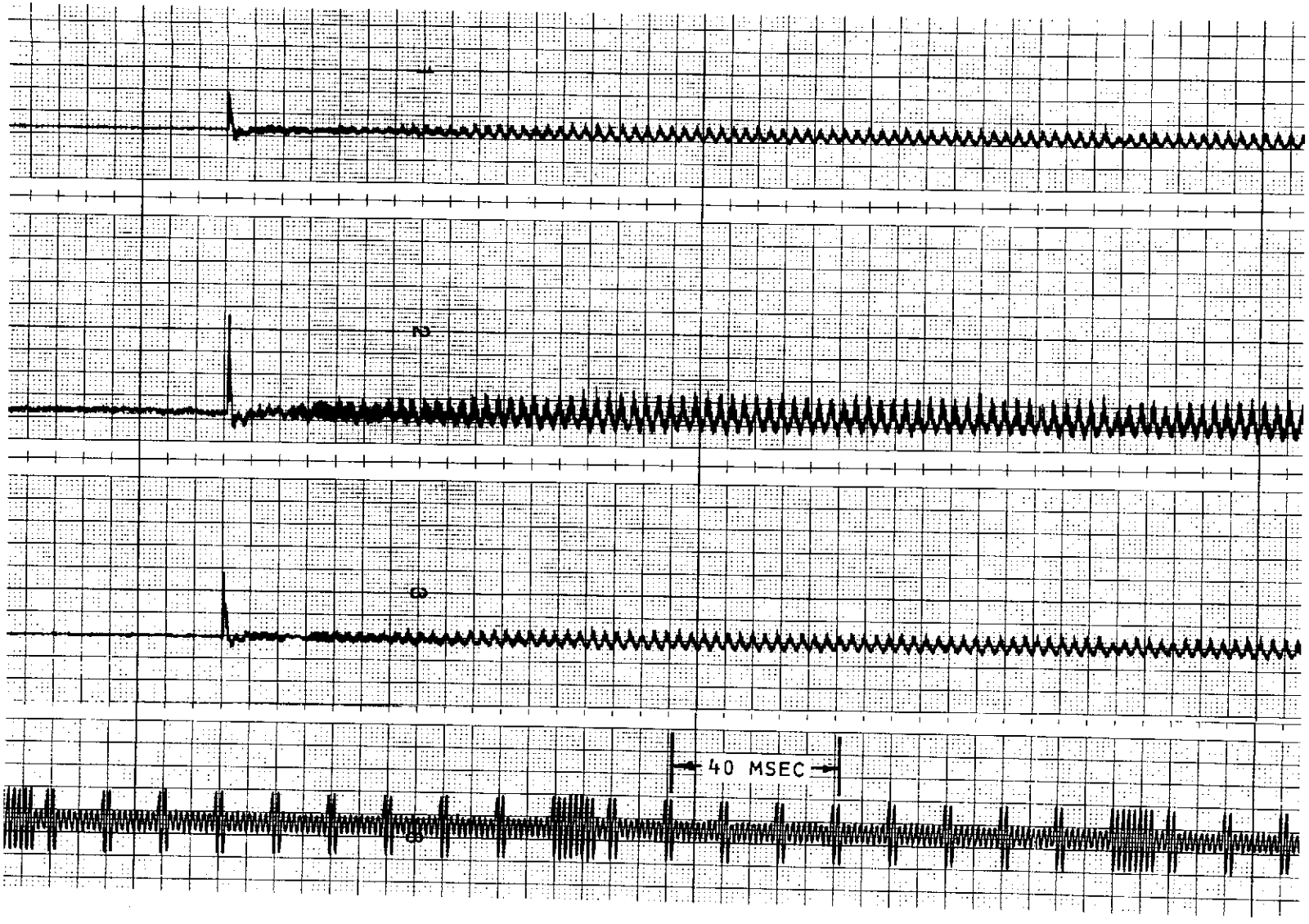

Figure 16. Pressure Response From a Bomb Disturbance Exhibiting 2640- and 440-Hz Oscillation

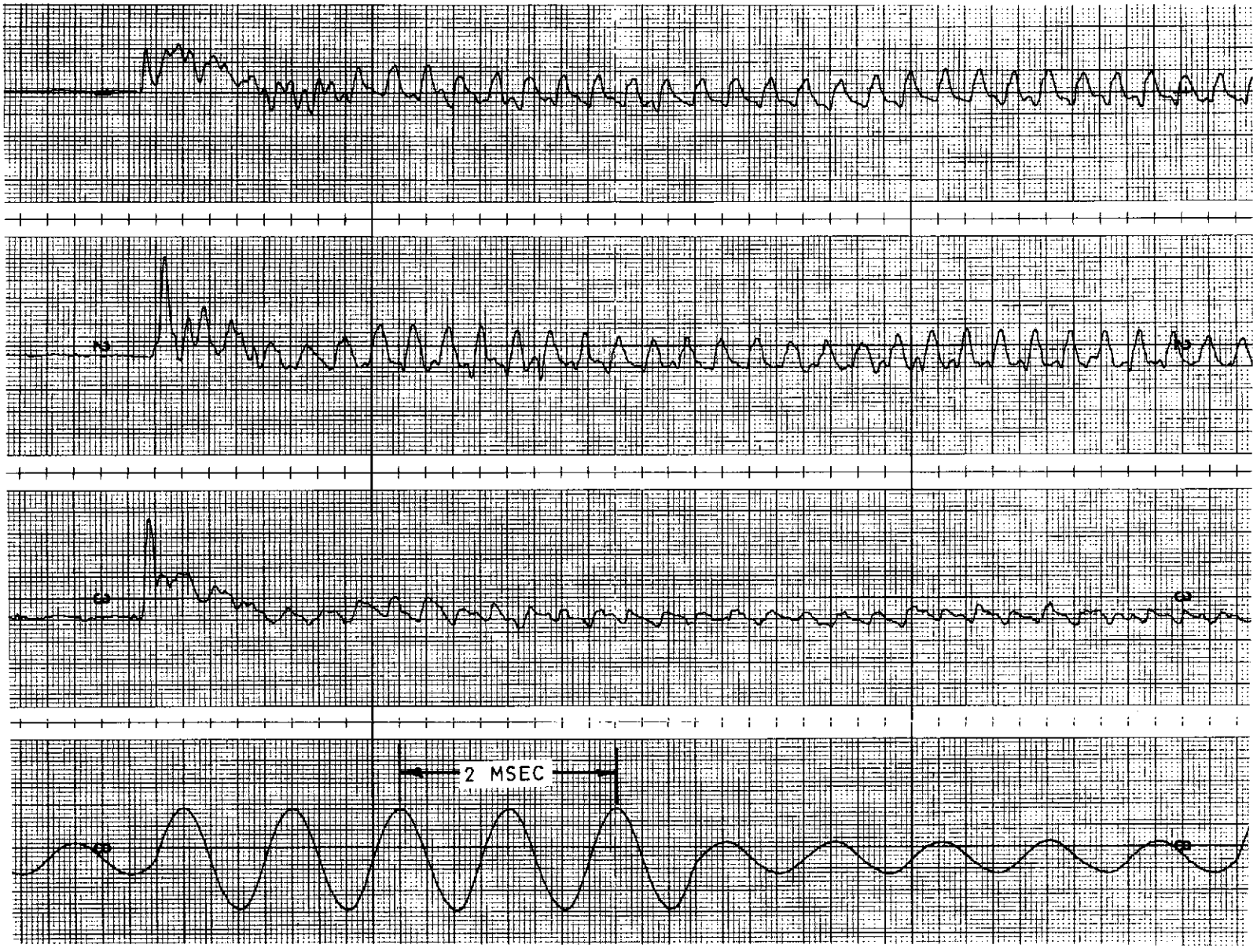

Figure 17. Pressure Response From a Bomb Disturbance Exhibiting 3000 Hz Instability

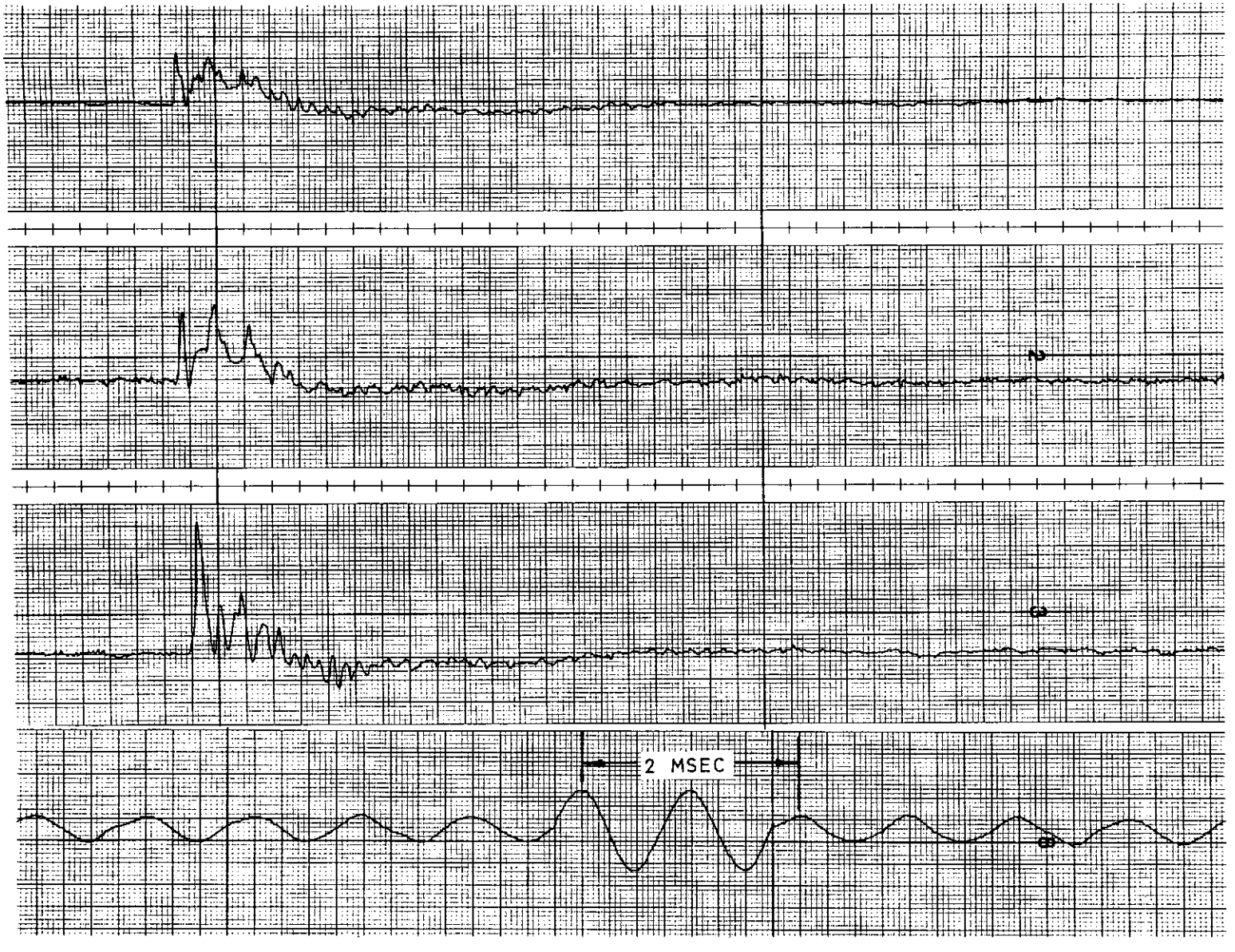

Figure 18. Pressure Response From a Bomb Disturbance Exhibiting Stable Behavior

TABLE 8. BOMB STABILITY RESULTS FROM SINGLE MODE TEST SERIES

Run	Bomb	Measured Overpressure* psi			Damp Time, msec	Rate of Pressure Rise**, psi/msec
		Photocon No. 1	Photocon No. 2	Photocon No. 3		
43	1	135	435	135	6	8
	2	145	185	75	4	-
	3	85	95	45	4	-
44	1	130	130	150	5	4
	2	160	235	85	4	4
	3	100	95	55	4	1.3
45	1	460	135	150	5	2.7
	2	170	225	140	Unstable	3.6
46	1	125	125	160	6	3.3
	2	140	210	---	6	8.0
47	1	165	140	145	6	3.7
	2	140	145	65	6	4.0
	3	175	250	85	28	4.0
48	1	150	185	135	6	4.0
	2	160	250	115	6	6.0
	3	95	100	50	5	-
49	1	160	235	150	7	4.0
	2	165	250	80	7	4.0
	3	90	95	50	6	1.6
50	1	250	170	150	8	5.0
	2	170	260	75	6	6.0
	3	135	110	60	7	-
51	1	130	180	150	8	4.8
	2	155	250	120	6	4.8
	3	95	105	55	5	2.0
52	1	195	185	155	7	5.0
	2	120	195	160	6	4.0
53	1	265	150	140	7	5.0
	2	170	250	410	7	6.0
	3	100	125	55	7	-
54	1	130	85	185	6	3.0
	2	140	80	95	7	-
	3	155	195	145	Unstable	-
55	1	215	175	270	5	6.0
	2	165	110	95	5	-
	3	130	70	105	5	2.4
56	1	180	110	270	5	6.8
	2	165	105	125	5	6.4
57	← No Bombs →					

TABLE 8. (Concluded)

Run	Bomb	Measured Overpressure*, psi			Damp Time, msec	Rate of Pressure Rise**, psi/msec
		Photocon No. 1	Photocon No. 2	Photocon No. 3		
58	1	390	180	135	5	-
	2	170	120	95	4	2.0
	3	120	75	90	4	-
59	1	135	80	100	6	2.0
	2	185	120	70	6	2.0
	3	130	75	60	6	-
60	1	110	110	60	5	2.0
	2	130	170	145	Overlap	3.0
	3	85	160	55	5	-
61	1	110	160	145	5	3.0
	2	95	150	85	4	1.0
	3	85	105	50	5	1.0
62	1	75	125	65	5	-
	2	125	170	150	5	2.0
	3	80	150	50	6	1.2
63	1	205	195	150	4	2.6
	2	100	170	80	5	-
	3	70	95	60	5	-
64	1	95	140	60	5	1.0
	2	110	165	150	6	-
	3	85	145	50	7	-
65	1	95	200	40	14	1.5
	2	105	460	110	95	1.4
66	1	180	460	70	9	3.0
	2	100	190	55	18	-
	3	95	170	30	6	2.0
67	1	105	210	40	5	1.0
	2	80	270	30	24	-
	3	115	210	60	70	-
68	1	90	290	30	6	2.0
	2	120	250	65	55	2.0
69	1	150	500	40	8	-
	2	105	205	40	38	-
	3	80	135	30	5	-

*Overpressure - maximum pressure reached minus pressure before disturbance.
**Selectively calculated from various overpressures to provide an indication of the rate of pressure rise.

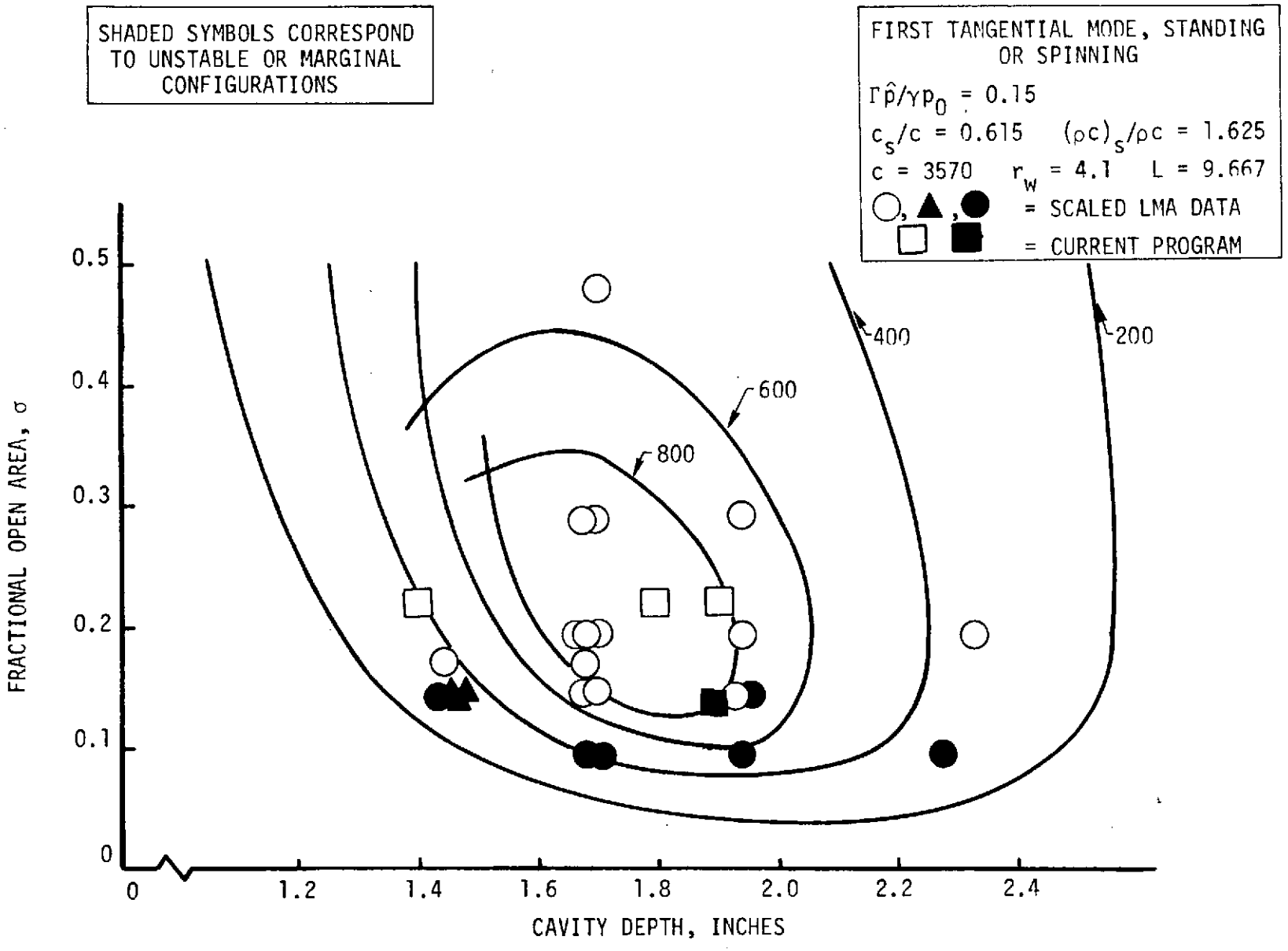

Figure 19. Comparison of Stability Results With Predicted Trends for Primary Cavity, $\Gamma\hat{p}/\gamma p_o = 0.15$

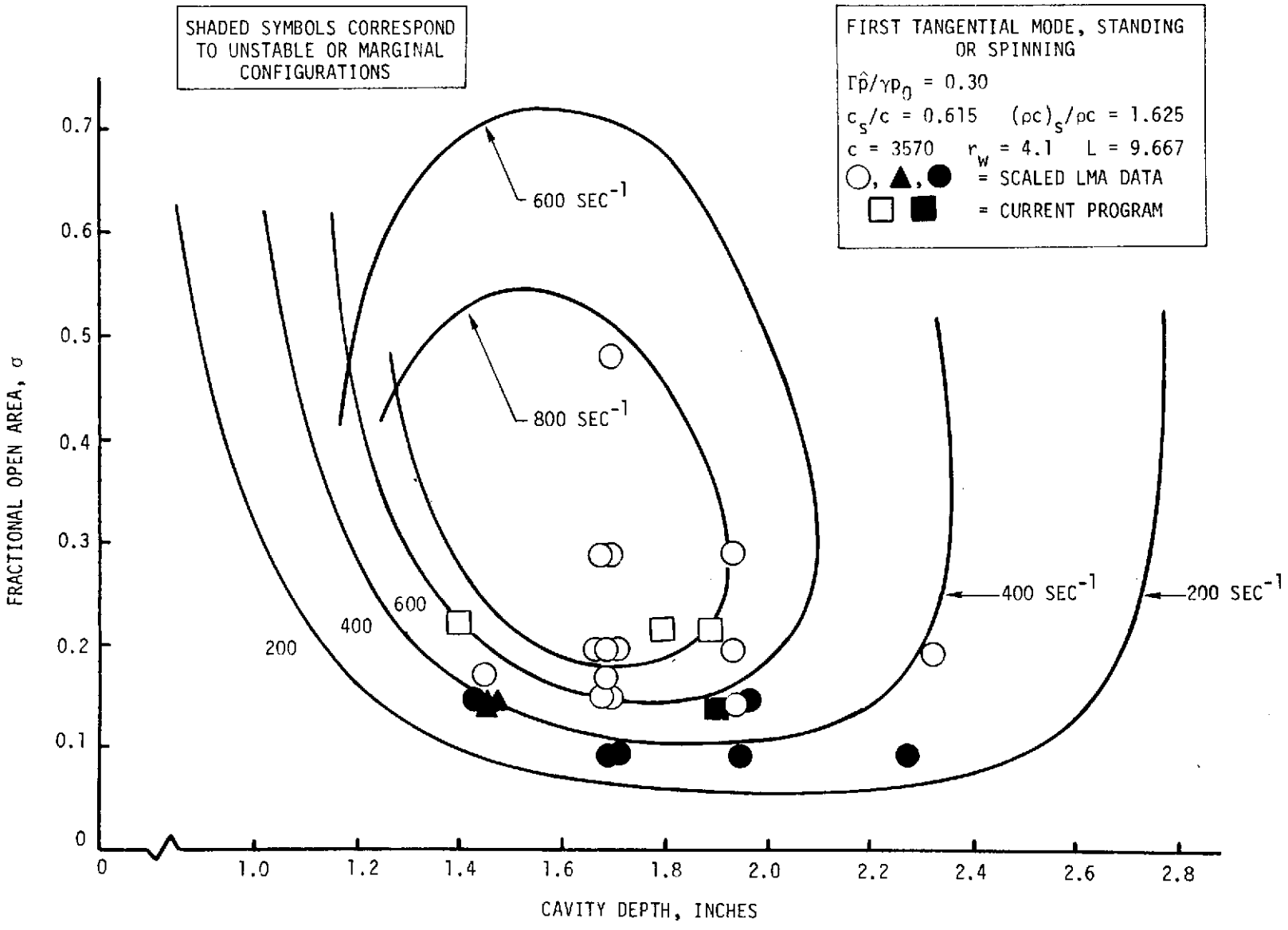

Figure 20. Comparison of Stability Results With Predicted Trends for Primary Cavity, $\Gamma\hat{p}/\gamma p_o$ = 0.30

Configurations which allowed a 2600-Hz oscillation, but not 3000-Hz oscillation, were considered stable to the first tangential mode. The predicted damping curves have been calculated for radially directed cavities with parameters chosen to correspond to estimated OME-type conditions. Values for the amplitude parameter $\Gamma\hat{p}/\gamma p_o$ have been chosen arbitrarily to best agree with the data. The values chosen of $\Gamma\hat{p}/\gamma p_o$ correspond to peak-to-peak amplitudes of ~100 percent of chamber pressure, if $\Gamma = 0.6$ is used. Such amplitudes are ordinarily considered far beyond the capabilities of the linearized analysis being used. However, in this analysis, the effect of increased amplitude is to increase the acoustic resistance of the cavity. The analysis may, therefore, still predict the damping effects of the cavity properly. Moreover, the amplitude parameter has been treated largely as an empirically derived coefficient, it being selected to give the best agreement between predicted and measured results.

Data relating to steady-state performance of the engine and cavity temperatures also were recorded and analyzed. These data will be described after discussion of the stability results from the second test series.

Stability Results from Multimode Suppression Tests

The completed test matrix for the multimode suppression tests is shown in Table 9 . The planned testing was directed toward defining the range of cavity configurations that would prevent all modes of instability and, in addition, confirming stability of a selected configuration over a range of operating conditions. Cavity configuration, mixture ratio, fuel temperature, and BLC flowrate were considered to be the most important stability-rated parameters. BLC flowrate was included because earlier company-funded tests had shown a significant effect of this flowrate on stability of the first radial and third tangential modes. BLC flowrate does not appear to have a significant effect on stability of the first tangential mode (Ref. 1).

Earlier company-funded testing with the injector used for this program had exhibited high-frequency instability at high BLC flowrates and seemed to worsen with increasing flowrate. The acoustic cavity, designed to suppress the first tangential mode, prevented that mode from occurring, but the first radial or third tangential modes, or both, with occasional transitions to the second tangential mode, developed during all initial tests. However, these modes were subsequently eliminated by a crude trial modification to the cavity configuration; every third resonator (4 out of 12) was retuned for the high-frequency modes by bonding filler blocks into these cavities to reduce their depth. With this modified cavity configuration, the engine was stable during subsequent firings (including one stability rating test with two bombs). Therefore, tests at moderate and high levels of BLC flowrate were included. In addition, excursions in overall mixture ratio and fuel temperature were included because of their likely significant effect or stability.

Stability results from this test series are summarized in Table 10. The testing showed that a 6600-Hz oscillation developed spontaneously at high BLC flowrate and with insufficient cavity suppression. This oscillation has been identified as coexisting first radial (1R) and third tangential (3T) modes of instability. This 3T/1R mode occurred spontaneously and was largely unaffected by the bomb disturbances. The bomb disturbances tended to cause the 3T/1R mode to damp temporarily

TABLE 9. TEST MATRIX FOR MULTIMODE SUPPRESSION TESTING

Objective	Number of Tests①	Primary Cavity		Secondary Cavity		Overall Mixture Ratio			Fuel Temperature, F		BLC Flowrate, percent	
		σ②	ℓ③, in.	σ	ℓ, in.	1.45	1.65	1.85	200	250	2.5	6.0
Confirm Unstable	3	0.228	1.75	0.0	0.0		X		X		X	
Third Tangential/	1	0.228	1.75	0.0	0.0		X		X			X
First Radial Mode	1	0.152	1.75	0.0	0.0		X		X		X	
↓	3	0.152	1.75	0.0	0.0		X		X			X
Define Required σ for	3	0.152	1.75	0.076	0.92		X		X		X	
Third Tangential/	4	0.152	1.75	0.076	0.92		X		X			X
First Radial Mode	2	0.140	1.75	0.083	0.92		X		X		X	
↓	4	0.140	1.75	0.083	0.92		X		X			X
↓	2	0.152	1.75	0.034	0.92		X		X		X	
↓	4	0.152	1.75	0.034	0.92		X		X			X
Define Required ℓ for	3	0.152	1.75	0.076	0.7		X		X		X	
Third Tangential/	3	0.152	1.75	0.076	0.7		X		X			X
First Radial Mode	3	0.152	1.75	0.076	1.3		X		X		X	
↓	3	0.152	1.75	0.076	1.3		X		X			X
Confirm Stable Over	3	0.152	1.75	0.076	0.92	X			X			X
Operating Range	3	↓	↓	↓	↓			X	X			X
↓	3						X			X		X
↓	3④	↓	↓	↓	↓		X		X			X
Total Tests	51											

① Three bombs are planned for each test unless terminated by an instability.

② σ = Fractional open area based on injector face area.

③ ℓ = Effective depth.

④ Planned to be made with elevated chamber pressure.

TABLE 10. SUMMARY OF STABILITY RESULTS FROM MULTIMODE SUPPRESSION TEST SERIES

Primary Cavity		Secondary Cavity		Number of Tests/Bombs[3]	Average Mixture Ratio	Average Fuel Temperature, F	Average BLC Flowrate, percent	Stability	Maximum Damp Time, msec	Number of Instabilities/ Tests[4]	Frequency Duration, Hz/msec
σ[1]	ℓ[2], in.	σ[1]	ℓ[2], in.								
0.228	1.75	0.00	0.00	3/9	1.69	188	1.9	Stable	16	0/3	
0.228	1.75	0.00	0.00	1/2	1.59	193	4.6	Unstable	--	1/1	6600/Full
0.152	1.75	0.076	0.92	3/8	1.66	192	2.5	Stable	11	0/3	
0.152	1.75	0.076	0.92	4/10	1.58	190	5.6		12	0/4	
0.152	1.75	0.076	0.70	3/6	1.66	194	2.5		10	0/3	
0.152	1.75	0.076	0.70	3/7	1.60	185	5.9		10	0/3	
0.152	1.75	0.076	1.30	3/9	1.65	205	2.5		8	0/3	
0.152	1.75	0.076	1.30	3/8	1.61	199	5.9	Marginal	26	2/3	2570/23
0.140	1.75	0.083	0.92	2/4	1.62	194	2.6	Stable	12	1/4	
0.140	1.75	0.083	0.92	4/11	1.60	192	6.0	Unstable	23[5]	3/3	6600/Full
0.152	1.75	0.00	0.00	1/3	1.64	190	2.5	Stable	15	0/1	
0.152	1.75	0.00	0.00	3/9	1.57	194	6.0	Unstable	19	2/3	6550/Full
0.152	1.75	0.034	0.92	2/6	1.72	194	2.5	Stable	10	0/3	
0.152	1.75	0.034	0.92	4/11	1.64	187	5.8		12		
0.152	1.75	0.076	0.92	3/9	1.87	184	5.5		9		
0.152	1.75	0.076	0.92	3/9	1.46	195	5.3		12		
0.152[6]	1.75	0.076	0.92	3/9	1.63	179	4.8[6]		12		
0.152	1.75	0.076	0.92	3/8	1.65	217	5.9		14		

[1] σ = Fractional open area based on injector face area.

[2] ℓ = Effective cavity depth.

[3] Three bombs were installed for each test.

[4] All 6600-Hz instabilities occurred spontaneously; none was triggered by bomb.

[5] Long damp time due to 2640-Hz oscillation; bomb caused 6600 Hz to damp and redevelop spontaneously subsequent to damping of disturbance.

[6] Tests made at high chamber pressure (140 psia); all others at nominal pressure (125 psia).

and then redevelop spontaneously. In no case did it appear that a radial mode or 3T/1R coexistent modes were initiated by a bomb disturbance, although one of the three bombs was mounted along the centerline of the chamber to maximize the likelihood of initiating the first radial mode. In addition, the spontaneous 3T/1R oscillation never reached high amplitudes, but tended to be sustained at amplitudes near 20 psi peak-to-peak (16 percent of chamber pressure).

Additional evidence of a 2600-Hz oscillation was encountered during this test series. During two tests, this 2600-Hz oscillation continued for longer than 20 milliseconds but damped subsequently. A number of other tests was made that clearly exhibited this type of oscillation but damped in less than 20 milliseconds. Thus, there appears to be a clear tendency for this mode to occur but in a largely random manner. Larger numbers of tests would be required to determine whether or not it is suppressed by some of the cavity configurations. Results from a detailed analysis of the high-frequency pressure data are summarized in Table 11. In those cases where an overpressure is listed with a "greater than" sign (>), the oscillogram showed clear evidence of saturation of the oscillograph systems, thus indicating the actual pressure exceeded the tabulated level. Amplitudes of sustained oscillations are shown in parenthesis.

The stability results from this test series have been plotted in Fig. 21 in the form of a stability map of the type shown previously for the first tangential mode. Also shown are two predicted damping curves for two values of the amplitude parameter, $\Gamma\hat{p}/\gamma p_o$. These curves were calculated for a circumferentially uniform radial cavity, whereas the actual cavity was nonuniform comprising resonators with two depths. Therefore, the theoretical curves are not completely comparable to the experimental results. However, the computer program for predicting cavity damping has not yet been modified to permit analysis of this cavity arrangement, although the necessary equations have been developed (Appendix A). Nevertheless, it appears likely that the trends in predicted damping would not change enormously between the uniform and nonuniform cases with equal open area. If this assumption is valid, the predicted curves are useful for comparison.

This comparison, shown in Fig. 21 , is not very satisfying from the standpoint of agreement between analytical and experimental results. First, the predicted damping suggests a much smaller range of cavity depths to achieve stability than implied by the data. Secondly, the cavity with the largest open area was the only configuration that failed to stabilize the engine; however, the latter effect can at least be rationalized through a simplified analysis. The damping effect of the acoustic cavities is expected to be approximately proportional to the surface integral:

$$\alpha \sim \int_{\text{cavity}} p^2 \, dS$$

TABLE 11. SUMMARY OF BOMB STABILITY RESULTS FROM MULTIMODE SUPPRESSION TEST SERIES

Run	Bomb	Overpressure*, psi			Damp Time, msec	Frequencies/ Duration, Hz/msec
		Photocon No. 1	Kistler No. 1	Kistler No. 2		
138	1	>160	120	160	15	
	2	160	90	160	10	
	3	160	100	120	12	
139	1	>140	140	160	11	
	2	-	160	160	15	
	3	>140	100	120	15	
140	1	>160	100	140	12	
	2	>160	140	160	16	
	3	150	100	140	16	
141	-	(40)*	(40)	(30)	-	6600/throughout
142	1	120	120	120	6	
	2	-	50	60	8	
143	1	>120	110	120	7	
	1	120	100	100	8	
	3	80	60	40	7	
144	1	>130	110	110	7	
	2	>130	90	110	11	2480/5 msec
	3	90	50	60	8	
145	1	>130	110	100	8	
	2	140	110	100	8	
	3	90	60	60	7	
146	1	>140	80	70	9	
	2	90	50	50	7	
147	1	120	90	100	8	
	2	90	40	50	6	
148	1	>130	120	100	7	
	2	90	40	60	7	
	3	130	110	130	12	
149	1,2	>100	120	100	10	
150	1	90	50	50	6	
	2	110	90	70	10	2480/6 msec
151	1	>110	130	90	8	
	2	80	40	30	8	
152	1	>140	180	110	8	
	2	90	60	50	7	
153	1	>140	80	170	7	
	2	100	80	80	8	
154	1	>120	90	100	10	
	2	>120	60	-	9	
	3	100	80	-	8	

TABLE 11. (Continued)

Run	Bomb	Overpressure*, psi			Damp Time, msec	Frequencies/ Duration, Hz/msec
		Photocon No. 1	Kistler No. 1	Kistler No. 2		
155	1	>110	70	80	6	
	2	100	100	100	8	
	3	40	40	60	8	
156	1	100	60	100	8	
	2	>100	110	120	8	
	3	70	60	120	8	
157	1	70	60	50	6	
	2	80	50	60	8	
	3	110	130	80	8	
158	1	>140	60	70	7	
	2	>140	90	70	23	2560/22 msec
	3	60	50	40	6	
159	1	>140	160	80	9	
	2	140	140	60	-	
	3	100	80	40	26	2580/24 msec
160	1	>140	80	50	8	
	2	60	60	30	6	
164	1	>140	100	100	12	
165	1	>140	100	100	10	
	2	140	100	50	10	
	3	100	40	20	10	
166	1	140	-	100	10	
	2	-	-	120	15	
	3	100	-	50	10	
167	-	-	(30)	(10)	-	6600/throughout
	1	>130	70	100	12	
	2	140	100	100	12	
	3	140	100	100	-	
	-	-	(60)	(30)	-	6600/throughout
168	-	-	-	(10)	-	6600/throughout
	1	140	-	(10)	-	
	2	140	-	100	14	
	3	80	-	40	8	
169	-	-	(20)	(10)	-	6600/throughout
	1	>140	100	100	23	2640/21 msec
	2	>140	100	100	12	
170	-	(30)	-	-	-	6500
	1	>140	220	-	10	
	2	>150	220	-	-	
	3	120	120	-	15	

TABLE 11. (Continued)

Run	Bomb	Overpressure*, psi			Damp Time, msec	Frequencies/ Duration, Hz/msec
		Photocon No. 1	Kistler No. 1	Kistler No. 2		
171	-	(25)	-	(10)	-	6600
	1	-	-	180	17	
	2	>140	150	190	12	
	3	>140	110	80	10	
172	1	-	-	120	12	
	2	-	-	120	19	
	3	-	-	100	15	
173	1	-	-	80	10	
	2	-	120	110	15	
	3	-	110	40	12	
174	1	400	-	200	5	
	2	500	250	150	7	
	3	250	150	100	9	
175	1	350	250	-	8	
	2	300	200	150	10	
	3	200	130	-	10	
176	1	300	250	200	10	
	2	300	250	-	12	
177	1	500	200	-	8	
	2	500	250	-	11	
	3	250	200	-	10	
178	1	500	300	200	8	
	2	250	250	200	10	
	3	300	250	-	10	
179	1	450	200	-	7	
	2	500	200	-	7	
	3	300	150	-	10	
180	1	450	300	300	9	
	2	350	300	150	7	
	3	300	150	200	9	
181	1	450	200	300	8	
	2	250	250	200	5	
	3	300	200	200	9	
182	1	400	200	250	9	
	2	400	300	200	9	
	3	200	100	50	8	
183	1	300	200	300	7	
	2	250	250	150	12	
	3	250	200	150	10	
184	1	350	300	200	8	
	2	300	250	200	10	
	3	200	100	50	5	

TABLE 11. (Concluded)

Run	Bomb	Overpressure*, psi			Damp Time, msec	Frequencies Duration, Hz/msec
		Photocon No. 1	Kistler No. 1	Kistler No. 2		
185	1	350	200	200	8	
	2	200	200	100	7	
	3	200	100	50	10	
186	1	250	150	150	7	
	2	250	150	150	10	
	3	200	200	100	8	
187	1	300	200	150	8	
	2	250	200	150	12	
	3	250	200	100	8	
188	1	350	300	200	12	
	2	250	300	100	8	
	3	300	300	150	10	
189	1	450	250	250	10	
	2	350	200	100	10	
	3	200	150	100	10	
190	1	>200	200	200	12	
	2	>200	300	150	14	
	3	150	100	50	10	
191	1	400	250	150	12	
	2	200	100	50	12	

*Values in parentheses denote sustained instability amplitudes.

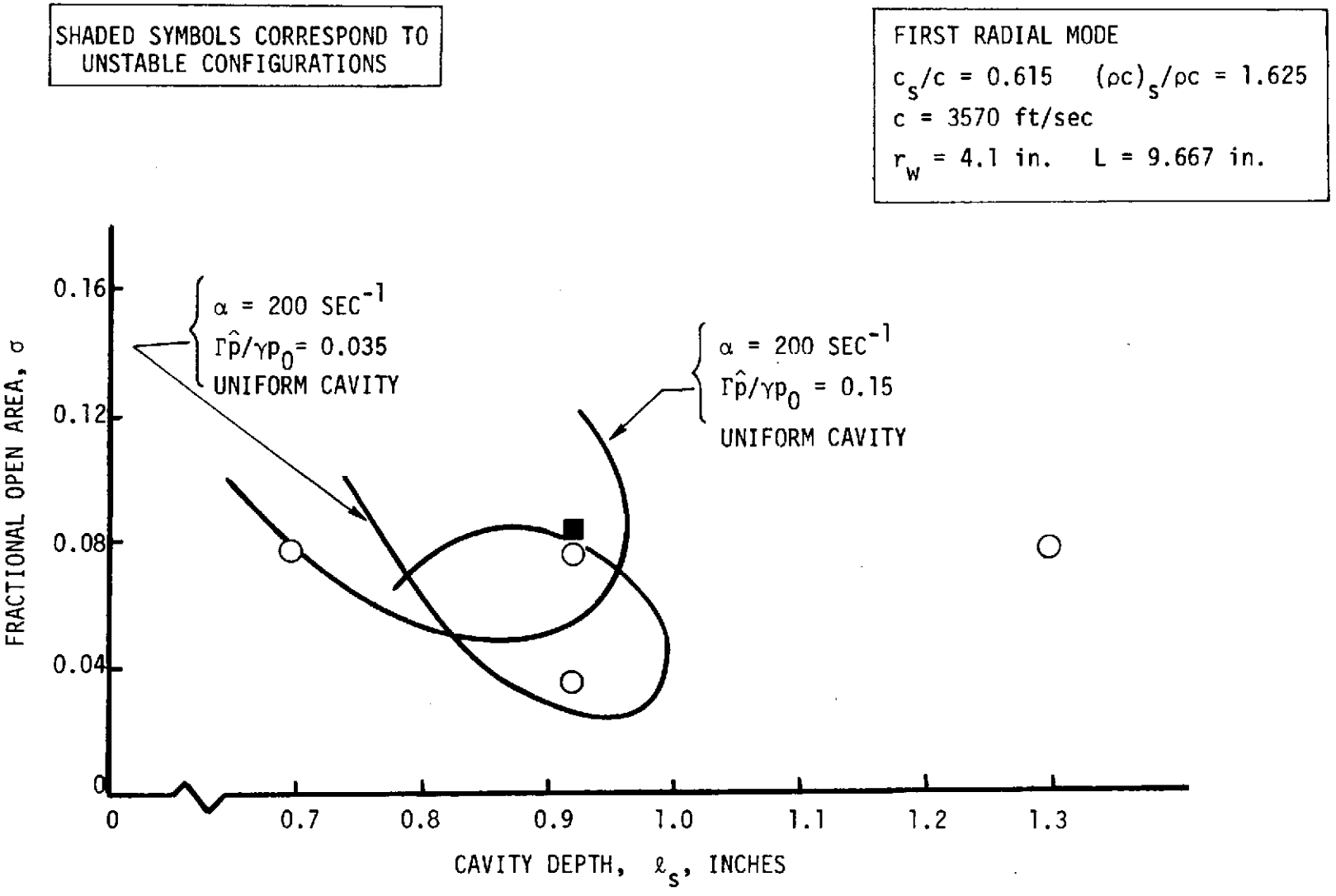

Figure 21. Comparison of Stability Results From Multimode Test Series With Predicted Trends for Circumferentially Uniform Secondary Cavity

If the pressure is assumed to vary only as cos (m θ) over the cavity entrance region, an effectiveness factor may be defined as:

$$\varepsilon = \frac{\left[\int p^2 \, dS\right]_{\text{nonuniform cavity}}}{\left[\int p^2 \, dS\right]_{\text{equal area uniform cavity}}}$$

$$= \frac{2\overline{n}}{\sum_i \Delta\theta_i} \quad \frac{\int f(\theta) \cos^2 m (\theta - \theta_o) \, d\theta}{\int \cos^2 m (\theta - \theta_o) \, d\theta}$$

where $f(\theta)$ denotes the angular distribution of cavities and $\Delta\theta_i$ denotes the angular size of the cavity entrance for the i^{th} cavity. In some cases, this effectiveness factor depends on the angle θ_o at which the mode stands relative to the coordinate origin. However, it appears reasonable to assume that a standing mode will rotate to minimize the damping of cavities.

Consequently, this factor was evaluated for the three angular distributions of cavities tested, with the following results (third tangential mode):

Open Areas	ε
0.152/0.076	1.000
0.140/0.083	0.631
0.152/0.034	1.000

This implies the 8.3-percent open area cavity with the chosen angular distribution will produce only 63 percent as much damping as a circumferentially uniform cavity with the same open area, or four equally spaced and equal size cavities with the same total open area. Therefore, with respect to Fig. 21, the 8.3-percent cavity corresponds to a larger open area uniform cavity with the same damping (assuming this open area corresponds to greater than maximum damping). Although this argument is speculative, it does indicate the importance of the angular distribution of cavities.

Clearly, cavity damping calculations which properly account for the angular distribution of cavities are needed. Nonetheless, a relatively large range of cavity sizes has been shown to stabilize the engine for these modes (first radial and third tangential modes).

Performance

The performance results obtained from the like doublet No. 2 injector in the 12-inch OME thrust chamber are summarized in Table 12. Performance has been

TABLE 12. SUMMARY OF PERFORMANCE MEASURED DURING OME STABILITY RATING TESTS

Run	Flowrate, lb/sec	Mixture Ratio	BLC, percent	Fuel Temperature, F	Injector Face Pressure, psia	Sidewall Chamber Pressure, psia	Nozzle Stagnation Pressure, psia	η_{c^*}	Stability
43	18.96	1.49	0.0	198	126.5	118.8	119.8	0.955	Stable
44	19.78	1.68		196	131.7	123.6	125.0	0.950	Stable
45	19.44	1.80		200	132.8	121.0	126.3	0.979	Unstable
46	19.53	1.76		203	130.2	122.5	123.8	0.954	Stable
47	19.33	1.87		194	129.7	---	123.2	0.963	Marginal
48	19.47	1.71		234	129.9	122.2	123.2	0.952	Stable
49	19.37	1.67		253	129.1	121.6	122.6	0.952	
50	19.40	1.73		253	129.0	121.6	122.6	0.951	
51	19.52	1.73		252	129.9	122.7	123.4	0.951	
52	19.38	1.89		249	128.3	121.1	122.0	0.951	
53	19.84	1.71	0.0	200	131.6	123.9	124.9	0.947	Stable
54	19.44	1.78	0.0	198	128.5*	120.6	122.6	0.945	Unstable
55	19.68	1.84		205	131.0*	123.1	124.9	0.952	Stable
56	19.71	1.78		204	131.0*	123.1	124.9	0.950	Stable
57	19.91	1.80		249	132.4*	124.4	126.2	0.950	Premature Bombs
58	19.96	1.80		241	132.8*	124.8	126.6	0.951	Stable
59	19.82	1.77		252	131.8*	123.9	125.7	0.951	
60	19.74	1.81		201	131.1*	123.2	125.0	0.949	
61	19.78	1.83		198	131.5*	123.6	125.4	0.950	
62	19.72	1.83		205	131.4*	123.5	125.3	0.953	
63	19.86	1.76		252	132.5*	124.5	126.3	0.953	
64	19.92	1.78		249	132.5*	124.5	126.3	0.950	
65	19.98	1.82		192	132.4*	124.4	126.2	0.947	Marginal
66	19.92	1.80		201	132.1*	124.2	125.9	0.948	Stable
67	19.93	1.85		204	132.1*	124.2	125.9	0.948	Marginal
68	20.07	1.79		237	132.7*	124.7	126.5	0.945	
69	20.14	1.77	0.0	249	133.5*	125.7	127.3	0.947	
138	20.36	1.72	1.9	186	132.2	124.3	125.3	0.940	Stable
139	20.58	1.70	1.9	191	133.2	125.1	126.3	0.937	
140	20.54	1.65	1.9	188	132.7	124.5	125.8	0.936	
141	21.36	1.59	4.6	193	134.0	128.3	127.0	0.934	Unstable
142	20.62	1.69	2.5	189	132.4	124.8	125.5	0.935	Stable
143	20.77	1.63	2.5	196	132.6	125.0	125.7	0.930	
144	20.53	1.65	2.5	192	131.0	123.4	124.2	0.929	
145	21.69	1.47	5.1	191	134.4	126.9	127.4	0.929	
146	21.66	1.60	5.6	190	131.9	124.8	125.0	0.915	
147	21.34	1.61	5.8	187	130.7	123.7	123.9	0.921	
148	21.70	1.63	5.7	190	132.9	125.7	126.0	0.920	
149	20.90	1.64	2.5	188	132.5	124.7	125.6	0.930	
150	20.96	1.69	2.5	190	132.8	124.8	125.9	0.928	
151	20.61	1.65	2.5	204	131.9	124.1	125.0	0.932	Stable

*Chamber pressure measured at bottom of radial cavity in chamber sidewall.

TABLE 12. (Concluded)

Run	Flowrate, lb/sec	Mixture Ratio	BLC, percent	Fuel Temperature, F	Injector Face Pressure, psia	Sidewall Chamber Pressure, psia	Nozzle Stagnation Pressure, psia	η_{c^*}	Stability
152	21.78	1.63	5.9	194	132.4	125.0	125.5	0.922	Stable
153	21.78	1.60	5.9	179	131.9	124.6	125.0	0.921	
154	21.67	1.57	6.0	183	131.9	124.6	125.0	0.924	
155	20.53	1.68	2.5	201	132.2	124.2	125.3	0.938	
156	20.56	1.68	2.5	204	132.0	124.0	125.1	0.935	
157	20.52	1.60	2.6	210	132.1	124.1	125.2	0.939	Stable
158	21.83	1.59	6.0	205	134.0	126.5	127.0	0.926	Marginal
159	21.49	1.62	5.9	203	131.7	124.2	124.9	0.923	Marginal
160	21.76	1.62	5.9	190	132.9	125.4	126.0	0.924	Stable
161	20.62	1.59	2.6	185	132.7	124.1	125.5	0.937	
162	20.62	1.61	2.6	196	133.3	124.9	126.4	0.945	
163									Test too short
164	20.49	1.60	2.6	193	131.6	123.7	124.8	0.937	Stable
165	20.70	1.69	2.5	200	133.4	125.4	126.5	0.939	
166	21.58	1.59	5.9	191	132.6	125.1	125.7	0.926	
167	21.61	1.60	6.0	188	132.7	125.5	125.8	0.925	
168	21.69	1.60	6.0	196	133.1	126.1	126.2	0.925	
169	21.79	1.59	6.0	195	133.9	126.5	127.0	0.927	
170		1.55	6.1	195	133.0	126.7	125.7	0.923	
171		1.58	5.9	192	132.2	124.5	124.8	0.923	
172		1.58	5.9	194	133.8	125.8	126.1	0.920	
173		1.64	2.5	190	133.9	125.5	126.3	0.935	
174	21.08	1.74	2.5	192	135.0	127.2	128.0	0.933	
175	20.67	1.71	2.5	196	132.6	124.8	125.7	0.934	
176	21.77	1.65	5.8	185	133.6	126.2	126.6	0.922	
177	21.66	1.64	5.8	193	133.0	125.6	126.1	0.924	
178	21.70	1.68	5.7	187	133.0	125.7	126.1	0.921	
179	21.70	1.60	6.0	183	133.0	125.6	126.1	0.924	
180	21.76	1.85	5.5	181	132.4	125.0	125.5	0.913	
181	21.70	1.87	5.5	185	131.9	124.6	125.1	0.913	
182	21.70	1.88	5.5	185	132.0	124.7	125.1	0.913	
183	21.93	1.47	5.3	193	135.7	127.9	128.7	0.930	
184	21.60	1.45	5.3	197	133.9	126.2	127.0	0.932	
185	21.36	1.45	5.4	195	132.1	124.5	125.2	0.930	
186	23.81	1.62	4.8	178	147.6	139.3	139.9	0.924	
187	23.93	1.63	4.8	169	148.6	140.2	140.9	0.925	
188	23.71	1.65	4.7	189	147.4	139.1	139.7	0.925	
189	21.65	1.59	6.0	209	132.3	124.6	125.4	0.921	
190	21.54	1.68	5.8	221	131.3	124.3	124.5	0.917	
191	21.70	1.68	5.9	220	132.7	125.4	125.8	0.920	Stable

*Chamber pressure measured at bottom of radial cavity in chamber sidewall

characterized in terms of the characteristic exhaust velocity efficiency, η_{c^*}, which, in turn, was calculated from the data through use of the conventional relationship:

$$\eta_{c^*} = \frac{p_o A^* g}{\dot{w} c^*_t}$$

where

p_o = nozzle stagnation pressure

A^* = area of the throat

g = mass/force conversion factor

$\dot{w}$ = total propellant flowrate

c^*_t = theoretical characteristic exhaust velocity for the mixture ratio

The value of η_{c^*} represents an uncorrected efficiency because no corrections have been made for nozzle wall thermal expansion or boundary layer buildup (these effects tend to cancel each other) or for flow stratification losses associated with the use of BLC on the chamber walls. The nozzle stagnation pressure, p_o, was calculated from the static pressure at the injector face, p_I, by:

$$\frac{p_I}{p_o} = \frac{1 + \gamma M_{NE}^2}{\left(1 + \frac{\gamma - 1}{2} M_{NE}^2\right)^{\gamma/\gamma - 1}}$$

where M_{NE} is the combustion gas Mach number at the nozzle entrance. This equation accounts for the Rayleigh heating loss in the combustion chamber under the assumption that the stagnation pressure remains constant through the nozzle contraction region.

During firings made with axial cavities, a direct measurement was made of the injector face pressure through a pressure tap located in the cavities. However, when the radially directed cavities were tested (runs 54 through 69), the axial cavity containing the injector pressure tap was closed off. Therefore, the chamber pressure was measured only at a downstream location, 4.05 inch from the injector face. Results from available combustion model calculations were used to obtain a correction for relating pressure at this location to that at the injector face. The validity of the correction was verified by comparison with results from the axial cavity tests wherein pressures were measured both at the injector face and 3.0 inches downstream.

Figure 22 shows the variation of the measured values of η_{c^*} with mixture ratio and with BLC flowrate as a parameter. These results indicate that performance is independent of mixture ratio when the BLC flowrate is low. However, η_{c^*} is reduced approximately 1 to 1.5 percent by use of 2 to 2.5 percent BLC, and is reduced by 2.5 to 3

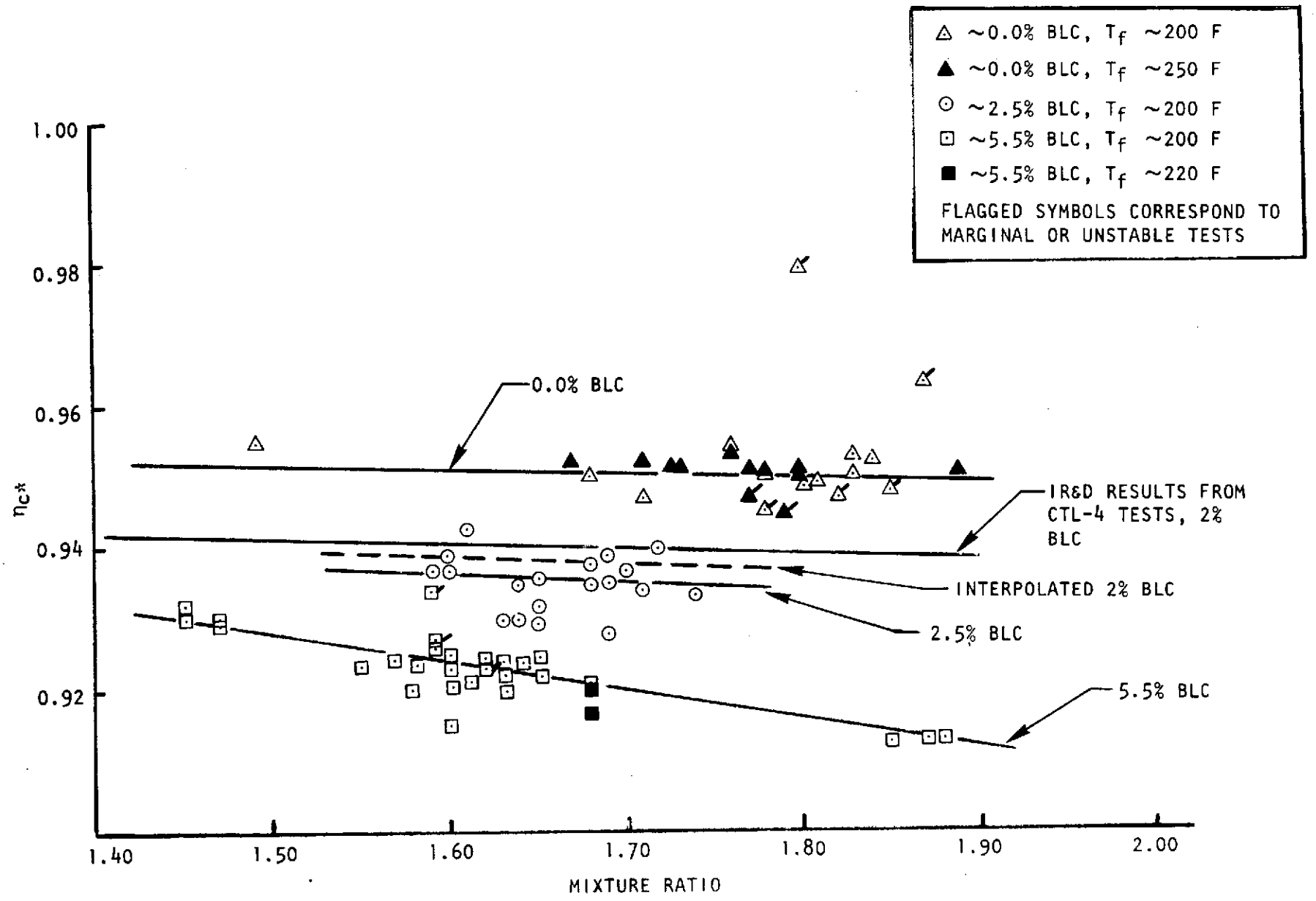

Figure 22. Variation of c* Efficiency (Based on Chamber Pressure) With Mixture Ratio (Obtained With Improved Like-Doublet Injector (OME) in 12-Inch-Long Chamber)

percent by the use of 5 to 6 percent BLC. The decrease in η_{c^*} with mixture ratio at high BLC flowrate probably reflects the interaction of the decrease in theoretical c* with mixture ratio (MR) for MR > 1.7 combined with the substantial difference between the core flow and overall mixture ratios at high BLC flowrates. Examination of the data indicates that there was no clearly defined correlation between stability and performance.

Cavity Gas Temperature

Measurements of cavity gas temperature were made during runs 43 through 53 with axial primary cavities, during runs 54 through 69 with the three radial primary cavities, and during runs 174 through 191 with the dual-mode array of axial cavities. The results from these three series of temperature measurements are summarized in Tables 13 through 15. Omissions in the tables where no temperatures are recorded correspond to failure of the thermocouples. The location of the thermocouple junction within the cavity for the axial cavities is shown in Tables 3 and 4 as cavity depth and transverse position. Positions of the thermocouples in the radial cavities are shown in Table 5 . Also shown in Table 15 is an effective depth position of the thermocouple for the L-shaped radial cavity which was calculated as the distance along the midwidth centerline of the cavity and represents an average flow path. Use of this coordinate as an alternate to the Δr of Table 5 for the cavity depth in the correlations of temperature distribution is suggested by success obtained with its prior usage in the cavity technology program reported in Ref. 4.

The measured cavity gas temperatures are shown in Fig. 23 and 24 as functions of depth measured from the cavity entrance. As is often the case with acoustic cavity temperature data, the data for both the axial or radial cavities show substantial scatter. The temperatures recorded by the various thermocouples ranged form 3255 down to 630 F. Measured temperatures also varied widely during individual tests. For example, at thermocouple T_{AX} -7, the range was from 3255 to 1930 F, and at T_{AX} -6, the range was from 2535 to 1735 F (Table 13). Therefore, development of a correlation for either the average cavity gas temperature or for the temperature distribution for use in the theoretical damping model is restricted by these limitations. In addition, a review was made of the cavity temperatures measured during an earlier experimental program in which tests were made with the same OME thrust chamber but with a different injector made up of unlike doublet injection elements. These data are shown in Table 16. These temperatures are (as expected) substantially different from those measured during the current program. These data clearly show a substantial increase in temperature between stable and unstable tests, especially deep in the cavity.

An examination of data from the current program showed that temperatures measured during unstable or marginally stable tests were more apt to vary in an erratic manner than temperatures measured during stable tests. Because the goal of the program was to develop the technology to design stable engines, the temperature data obtained during unstable tests were rejected for correlation purposes.

The variation with mixture ratio in the temperature measured at several selected thermocouples was also examined, as shown in Fig. 25. The obvious effect of mixture ratio for each thermocouple is not surprising in a region close to the

TABLE 13. SUMMARY OF AXIAL CAVITY GAS TEMPERATURE RESULTS (RUNS 43 THROUGH 53)

Run	Gas Temperature In Cavity, F										Stability
	T_{AX} -1 D = 0.0 η = 0.1*	T_{AX} -2 D = 0.1 η = 1.0**	T_{AX} -3 D - 0.3 η = 0.1	T_{AX} -4 D - 0.5 η = 1.0	T_{AX} -5 D - 0.7 η = 0.1	T_{AX} -6 D - 0.2 η = 0.1	T_{AX} -7 D = 0.4 η = 1.0	T_{AX} -8 D = 0.5 η = 0.1	T_{AX} -9 D = 0.7 η = 1.0	T_{AX} -10 D = 0.8 η = 0.1	
43	2495	2605	1880	2270	2205	2535	3255	2277	2245	3023	Stable
44	2160	2885	2065	2271	1824	1965	2915	1785	--	1441	Stable
45	1935	2000	1755	1801	1571	1925	1930	1702	2183	1596	Unstable
46	1895	2600	1820	2299	1629	1785	2495	1824	2037	1318	Stable
47	1870	2610	1825	2149	1657	1790	2235	1384	1729	1572	Marginal
48	2000	2680	1950	--	1770	1840	2345	1519	--	1437	Stable
49	2070	2750	1950	--	1937	1835	2660	1665	--	1500	↓
50	1985	2550	1890	--	1762	1995	2710	1632	--	1482	
51	2000	2690	1915	--	1823	1890	2435	1514	--	1429	
52	1915	2490	1765	--	1678	1735	2310	1502	--	1470	
53	1980	2550	1835	--	1716	1840	2460	1548	--	1448	

*Thermocouples coded η = 0.1 are located approximately 0.1 inch from the partitions that separate the acoustic cavities.

**Thermocouples coded η = 1.0 are located along the centerline of the cavities.

TABLE 14. SUMMARY OF RADIAL CAVITY GAS TEMPERATURE RESULTS (RUNS 54 THROUGH 69)

Run	Cavity Temperature, F											Stability
	Cavity	TC-1	TC-2	TC-3	TC-4	TC-5	TC-6	TC-7	TC-8	TC-9	TC-10	
54	Radial No. 3	2165	1721	1855	1935	1655	1915	1752	1740	1870	1567	Unstable
55	↓	1850	1347	2135	2170	1336	1965	1848	1660	2045	1386	Stable
56	↓	1965	1493	2130	2045	1168	1990	1861	1670	2145	1438	Stable
57	↓	1765	--	2150	2015	--	1985	1824	1750	2160	1422	Premature Bombs
58	↓	1955	1533	2140	2105	--	2095	1893	1730	2110	1414	Stable
59	Radial No. 3	1865	1244	2170	2130	--	2135	1986	1720	2115	1523	↓
60	Radial No. 2	--	1425	1955	2035	1075	2030	1570	1760	2055	1450	↓
61	↓	--	--	2085	2085	1167	2080	1670	1710	2050	1490	↓
62	↓	--	--	2090	2135	1173	2045	1640	1710	2055	1497	↓
63	↓	--	--	2155	2200	1330	2115	1715	1815	2120	1532	↓
64	Radial No. 2	--	--	2160	2180	1311	2130	1705	1805	2095	1552	↓
65	Radial No. 1	--	--	--	1670	817	--	630	1270	810	1459	Marginal
66	↓	--	--	--	1930	1017	--	765	1375	1340	1473	Stable
67	↓	--	--	--	1780	1199	--	1095	1255	865	1337	Marginal
68	↓	--	--	--	1980	1162	--	1000	1315	--	1469	
69	Radial No. 1	--	--	--	2005	1008	--	1030	1060	--	1585	

TABLE 15. SUMMARY OF AXIAL CAVITY GAS TEMPERATURE RESULTS (RUNS 174 THROUGH 191)

Run No.	Mixture Ratio	T_{AX} -1 D = 1.0 η = 0.1	T_{AX} -1 D = 0.6 η = 1.0	T_{AX} -3 D = 1.0 η = 0.1	T_{AX} -4 D = 0.6 η = 0.1	T_{AX} -5 D = 0.4 η = 0.1	T_{AX} -6 D = 0.8 η = 0.1	Stability
174	1.74	1703	2082	----	2129	1415	1379	Stable
175	1.71	1734	2130	----	2053	1434	1420	
176	1.65	1578	1995	2483	2073	1348	1344	
177	1.64	1622	2169	2172	2112	1315	1432	
178	1.68	1544	1801	2061	2335	1350	1149	
179	1.60	1591	2066	1649	2042	1306	1188	
180	1.85	1543	1652	----	1983	1306	901	
181	1.87	1515	1685	----	1749	1261	942	
182	1.88	1567	1619	----	1744	1190	903	
183	1.47	1816	2145	----	2175	1528	1351	
184	1.45	1853	1952	----	1949	1805	1180	
185	1.45	1835	1980	----	1992	1474	1208	
186	1.62	1706	1878	----	1645	1349	1057	
187	1.63	1624	2181	----	2208	1770	1403	
188	1.65	1661	1917	----	2144	1323	1037	
189	1.59	1636	2066	----	2167	1484	1255	
190	1.68	1564	1800	----	2045	1297	1035	
191	1.68	1551	1764	----	2005	1410	1050	

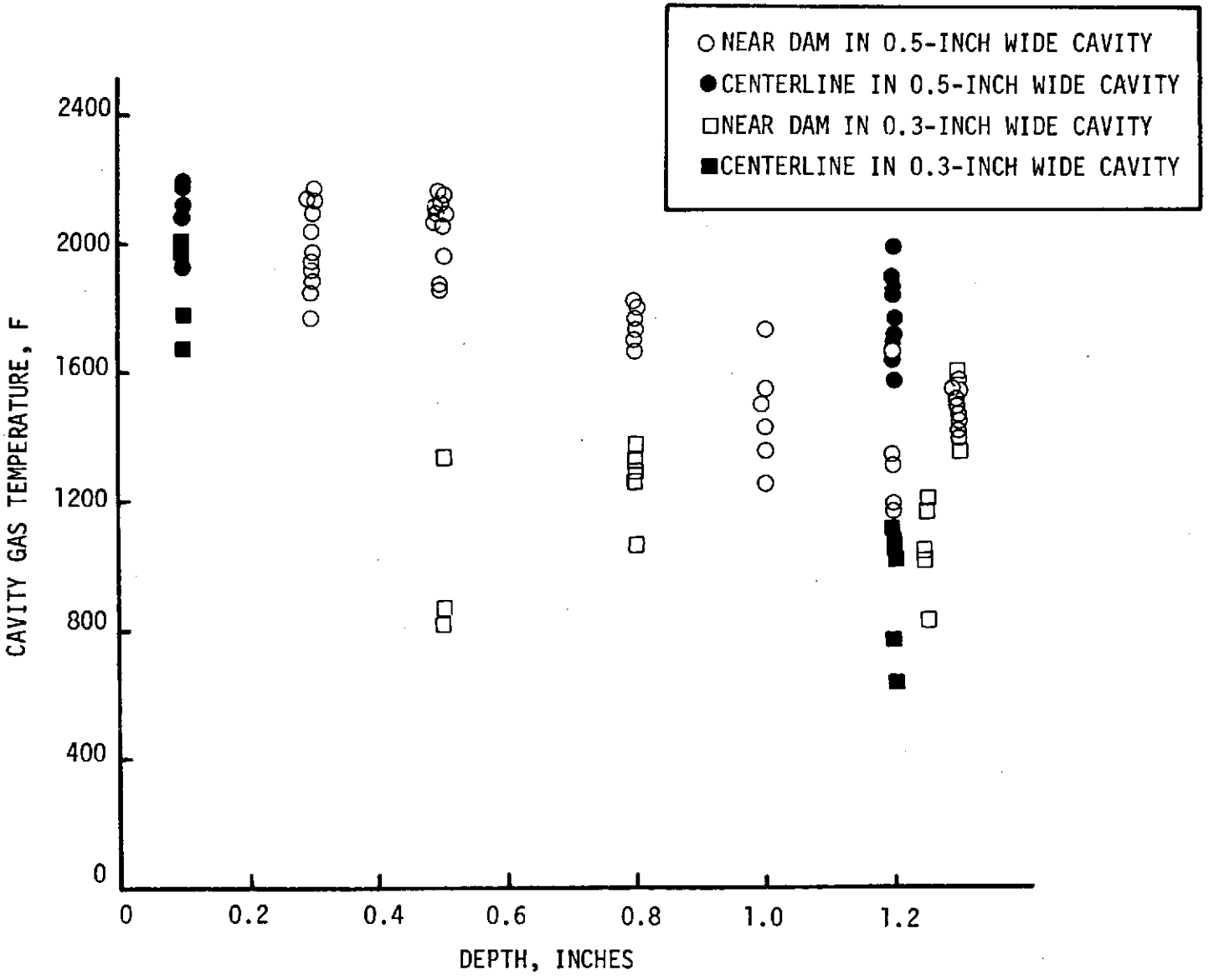

Figure 23. Variation of Cavity Gas Temperature with Depth in Radial Primary Cavities (Runs 54-69)

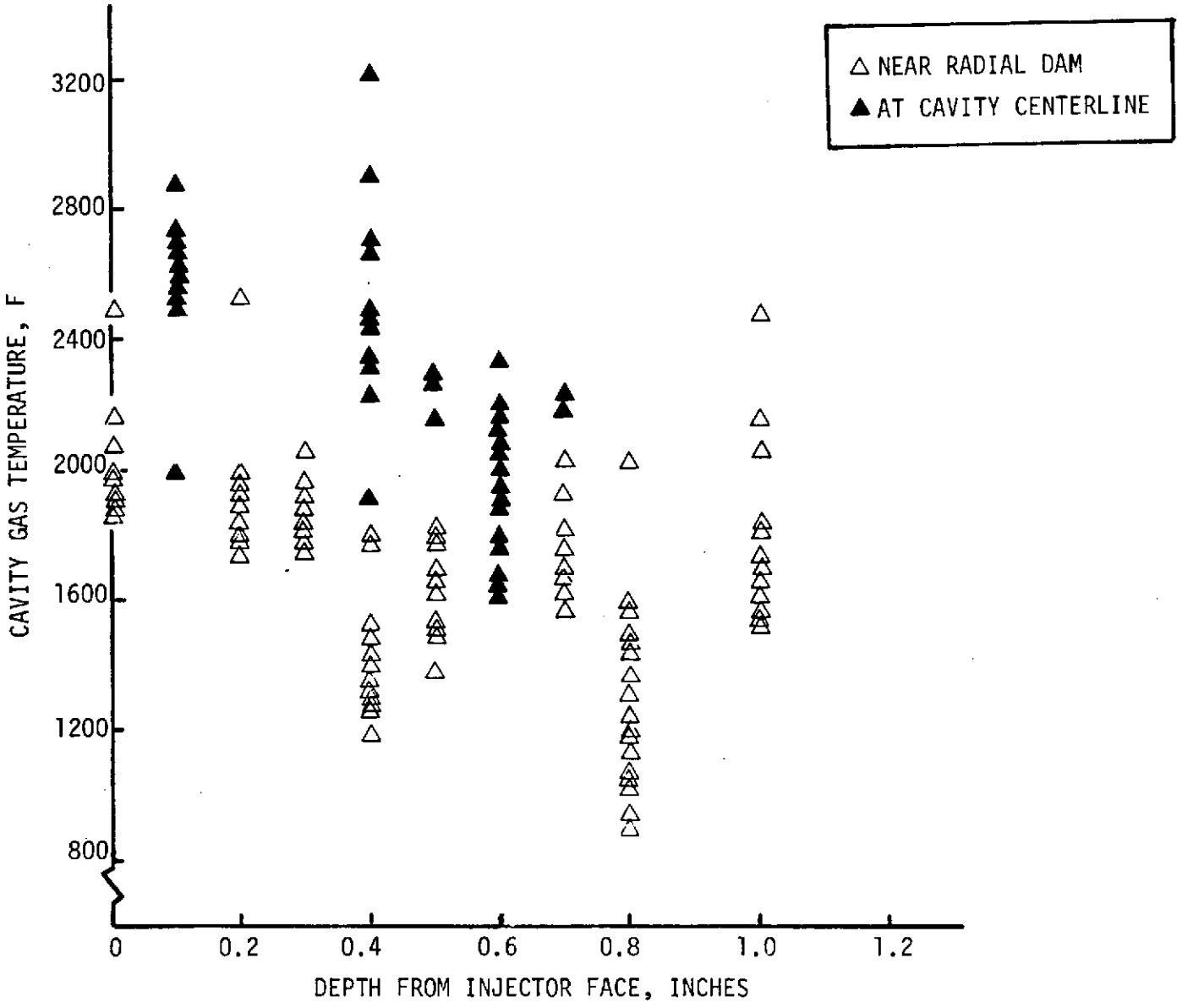

Figure 24. Variation of Cavity Gas Temperature With Depth in Axial Primary Cavities

TABLE 16. ACOUSTIC CAVITY GAS TEMPERATURE MEASUREMENTS DURING N_2O_4/MMH MOTOR FIRINGS WITH AN UNLIKE DOUBLET INJECTOR

Run	Mixture Ratio	Chamber Pressure, psia	Gas Temperature at Given Distances (inch) From Cavity Opening, F					Stability
			0.0	0.1	0.3	0.5	0.75	
86	1.43	126.6	4380	3300	3800	2110	1030	Stable
87	1.37	130.1	>6000	2920	3650	2550	2310	Unstable
88	1.52	128.2	----*	1960	2610	1960	770	Stable
89	1.58	128.6	----	----	2430	2550	2210	Unstable
90	1.51	129.7	----	----	----	2050	870	Stable
91	1.73	132.6	----	----	----	1760	580	↓
92	1.63	131.9	----	----	----	2000	660	
93	1.60	129.7	----	----	----	1840	660	
94	1.50	132.3	----	----	----	----	2270	Unstable
95	1.60	128.7	----	----	----	----	740	Stable

*Indicates thermocouple has burned out.

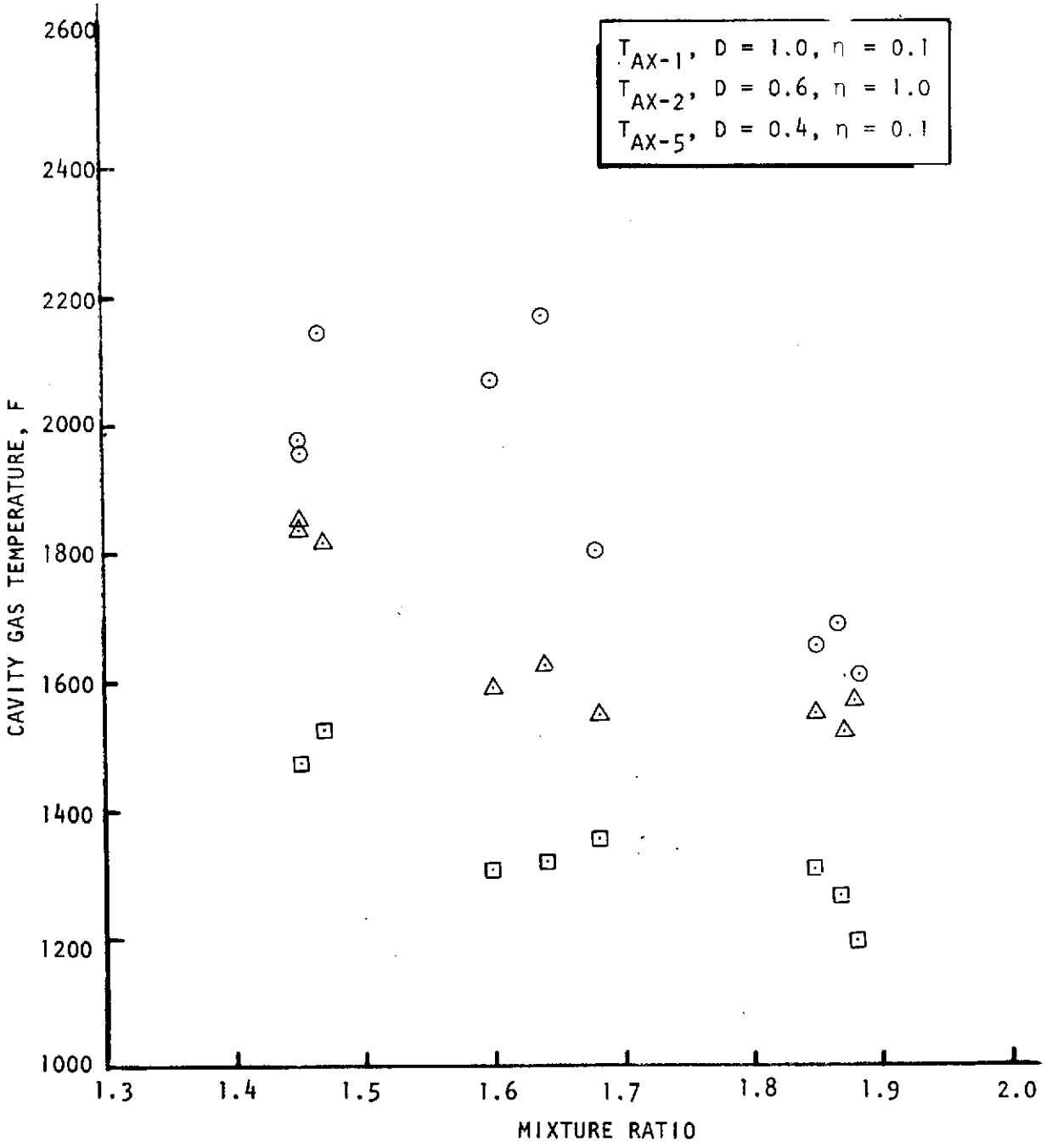

Figure 25. Variation of Measured Cavity Gas Temperature With Mixture Ratio During Runs 177-185

injector because the atomization and mixing characteristics of the impinging like-doublet pairs must be affected to some degree by the variation in spray fan momenta with mixture ratio. However, it should be noted in Fig. 25 that the effects of mixture ratio on the individual thermocouple responses were not the same; consequently, development of a good correlation of mixture ratio effects was considered unlikely with the limited mixture ratio excursions that were made during the hot-firing program. Correlation of cavity gas temperatures was, therefore, undertaken only for the tests at the nominal OME mixture ratio.

The variation of measured gas temperatures with effective cavity depth during tests at nominal mixture ratio, which were used for correlation purposes, is shown in Fig. 26 for the axial cavities, and in Fig. 27 for the radial cavities. Although there is still appreciable scatter in the data, four definite trends appear:

1. The temperature decreases with increasing cavity depth for both axial and radial cavities.
2. The temperature close to the partitions separating the cavity compartments (η = 0.1 inch) is lower than that at the centerline of an axial cavity. However, there is little difference between the centerline and near-partition results for radial cavities.
3. Gas temperatures are lower in the radial cavities than in the axial cavities.
4. The temperatures inside the 0.3-inch-wide radial cavity are lower than those in the 0.5-inch-wide cavity.

During a previous acoustic cavity investigation, made with an LM ascent-type thrust chamber assembly and the N_2O_4/N_2H_4-UDMH (50-50) propellant combination (Ref. 1), a correlation for cavity gas temperatures was developed:

$$\frac{T_g(y) - T_w}{T_g(0) - T_w} = C_1 e^{-C_2 y} - C_3 e^{-C_4 y}$$

where

$T_g(0)$, $T_g(y)$ = gas temperatures at the entrance and depth position y in the cavity, respectively

T_w = wall temperature (assumed constant)

C_1, C_2, C_3, C_4 = empirical coefficients related to the cavity width, distance from the injector, and cavity type (axial or radial)

Cavity temperature results from a more recent cavity technology program (Ref. 4), during which tests were made with the H_2/O_2 propellant combination with a gas/liquid coaxial injector, were correlated with the expression:

$$\frac{T_g(\zeta) - T_w}{T_g(0) - T_w} = e^{-M\zeta}$$

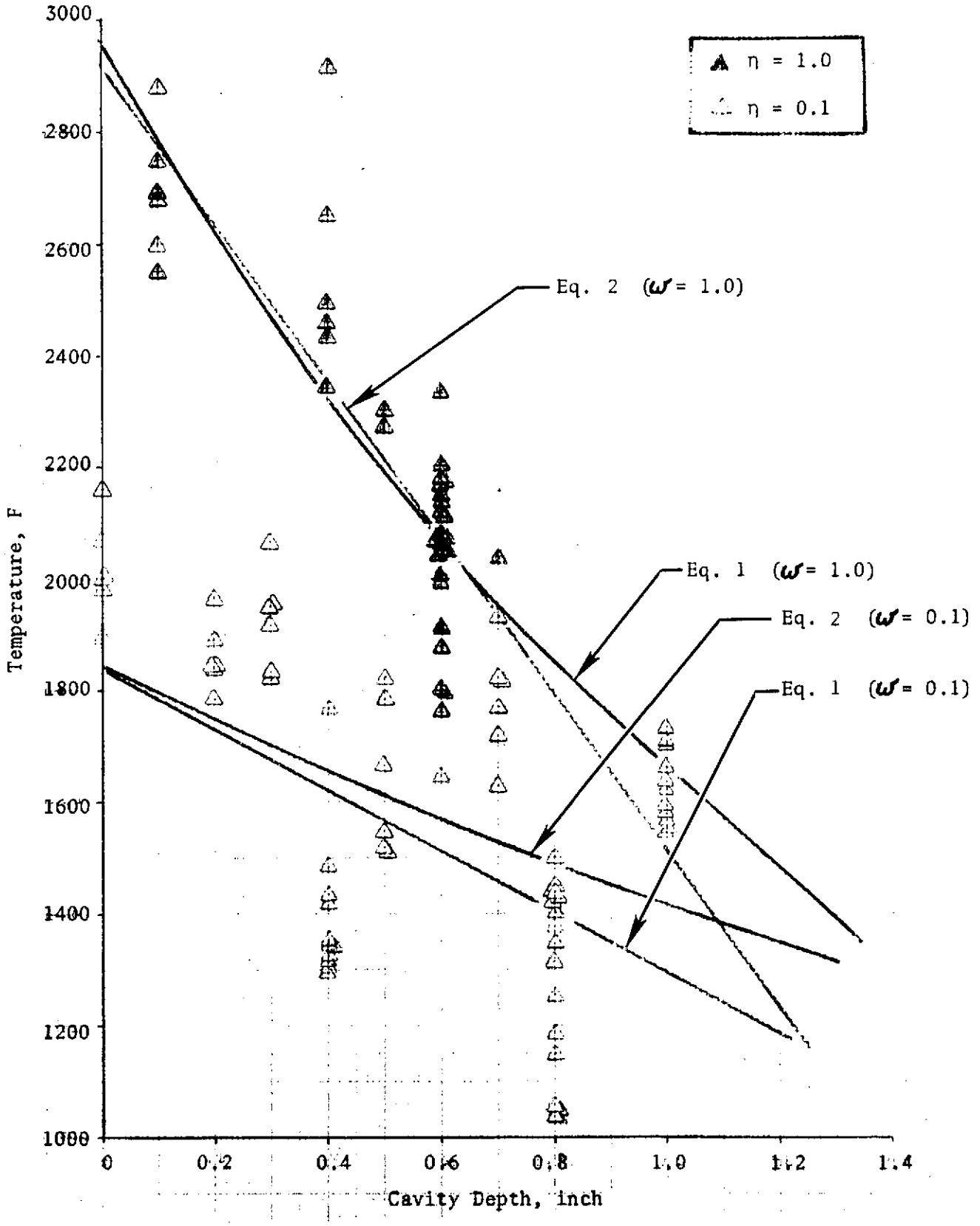

Figure 26. Variation of Gas Temperature With Depth for Axial Cavities (Only Stable Tests at Nominal Mixture Ratio)

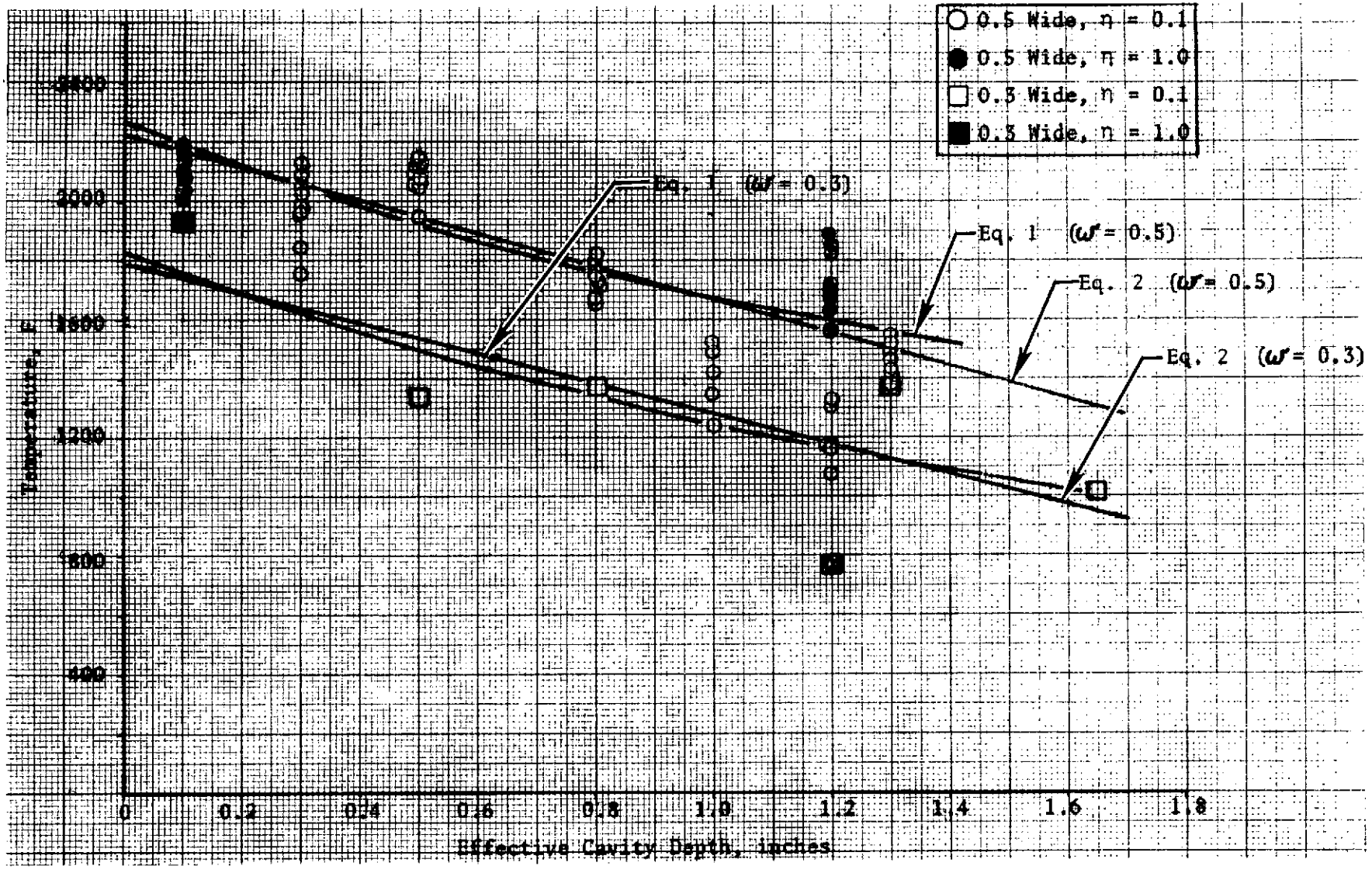

Figure 27. Variation of Gas Temperature With Effective Depth for Radial Cavities (Stable Tests at Nominal Mixture Ratio Only)

where

ζ = effective depth measured along the cavity centerline

M = empirical coefficient which is a function of cavity width and any internal cavity purge flow (the remaining variables have the same meaning as given above)

Neither of these correlations was expected to be directly applicable for the current investigation. The correlation for the LM ascent system was based on an assumed penetration of liquid propellant into the cavities so that subsequent vaporization, with either monopropellant or bipropellant exothermic reactions within the cavities, provided a volumetric heat source in the cavity. The volumetric heat source assemption was needed to explain measured cavity temperature distributions which consistently maximized at a significant depth within the cavity rather than at the cavity entrance, an impossibility for simple convention of sensible heat. During the current program, the cavity temperatures (Fig. 27) appear to maximize at or near the cavity entrance; consequently, no internal heat generation term is needed. The correlation procedure developed to describe the cavity gas temperature distribution for the gas/liquid H_2/O_2 engine was based on the use of a computer model for the coaxial jet combustion (Ref. 4), which provided a good estimate of gas mixture ratio and temperature at the cavity entrance. This procedure allowed an independent definition of $T_g(0)$ so that (with one variable eliminated) only the parameter M needed to be determined from limited data. For a liquid/liquid injector, as used with the OME thrust chamber, no adequate corresponding model for the near-injection gaseous flowfield is available for apriori definition of $T_g(0)$.

Consequently, least-squares data-fitting procedure was used to correlate the cavity temperature measurements with several simple expressions in which cavity depth was the only parameter. Separate correlations were made for the data obtained in the axial and radial cavities and (in the case of the axial cavities) for the data obtained by thermocouples along the cavity centerlines and by the thermocouples located near the compartment separating dams. The best correlations were obtained with two equations:

$$\frac{T_g(\zeta) - T_w}{T_g(0) - T_w} = e^{-B_1\zeta} \tag{1}$$

with T_w arbitrarily chosen as 100 F and

$$T_g(\zeta) = T_g(0) - B_2\zeta \tag{2}$$

The correlating procedure yields values for the empirical coefficients $T_g(0)$, B_1 and B_2, which are shown in Table 17. The temperature distributions calculated from Eq. 1 and 2 are shown in Fig. 26 and 27 along with the data.

TABLE 17. CORRELATION COEFFICIENTS FOR ACOUSTIC CAVITY TEMPERATURE DISTRIBUTIONS

Cavity and Location	Correlation Coefficients			
	$T_g(0)$ (Eq. 1)	B_1 (Eq. 1)	$T_g(0)$ (Eq. 2)	B_2 (Eq. 2)
Axial Cavities (Along Centerline, η = 1.0)	2966	0.63	2913 F	1400
Axial Cavities (Near Partition, η = 0.1)	1842	0.29	1858	455
Radial Cavities, ω' = 0.5 (Combined values of η)	2272	0.34	2229	571
Radial Cavities, ω' = 0.3 (Combined values of η)	1804	0.39	1793	515

Each of these equations describes the data equally well, and a choice between them cannot be made on this basis. The form of Eq. 1 causes the predicted gas temperature to approach an essentially earth ambient temperature (T_w = 100 F) for large cavity depths as a limit, whereas Eq. 2 fails in this regard. However, for cavities with an effective depth (measured from either the injector face in the case of axial cavities or the chamber wall in the case of radial cavities) less than 1.25 inch, the simpler form of Eq. 2 is adequate.

A simple expression for a spatial average cavity gas temperature has been obtained from the correlations for gas temperature along the centerline and near the dam, as described in Appendix B. This expression is:

$$\overline{T}_g(\ell) = \left(T_{0,0} - \frac{B_{2,0}}{2}\ell\right)\left(1 - \frac{b^2}{3a_1^2}\right) + \left(T_{0,1} - \frac{B_{2,1}}{2}\ell\right)\frac{b^2}{3a_1^2} \qquad (3)$$

where

ℓ = cavity depth

b = cavity half width (between partitions)

$T_{0,0}$ ≈ constant $T_g(0)$ of Eq. 2 for the cavity centerline

$T_{0,1}$ ≈ constant $T_g(0)$ of Eq. 2 near the cavity wall

a_1 = b - n

$B_{2,0}$ and $B_{2,1}$ are the correlation coefficients, B_2, of Eq. 2 at the cavity centerline and near the cavity wall, respectively.

For the primary axial cavities of the present investigation, ℓ is approximately 1.2 inch, b is approximately 1.0 inch, and a_1 is approximately 0.9 inch, so that the corresponding predicted spatial average temperature is:

$$\overline{T}_g(1.2) = \left(2966 - \frac{1400}{2}(1.2)\right)\left(1 - \frac{1}{3(0.9)^2}\right) + \left(1858 - \frac{455}{2}(1.2)\right)$$

$$= 1904 \text{ F}$$

For the three radial cavities used in the investigation, the predicted average temperatures are:

$\overline{T}_g$ = 1355 F for radial No. 1 (ℓ = 1.9, w = 0.5)

$\overline{T}_g$ = 1758 F for radial No. 2 (ℓ = 1.8, w = 0.5)

$\overline{T}_g$ = 1872 F for radial No. 3 (ℓ = 1.4, w = 0.3)

CONCLUSIONS

The results from this program clearly indicate that dynamic stability can be ensured in regeneratively cooled OMS enginesthrough the use of acoustic cavities. Stable operation has been demonstrated with a range of cavity configurations that indicates at least a moderate stability margin can be obtained. Further, adequate suppression has been demonstrated with doubly tuned cavity configurations that prevented the first and third tangential modes and the first radial mode from occurring. All three of these modes were encountered when insufficient suppression was provided.

The ability to suppress multiple modes of instability is an important aspect of the use of acoustic cavities because multiple modes are often encountered. Further, the observed relationship of the stability and amplitude of the first radial/third tangential modes to the BLC flowrate with the OME-type hardware used during the test program is interesting and is considered significant. Nevertheless, the same modes were never triggered by the stability-rating bombs. Also, the circumferential distribution of multiple-tuned cavities to suppress multiple modes of instability was shown to be important.

Acoustic model tests during the program were found to be an effective means of characterizing the resonance characteristics of practical but geometrically complex cavity configurations that could not be readily analyzed mathematically.

At the completion of this contract, a copy of the computerized analytical model, used for prediction of cavity damping, was delivered to NASA-JSC, along with an operating manual.

Although the utility of acoustic cavities has been demonstrated and much has been learned, several areas are still uncertain. Among these is the 2600-Hz oscillation that occurred repeatedly during the test program. This mode of oscillation has been tentatively identified as associated with the feed system, but no significant effort was devoted to suppression or analysis of it. This mode may not be significant relative to the use of acoustic cavities, assuming it may be eliminated by modifying the feed system, but it could be a significant stability problem for an engine development program.

In addition, the ranges of cavity configurations that will prevent one or more modes of instability have not been determined sufficiently to allow an adequate evaluation of the predicted stability characteristics. A more complete definition of this range of cavity dimensions would permit current design techniques to be evaluated properly and would also permit improvements to be made. A related problem is the interpretation of the cavity temperature data. These data, assuming they are representative of the cavity gas temperatures (and ignoring temperature gradients), may often be interpreted to indicate improper cavity tuning when the cavities are clearly suppressing an instability. Better definition of the cavity tuning required for stability and further evaluation of temperature effects are needed.

APPENDIX A

ITERATIVE EQUATIONS FOR PREDICTION OF CAVITY DAMPING FROM A CIRCUMFERENTIALLY NONUNIFORM RADIALLY DIRECTED CAVITY

An analytical model was developed previously for predicting the damping caused by an acoustic cavity. However, the analysis and calculations made to date have been based on a simplifying assumption that the acoustic impedance of the cavity was circumferentially uniform, which simplifies the analysis considerably. Nonetheless, the method can be applied easily to the circumferentially nonuniform case.

Employing the method used previously, the cavity damping may be predicted by solving a characteristic equation which may be written as:

$$\int y(S) \quad \xi^{(i)} \left\{ \xi^{(i)} - \xi^{(i+1)} \right\} dS = 0$$

The corresponding characteristic equation may be written as:

$$\sum_{m\nu\eta q} \left\{ {}^{(i)}_{a_{m\nu}} \; {}^{(1)}_{I_{m\eta}} \left({}^{(i)}_{a_{\eta q}} - {}^{(i+1)}_{a_{\eta q}} \right) + {}^{(i)}_{a_{m\nu}} \; {}^{(2)}_{I_{m\eta}} \left({}^{(i)}_{b_{\eta q}} - {}^{(i+1)}_{b_{\eta q}} \right) + \right.$$

$$\left. {}^{(i)}_{b_{m\nu}} \; {}^{(3)}_{I_{m\eta}} \left({}^{(i)}_{a_{\eta q}} - {}^{(i+1)}_{a_{\eta q}} \right) + {}^{(i)}_{b_{m\nu}} \; {}^{(4)}_{I_{m\eta}} \left({}^{(i)}_{b_{\eta q}} - {}^{(i+1)}_{b_{\eta q}} \right) \right\} G_{\nu q} = 0$$

With circumferentially uniform cavity, the characteristic equation contains a double summation, rather than the quadruple summation shown above, and only one set of coefficient terms (corresponding to the four sets shown above).

These equations have not yet been programmed for numerical solution.

In addition, the oscillatory pressure may be expressed as:

$$p = -j \; k \int y \; G \; p \; dS$$

where G is a Green's function which may be expressed as:

$$G(r|r_m) = \sum_{m,\nu} \frac{\varepsilon_m \; \varepsilon_\nu}{2 \; \pi \; L} \; \frac{\cos m(\theta - \theta_o) \; \cos \frac{\nu \pi z}{L} \; \cos \frac{\nu \pi z_o}{L} \; J_m \; (k_{m\nu} \; r)}{k_{m\nu} \; J'_m \; (k_{m\nu} \; r_w)}$$

Therefore,

$$p = -j\ k \sum_{m,\nu} \frac{\varepsilon_m\ \varepsilon_\nu}{2\ \pi\ L}\ \frac{\cos\ \frac{\nu\pi z}{L}\ J_m\ (k_{m\nu}\ r)}{k_{m\nu}\ J'_m\ (k_{m\nu}\ r_w)}$$

$$\left\{\cos\ m\theta \int r_w y\ (z,\theta)\ \cos\ m\theta_o\ \cos\ \frac{\nu\pi z_o}{L}\ dz\ +\right.$$

$$\left.\sin\ m\theta \int r_m y\ (z,\theta)\ \sin\ m\theta_o\ \cos\ \frac{\nu\pi z_o}{L}\ dz_o\ d\theta_o\right\}$$

This expression is of the form:

$$p = \sum_{m,\nu} \left(k_{m\nu}\ \cos\ m\theta + b_{m\nu}\ \sin\ m\theta\right)\ \cos\ \frac{\nu\pi z}{L}\ \frac{J_m\ (k_{m\nu}\ r)}{J_m\ (k_{m\nu}\ r_w)}$$

This form is used to define iterated coefficients from the integral equation for pressure. The iterated expression for pressure is defined as:

$$\xi^{(i+1)} = -j\ K \int y\ G\ \xi^{(i)}\ dS$$

Corresponding with:

$$\xi^{(i)} = \sum_{m,\nu} \left(a^{(i)}_{m\nu}\ \cos\ m\theta + b^{(i)}_{m}\ \sin\ m\theta\right)\ \cos\ \frac{\nu\pi z}{L}$$

From evaluating the pressure integral above, the iterated coefficients may be obtained as:

$$a^{(i+1)}_{m\nu} = -j\ k\ \frac{\varepsilon_m\ \varepsilon_\nu}{2\ \pi\ L}\ \frac{J_m\ (k_{m\nu}\ r_w)}{k_{m\nu}\ J'_m\ (k_{m\nu}\ r_w)}\ \sum_{\eta q} \left(a^{(i)}_{\eta q}\ I^{(1)}_{m\eta} + b^{(i)}_{\eta q}\ I^{(2)}_{m\eta}\right) G_{\nu q}$$

$$b^{(i+1)}_{m} = -j\ k\ \frac{\varepsilon_m\ \varepsilon_\nu}{2\ \pi\ L}\ \frac{J_m\ (k_{m\nu}\ r_w)}{k_{m\nu}\ J'_m\ (k_{m\nu}\ r_w)}\ \sum_{\eta q} \left(a^{(i)}_{\eta q}\ I^{(3)}_{m\eta} + b^{(i)}_{\eta q}\ I^{(4)}_{m\eta}\right) G_{\nu q}$$

where

$$I^{(1)}_{m\eta} = \int y \cos m\theta \cos \eta\theta \, d\theta$$

$$I^{(2)}_{m\eta} = \int y \cos m\theta \sin \eta\theta \, d\theta$$

$$I^{(3)}_{m\eta} = I^{(2)}_{\eta m}$$

$$I^{(4)}_{m\eta} = \int y \sin m\theta \sin \eta\theta \, d\theta$$

$$G_{\nu g} = \int \cos \frac{\nu\pi z}{L} \cos \frac{\nu\pi z}{L} \, dz$$

APPENDIX B

DERIVATION OF EXPRESSION FOR SPATIAL AVERAGE TEMPERATURE IN AXIAL CAVITIES

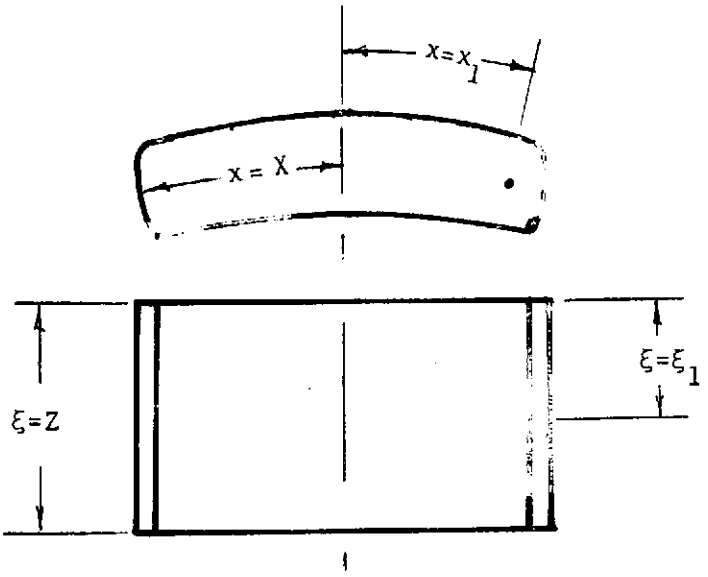

For the cavity geometry shown in the sketch above, the simplest relation for the temperature, $T(\xi = \xi_1)$, in any plane, ξ_1, which satisfies the requirement:

$$\frac{\partial T}{\partial x} = 0 \text{ at } x = 0$$

and which can be expressed in terms of empirically determined local temperatures at $x = 0$ and $x = x_1$* is:

$$T = T(x = 0) - Nx^2 = T_o - Nx^2$$

where N is an empirical coefficient.

The corresponding spatial average temperature in plane ξ_1 is:

$$\frac{\int_0^X T dx}{X} = \frac{T_0 X - \frac{NX^3}{3}}{X} = T_0 - \frac{NX^2}{3}$$

*The coordinate x is the inverse of the coordinate η used in the main test of the report, i.e.,

$$\eta = X - x$$

The coefficient N can be determined from the empirical temperatures T_0 and T_1 as:

$$N = \frac{T_0 - T_1}{x_1^2}$$

so that the average temperature becomes:

$$\overline{T}_g = T_0 - \frac{X^2}{3}\left(\frac{T_0}{x_1^2} - \frac{T_1}{x_1^2}\right)$$

$$\overline{T}_g(\xi) = T_0(\xi)\left(1 - \frac{X^2}{3x_1^2}\right) + \frac{X^2 T_1(\xi)}{3x_1^2}$$

But the empirical temperatures $T_0(\xi)$ and $T_1(\xi)$ are conveniently defined by the correlations:

$$T_0(\xi) = T_{0,0} - B_{2,0}\,\xi$$

$$T_1(\xi) = T_{0,1} - B_{2,0}\,\xi$$

so that:

$$\overline{T}_g(\xi) = (T_{0,0} - B_{2,0}\,\xi)\,(1 - \frac{X^2}{3x_1^2}) + (T_{0,1} - B_{2,1}\,\xi)\,\frac{X^2}{3x_1^2}$$

The spatial average temperature for a cavity of total depth Z is then given by:

$$\overline{T}_g(Z) = \left[(T_{0,0} - \frac{B_{2,0}}{2}\,Z)\,(1 - \frac{X^2}{3x_1^2}) + (T_{0,1} - \frac{B_{2,1}}{2}\,Z)\,\frac{X^2}{3x_1^2}\right]$$

REFERENCES

1. Oberg, C. L. et al., Final Report: Evaluation of Acoustic Cavities for Combustion Stabilization, NASA CR-115087, R-8757, Rocketdyne Division, Rockwell International, Canoga Park, California, July 1971.

2. Oberg, C. L. et al., Analysis of Combustion Instability in Liquid Propellant Engines With or Without Acoustic Cavities, R-9353, Rocketdyne Division, Rockwell International, Canoga Park, California, May 1974.

3. Oberg, C. L. et al., Analysis of the Wave Motion in Baffled Combustion Chambers, NASA CR-72879, R-8758, Rocketdyne Division, Rockwell International, Canoga Park, California, October 1971.

4. Hines, W. S. et al., Final Report: Advanced Acoustic Cavity Technology, R-9136, Rocketdyne Division, Rockwell International, Canoga Park, California, May 1974.